

Fluorinated building blocks for the next-generation polymer electrolyte membrane fuel cells

Mohan N. Wadekar

To,
Madhavi, Vedinee, Aai, Baba and Kaustubh.....
माधवी, वेदिनी, आई, बाबा आणि कौस्तुभ यांस.....

Fluorinated building blocks for the next-generation polymer electrolyte membrane fuel cells

Proefschrift

ter verkrijging van de graad van doctor
aan de Technische Universiteit Delft,
op gezag van de Rector Magnificus Prof. ir. K.C.A.M. Luyben,
voorzitter van het College voor Promoties,
in het openbaar te verdedigen

op woensdag, 07 november 2012 om 10:00 uur

door

Mohan N. Wadekar

Master of Science, Post Graduate Teaching Center,
Shivaji University, Solapur

Geboren te Satara, Indie (India).

Dit proefschrift is goedgekeurd door de promotor:
Prof.dr. S. J. Picken

Copromotor:
Dr. W. F. Jager

Samenstelling promotiecommissie:

Rector Magnificus,	voorzitter
Prof. Dr. S.J. Picken,	Technische Universiteit Delft, promotor
Dr. W.F. Jager,	Technische Universiteit Delft, copromotor
Prof. Dr. B. Ameduri,	University of Montpellier II
Prof. Dr. E.J.R. Sudhölter,	Technische Universiteit Delft
Prof. Dr. J.H. van Esch,	Technische Universiteit Delft
Dr.ing. G.J.M. Koper	Technische Universiteit Delft
Dr. G.J.M. Janssen	Energieonderzoek Centrum Netherlands
Prof. Dr. A. Schmidt-Ott	Technische Universiteit Delft, reservelid

This thesis is part of the SANE-PEMFC project which was subsidised by The Ministry of Economic Affairs in the Netherlands via the EOS LT framework (EOS LT 02025). Partial support from the COST Action CM1101 and collaboration with the Energy research Centre of the Netherlands (ECN) also contributed to this thesis.

ISBN: 9789088915178

Copyright © 2012 by Mohan N. Wadekar

All right reserved. No part of this publication may be reproduced or utilized in any form or by any means, electronic, or mechanical, including photocopying, recording or by any information storage and retrieval system without written permission of the author.

Printed in the Netherlands.

Table of contents

Chapter 1. Introduction: Polymer Electrolyte Membrane Fuel Cell; operation, components and optimization challenges.....	1
1.1 Introduction	2
1.1.1 World Energy	2
1.1.2 Polymer Elelctrolyte Membrane Fuel Cell	3
1.1.3 Opertion and components of PEMFC	4
1.2 Scope of the thesis.....	9
1.3 Outline of the thesis chapters	11
1.4 References and Notes.....	13
 Chapter 2. Synthetic routes to couple fluorocarbons to aromatic molecules and for creation of styryl moiety.....	 15
2.1 Introduction	16
2.1.1 Design of the polymerizable fluorosurfactant	16
2.1.2 Chemistry of fluorocarbons	17
2.1.3 Choice of starting materials	18
2.1.4 Reactions on α carbon	18
2.2 Experimental Section	20
2.2.1 Instrumentation	20
2.2.2 Materials and synthesis	20
2.3 Results and discussion.....	25
2.4 Conclusions.....	30
2.5 References and Notes.....	32
 Chapter 3. Syntheses of the polymerizable hybrid fluorosurfactant 1 and nonpolymerizable analogue 2	 33
3.1 Introduction	34
3.2 Experimental	37
3.2.1 Instrumentation.....	37
3.2.2 Materials	38
3.3 Results and discussion.....	41

3.4	Conclusions.....	45
3.5	References and notes	47

Chapter 4. Micellization properties and thermodynamics of micellization of hybrid fluorosurfactants 1 and 2..... 49

4.1	Introduction	50
4.2	Experimental	52
4.3	Results and discussion.....	53
4.3.1	Surface tension experiments	53
4.3.2	Isothermal titration calorimetry	57
4.3.3	Ionic conductivity experiments	59
4.4	Conclusion	63
4.5	References and notes	65

Chapter 5. Supramolecular “Leeks” of the fluorinated hybrid amphiphile, 2 that self-assemble into a supramolecular columnar phase 67

5.1	Introduction	68
5.2	Experimental	70
5.2.1	Materials and Methods	70
5.3	Results and discussion.....	71
5.4	Conclusions.....	83
5.5	Appendix	83
5.6	References and notes	86

Chapter 6. Syntheses and characterization of (co)polymers from 1 89

6.1	Introduction	90
6.2	Experimental Section	90
6.2.1	Polymer Synthesis	90
6.2.2	Polymer characterization	91
6.3	Results and Discussion	92
6.3.1	Synthesis of polymers.....	92
6.3.2	FTIR spectra	95
6.3.3	NMR study	97
6.3.4	Comonomer ratio	99

6.3.5	Thermal characterization	100
6.3.6	Cryo-TEM study on the micelles of P1	103
6.4	Conclusions.....	105
6.5	References and notes	106
Chapter 7.	General conclusions and future recommendations.....	107
Summary		109
Sammenvatting		111
Acknowledgements		113
Curriculum Vitae		115
Publications		117

Chapter 1

Introduction: Polymer Electrolyte Membrane Fuel Cell; operation, components and optimization challenges

In this chapter, current global scenario for energy consumption is discussed. PEMFC operation and its components are described in detail. The technological and economical challenges to develop PEMFCs with satisfactory performance are discussed. After a brief overview of the past efforts to develop PEMFCs with low cost, good durability and optimum output, ideas to develop *self-assembled nanostructured membranes and electrodes* for better fuel cells are discussed. Project motivations, objectives and plan of actions of the project are discussed. At the end, the outline of the chapters is revealed.

1.1 Introduction

1.1.1 World Energy

As the world population is crossing seven billion at the starting of this decade, demands for energy consumption has increased to a record level of more than 12000 million tons of oil equivalent.¹ Crude oil, natural gas and coal have been the main sources of energy supply, with industrial and transportation sectors consuming the largest part of energy, (see Figure 1.1). With depleting their reserves and with increasing their prices, it has become increasingly imperative to strive for the sustainable solutions to produce energy from the renewable sources like, solar, wind energy, hydropower, and bio energy. For examples, European Union targets to use more than 20% of the energy from renewable resources by 2020.² Further, it is a big challenge to curb the emission of green house gases such as CO₂, SO₂ in the atmosphere generated due to the consumption of coal, crude oil and natural gas.

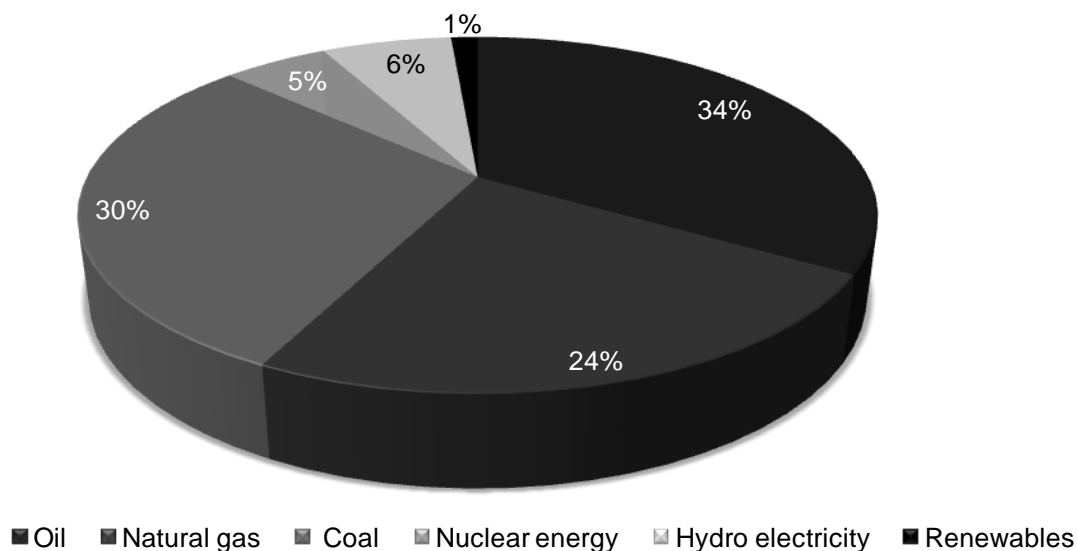


Figure 1.1. Distribution of the types of energy sources in the world's total energy consumption in 2010. The data has been taken from the Statistical Review of World Energy, June 2011 of British petroleum.¹

1.1.2 Polymer Electrolyte Fuel Cell (PEMFC)

Fuel cells are attractive options in that respect to convert chemical energy stored in fuel like hydrogen in to electrical energy. They are regarded as near-future technology to generate power for stationary applications like house hold energy supply as well as for the fields like transportation, telecommunication, space technology and portable electronic systems.³

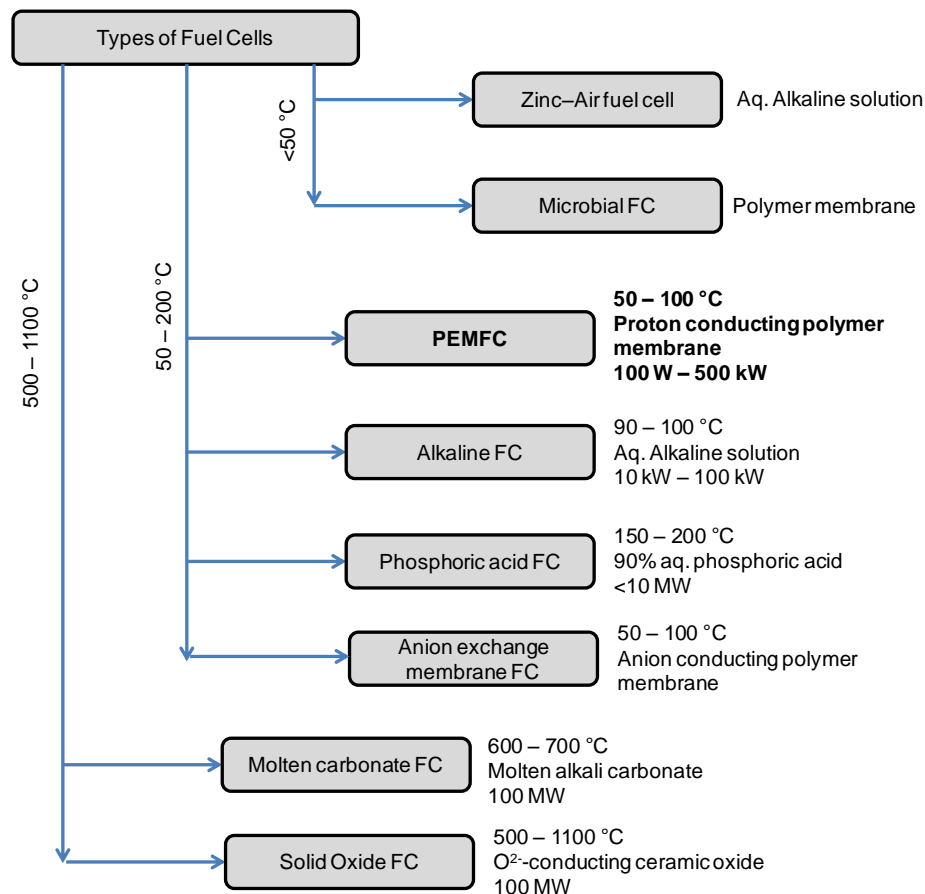


Figure 1.2. Various types of fuel cells, their operating temperature and the proton transporting medium used in them. Their power output range is also given.²

There are various types of fuel cells mainly based on the type of electrolyte medium used in them as well as on the temperature range at which they operate. Nevertheless, the type of electrolyte often depends upon the operating temperature. Figure 1.2 depicts various categories of fuel cells, the electrolyte type, operating temperature range used by them and power generated.

In solid oxide fuel cells, ceramic membrane made up of doped zirconium oxide and in alkaline fuel cells, sodium hydroxide or potassium hydroxide solution act as the

electrolyte. In polymer electrolyte membrane fuel cells (PEMFCs), proton transporting polymeric membrane is used as the electrolyte to transport protons. The main topic of discussion of this chapter is PEMFC (Figure 1.3) and the main objective of the whole work in this thesis is to improve the overall efficiency of PEMFCs and decrease their cost. Since, PEMFCs are seen as one of the most attractive options for the energy supply for transportation, there has been a sudden thrust in the PEMFC research for the last couple of decades to decrease their cost and improve overall output. A large part of research is also devoted to improve the thermal and chemical long duration stability of their components for steady performance, since they operate at elevated temperatures and very low pH and strongly oxidizing conditions.

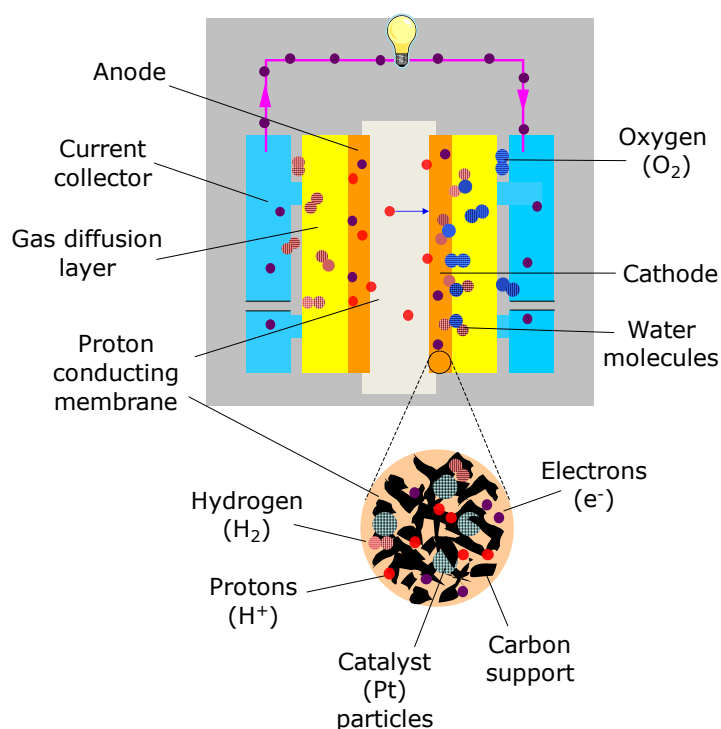


Figure 1.3. Pictorial representation of PEMFC and the operation. Also the morphology of the electrode layers is shown in insight.

1.1.3 Operation and components of PEMFC

In PEMFCs, hydrogen is introduced from anode side and oxygen from cathode side as shown in Figure 1.3. Hydrogen reacts on the surface of Pt catalyst nanoparticles

on the anode to liberate electrons and H^+ ions. The electrons pass through the outside circuit to supply electrical energy whereas protons transport through proton exchange membrane towards cathode side. There, they react with oxygen on the surface of catalyst particles to generate water molecules. Thus the chemical energy stored in hydrogen is converted into electricity. While doing so heat and water are generated as the byproducts. The main component of the PEMFCs where all these reactions take place is the membrane electrode assembly (MEA) which is the “heart” of the fuel cell. The MEA is made up of a thin **proton exchange membrane** (PEM) sandwiched between two **electrode** layers.

Proton exchange membrane. PEMs are typically made up of ~20 to 100 μm thick proton conducting polymer membranes, sandwiched between two electrodes. In the case of PEMFCs operating $<100\text{ }^\circ C$, they are made up of sulfonated ionomers with fully/partially fluorinated structures or various types of aromatic backbones. To make membranes for PEMFCs operating $\geq 100\text{ }^\circ C$, certain aromatic polymers (e.g. polybenzimidazoles) doped with inorganic nanoparticles or oxo- acids are used.⁴ Figure 1.4 illustrates the molecular structure of some proton conducting polymers used to make PEMs.^{3,5} The most commonly used and commercially available polymers are polymeric perfluorinated sulfonic acids (PFSA) like Nafion[®], Flemion[®], Aciplex[®], and Dow membranes. Other widely used polymers are aromatic sulfonic acid based polymers like sulfonated polystyrene, sulfonated poly(ether ether ketones), sulfonated poly(aryl ether sulfones), and sulfonated poly(benzimidazoles).

PEMs are prepared by solution casting of the ionomers into thin membranes. Due to the presence of sulfonate groups, the morphology of PEMs is microphase separated into nanodimensional interconnecting ionic channels and a nonionic hydrophobic matrix. The protons are transported over the sulfonate ($-SO_3^-$) groups or water molecules (as H_3O^+) through these percolating ionic channels. The presence of water molecules inside the proton conducting channels drastically enhances the proton conductivity hence, for high performance of current state-of-the-art PEMFCs, the PEMs need to have high relative humidity (RH, up to 100%). Apart from having sufficiently high proton conductivity ($>0.01\text{ S cm}^{-1}$), these hydrated PEMs need to have various properties like very low permeability for fuel and oxygen, reasonably

good mechanical properties as well as high thermal, and chemical and electrochemical stability for long duration.

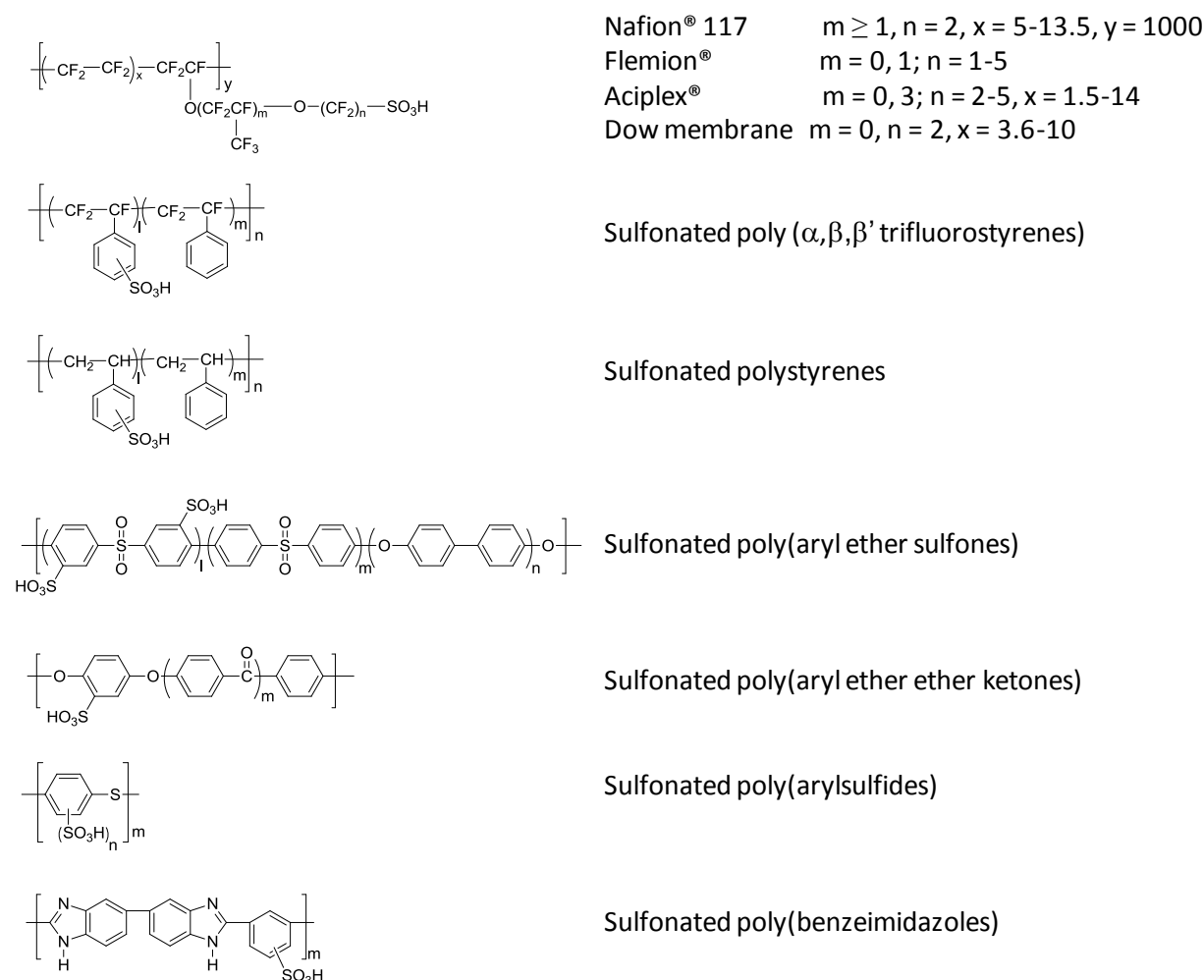


Figure 1.4. Molecular structures of some proton conducting polymers used to make PEMs.^{3,5}

Nafion® membranes are widely used PFSA materials in commercial PEMFCs. Typically, PFSA's like Nafion® are relatively expensive, protected by patents, and have limited percentage of proton transporting $-\text{SO}_3^-$ groups. They lose much of their activity above 100 °C due to loss of water. Further Nafion® is a random statistical copolymer, where the $-\text{SO}_3^-$ group containing repeating units are unevenly distributed throughout the polymer chains. This causes the poor control over the microstructure and thus the way it phase separates into proton conducting channels and fluorinated nonpolar matrix. The poorly optimized microstructure leads to several

dead ends of the ionic channel beyond which the protons cannot be transported further. Due to these reasons, the morphology of these membranes is kinetically trapped, less optimized.

Although the increase in the percentage of proton transporting groups increases proton conductivity in the polymer; water uptake and subsequent swelling also increase in parallel, resulting in inferior mechanical properties. Thus a substantial increase in the percentage of proton transporting groups without deterioration in other properties is a challenging task. Current state-of-the-art PEMFCs operate at around 60-80 °C with PFSA membranes, and high RH. Overall to improve the performance and decrease the cost per unit of PEMFC stack, it is necessary to engineer membranes with superior proton conductivity (probably by increasing the percentage of $-\text{SO}_3^-$ groups), reasonable mechanical properties as well as equally good thermal and chemical stability at operating temperatures >90 °C and at low RH of the feed gases.

b) Electrode layers. The PEMFC electrodes are fabricated by mixing the solution of carbon particles with the active catalyst metal nanoparticles adsorbed on them and solution of proton conducting polymer (generally PFSA's like Nafion[®] to act as a binder and proton conducting phase) and printing/pressing techniques on either electron transporting support like carbon paper or applying the mixture directly on both sides of proton exchange membranes followed by mechanical pressing.

The electrodes perform four functions. A) Carry out electrocatalytic reactions by metal nanoparticles. B) Transport of electrons through the conducting carbon particles phase on which the metal particles are adsorbed. C) Transport of protons towards PEM, that occurs through proton conducting polymer phase within the electrodes. D) Transport of reactants and products i.e. oxygen or hydrogen and water towards the catalytically active sites i.e. metal particles that occurs through the porous structures within electrodes and gas diffusion layer. To perform these tasks efficiently the triple phase points (Figure 1.5), where metal nanoparticles, carbon support and $-\text{SO}_3^-$ are in close contact with each other, play a very crucial role. More the number of triple phase points, more efficient is the electricity generation. Similarly, an important role is played by the water molecules diffusing through the

pores of the electrodes. At lower water content (RH) or higher temperature, *i)* there is increase in inefficient utilization of catalyst particles. Under wet conditions the fraction of metal nanoparticles connected to $-\text{SO}_3^-$ groups can be quite high as water can play connecting role. Under dry conditions this is less efficient and catalyst particles either get covered by polymer chains or they are away from $-\text{SO}_3^-$ groups on PFSA and thus do not form sufficient triple phase points which are necessary for effective transport of protons from the reaction sites. *ii)* The proton transportation between active sites and the membrane itself becomes more difficult. *iii)* The transport of reactant gases such as oxygen becomes more difficult as the permeability of dry PFSA is lower than of wet PFSA. In wet conditions, gas transports also occur more efficiently since the gases are also dissolved to some extent in water.

Thus the numbers of active metal nanoparticles exposed for the electrocatalytic reactions, the number of triple phase points, connectivity among the carbon particles as well as within the proton conducting polymer phase, and relative humidity are important parameters for a decent performance of fuel cell.

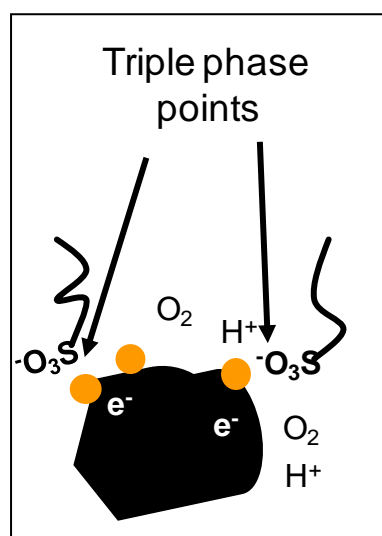


Figure 1.5. Triple phase points in the electrode microstructure.

The electrode fabrication accounts for almost 55% of the PEMFC cost.⁶ This is because of the highly expensive Pt, used as electrocatalyst for the oxidation reduction reaction (ORR) on cathode and hydrogen oxidation reaction (HOR) on

anode. It is the main ingredient of the electrodes on which all the reactions take place. These Pt nanoparticles usually are of size 3-5 nm. Pt is highly active catalyst and being a noble metal it is comparatively more stable than any other metal in strongly oxidizing conditions. Due to strongly acidic corrosive conditions, and elevated temperature, the catalyst particles need to be highly stable and catalytically active for long duration. Even Pt nanoparticles slowly dissolve and reprecipitate under these conditions (mainly on cathode side) leading to a decrease in the efficiency. Further their activity for ORR reactions is not as good as for HOR reactions and gases like carbon monoxide often decrease their activity by strongly binding them below 80 °C (fuel cell operating temperature). Degradation of the carbon (particles) support further decreases the electrode performance by destabilization of the binding between the support and catalyst particles. Although the amount of Pt in current state-of-the-art electrodes is minimum at $\sim 0.4 \text{ mg cm}^{-2}$ (this is for cathode, for anode it is 0.03 mg cm^{-2}), it still contributes to major part of the electrode cost.⁷ Due to random pore structure of carbon and because some Pt nanoparticles are covered by proton conducting polymer phase, not all catalyst particles in electrodes are accessible for the gases, thus reducing the number of active catalyst particles and the number of triple phase points. The traditional ways of preparing electrode layers although are easy; they do not ensure the optimal efficiency of the components and not all Pt nanoparticles are used during the electrocatalytic reactions with gases and there have been investigations to optimize the utilization and thus lower the loading of Pt nanoparticles on the electrodes.^{8,9} There is poor control over the microstructure of the electrode layers, which is why there are performance losses. It is said that almost one third of the performance losses in PEMFC occur at the electrodes (mainly at cathode).⁶ Researchers have attempted for robust and optimized electrode design by various electrode fabrication methods, synthesizing Pt catalyst by various ways, using better carbon support from various sources.⁸

1.2 Scope of the thesis

To improve the performance of PEMFC membranes and electrodes, it is necessary to improve their microstructures. As discussed in the previous sections, researchers have made efforts to improve their performances by using top-down approaches e.g.

PEMs were prepared from variety of PFSA or aromatic based polymers using different routes. Similarly electrodes were fabricated using carbon support from various sources, using Pt nanoparticles synthesized by variety of methods, and fabricating electrodes in many different ways. For instance, the designs of PEMFC electrodes to achieve optimum transport of gases, electrons and protons have been discussed in a review by McLean *et al.*⁸

However, hardly there have been efforts to improve the microstructures by bottom-up approach where, basic building blocks were synthesized and membranes as well as electrodes were fabricated by self-assembly of these building blocks. In rare examples, the efforts were made to improve the efficiency of PEMs by their fabrication from block or graft copolymers due to which well organized proton conducting channels can be created within the PEMs.^{10,11}

Our efforts were directed to create *self-assembled nanostructured PEMs and electrodes* by such a bottom-up approach. For this, we have synthesized a fluorinated polymerizable surfactant **1** and similar looking nonpolymerizable surfactant **2** (Figure 1.6) as our building blocks, resembling in molecular structure to Nafion®. Further, we have studied their phase behavior in water and the polymerization of **1**.

Surfactants in principle, form micelles in polar solvent like water. Initially they are spherical at low (<1%) surfactant concentration. With change in the relative concentrations of surfactant and water or on adding the third component like oil or salt, micelles of various shapes can be formed. For example, spherical micelles convert into rod-like micelles or bicontinuous irregularly shaped micelles or vesicles. At very high concentrations of surfactants ordered lyotropic liquid crystalline (LLC) phases are formed like, hexagonal phases with rod-like micelles or lamellar phases with sheets or cubic phases with ordered bicontinuous micelles.

To create *self-assembled nanostructured PEMs and electrodes* by bottom-up approach, we intend to first make an appropriate micellar phase of **1** with water and polymerize the whole phase without disrupting the morphologies. Thus PEMs will be made by polymerization of a thin layer of appropriate micellar phase of **1** with water.

To retain the mechanical integrity of the polymerized structure and to control the percentage of sulfonate groups, a comonomer (e.g. compound 3) or cross linking agents (like divinyl benzene) can be added as the third component. After polymerization, water will be removed. A similar procedure will be carried out to make electrodes but in the presence of Pt nanoparticles supported on carbon. Bicontinuous phases are most attractive phases for this purpose as they form continuous network of polar hydrophilic phase and nonpolar hydrophobic phase simultaneously and they have maximum interfacial area between hydrophobic phase and hydrophilic phase. Bicontinuous microemulsions of polymerizable hydrocarbon surfactants have been polymerized.¹² In general micellar phases will also ensure the arrangement of all $-\text{SO}_3^-$ groups in close vicinity with each other. Thus, proton conduction will essentially occur over $-\text{SO}_3^-$ groups and PEMs will rely less on the amount of water present. In case of the electrodes engineered using same approach, carbon particles are expected to have optimized microstructure due to their better organization within the self-assembled micellar phases of **1**.¹³

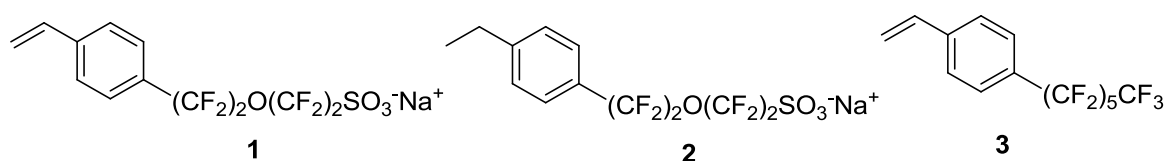


Figure 1.6. Polymerizable fluorosurfactant **1** and non-polymerizable fluorosurfactant **2**, and model comonomer.

1.3 Outline of the thesis chapters

This thesis describes the synthesis, phase behavior of the building blocks viz. **1** and **2**, and (co)polymerization behavior of **1**, which can be helpful in further development of procedures to create self-assembled nanostructured membranes and electrodes.

Chapter 2 explores some plausible schemes to synthesize polymerizable and nonpolymerizable fluorinated surfactants. Specific reactions suitable to develop necessary functionalities on the fluorocarbon molecules like sulfonatodehalogenation reaction on fluorocarbon halides and copper mediated coupling of fluorocarbon iodides with aromatic molecules are discussed in detail.

Syntheses of **1**, **2** are described in **Chapter 3**. Here to couple the fluorocarbon chain, copper mediated coupling reactions were applied to covalently attach fluorocarbon ether sulfonate molecule with aromatic molecules. The coupled aromatic moieties further were converted to styryl group using Wittig reaction.

In **Chapter 4**, micellization properties of fluorosurfactants **1** and **2** in water are discussed. Critical micelle concentration and aggregation numbers were estimated from surface tension, isothermal calorimetry experiments. The thermodynamics of micellization of the fluorosurfactants and effect of temperature on the thermodynamic properties studied by ionic conductivity measurements are discussed further.

Lyotropic mesophase behavior of **2** in water is described in **Chapter 5**. Here it is shown that it forms a lamellar phase and a novel columnar phase of multiwalled “Leek” shaped aggregates. Further details of these phases like their geometric parameters, their sizes and shapes are discussed.

In **Chapter 6**, free radical (co)polymerization of fluorosurfactant **1** and related compounds in solution is discussed. Polymer properties of these homo and copolymers are described. Cryo-TEM study of the homopolymer solution of **1** in water is also discussed which suggests that the polymer forms micelles (with ~5 nm diameters) by lateral self-assembly of 2-3 polymer chains.

The conclusions of the whole thesis and the recommendations for future research are detailed in **Chapter 7**.

1.4 References and Notes

- (1) http://www.bp.com/assets/bp_internet/globalbp/globalbp_uk_english/reports_and_publications/statistical_energy_review_2011/STAGING/local_assets/pdf/statistical_review_of_world_energy_full_report_2011.pdf.
- (2) http://en.wikipedia.org/wiki/Mandatory_renewable_energy_target#United_States.
- (3) Souzy, R.; Ameduri, B. *Prog. Polym. Sci.* **2005**, *30*, 644–687.
- (4) Jannasch, P. *Current Opinion Colloid Interf. Sci.* **2003**, *8*, 96–102.
- (5) Rikukawa, M.; Sanui, K. *Prog. Polym. Sci.* **2000**, *25*, 1463–1502.
- (6) Maiyalagan, T.; Pasupathi, S. *Mater. Sci. Forum* **2010**, *657*, 143–189.
- (7) Marcinkoski, J.; James, B. D.; Kalinoski, J. A.; Podolski, W.; Benjamin, T.; Kopasz, J. *J. Power Sources* **2011**, *196*, 5282–5292.
- (8) Litster, S.; McLean, G. *J. Power Sources* **2004**, *130*, 61–76.
- (9) Janssen, G.J.M.; Sitters, E.F. *J. Power Sources* **2007**, *171*, 8–17.
- (10) Peckham, T. J.; Holdcroft, S. *Adv. Mater.* **2010**, *22*, 4667–4690.
- (11) Zhang, Z.; Chalkova, E.; Fedkin, M.; Wang, C.; Lvov, S. N.; Komarneni, S.; Chung, T. C. M. *Macromolecules* **2008**, *41*, 9130–9139.
- (12) Lim, T. H.; Tham, M. P.; Liu, Z.; Hong, L.; Guo, B. *J. Membr. Sci.* **2007**, *290*, 146–152.
- (13) Microscopic/mesosopic particles due to their interaction with surfactants and due to elastic forces in the case of LLC phases, reorganize to minimize the surface energy. Wadekar, M. N.; Pasricha, R.; Gaikwad A. B.; Kumarswamy, G. *Chem. Mater.* **2005**, *17*, 2460–2465.

Chapter 2

Synthetic routes to couple fluorocarbons to aromatic molecules and for creation of styryl moiety

This chapter describes the molecular designs of the polymerizable fluorosurfactant, various synthetic approaches to couple fluorocarbons to aromatic molecules, to convert couple aromatic moieties to styryl group and to create sulfonate ($-\text{SO}_3^-$) group will be discussed. Sulfinatodehalogenation reaction and copper mediated cross coupling of pefluoro iodide or bromide with aromatic bromides were found to be of specific interest and studied further. Copper mediated cross coupling reactions were found to be promising to achieve the synthesis of the polymerizable fluorosurfactant. A dehydration reaction was studied to make styryl functionality.

2.1 Introduction

Fluorosurfactants are amphiphiles with partially or fully fluorinated hydrophobic tails. They are an interesting class of materials because of their exceptional chemical and thermal stability, oleophobic properties apart from hydrophobicity, and unusual surface properties.¹ As discussed in Chapter 1, our objective was to synthesize polymerizable fluorosurfactant and engineer nanostructured electrodes and membranes for PEMFC from various microphase separated morphologies of it. In this chapter, we discuss various synthetic strategies to i) couple aromatic molecules to fluorocarbons, ii) convert the coupled aromatic moiety to a styryl group, and iii) create sulfonate ($-\text{SO}_3^-$) on a fluorocarbon chain. These synthetic routes were first studied separately and later combined to make polymerizable surfactant with a backbone made up of fluorocarbon (either a fluoroalkane or fluoroalkoxy), $-\text{SO}_3^-$ group as the proton conducting group², and styryl functionality as polymerizable group.³ The choice of the styryl group was made particularly because it can be polymerized by all conventional methods and it has better chemical and thermal stability compared to other hydrocarbon based polymerizable functionalities. Although it is possible to couple fluorinated polymerizable groups like fluorinated vinyl or styryl groups, usually they cannot be easily polymerized by radical initiators. More discussion on the choice of polymerizable group as well as other aspects on the synthesis of the polymerizable fluorosurfactant follows in Chapter 3.

2.1.1 Design of the polymerizable fluorosurfactant

The molecular structure of polymerizable fluorosurfactants is schematically shown in Figure 2.1. It shows schematic depictions of the possible polymerizable fluorosurfactants with various architectures. The type of fluorocarbon chains, the head group moiety i.e. $-\text{SO}_3^-$ group and polymerizable group i.e. styryl moiety are shown in Figure 2.1. Initially the plan was to synthesize a polymerizable fluorosurfactant with one head, one tail and one polymerizable group. The surfactant molecules with two tails or two polymerizable groups are also possible as shown in Figure 2.1.

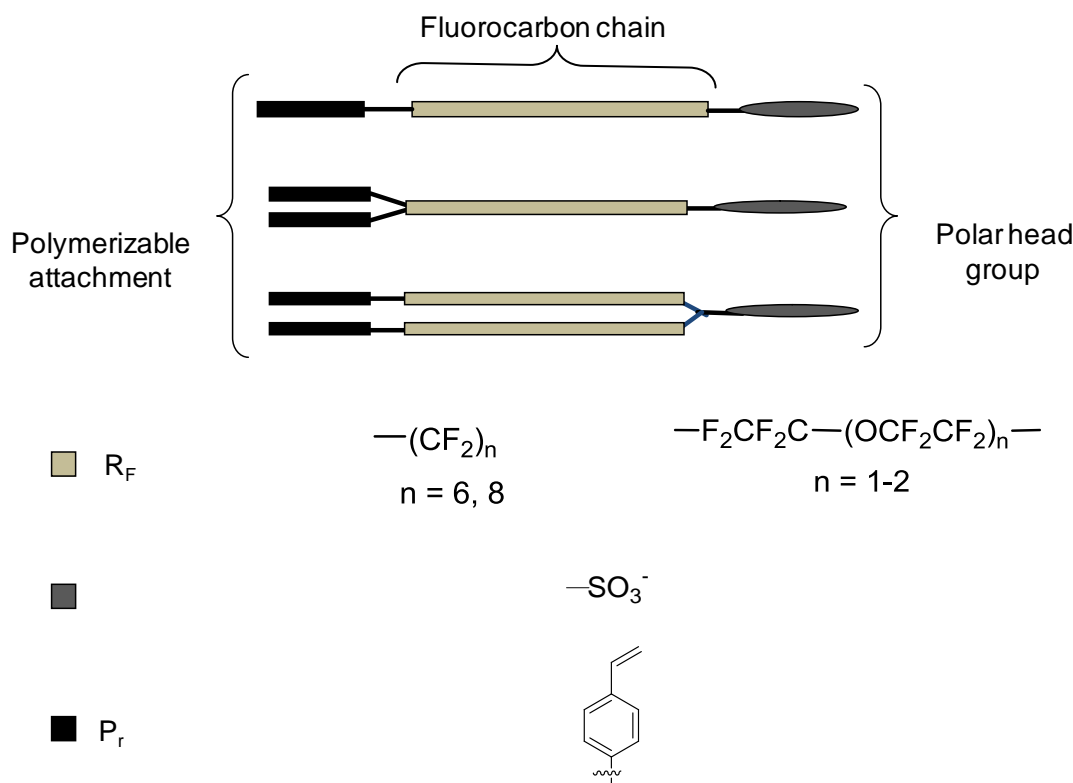


Figure 2.1. Various possible designs of the polymerizable fluorosurfactant.

2.1.2 Chemistry of fluorocarbons

The terminal (α) carbon atom ($\text{—CF}_2\text{X}$) on —R_F is the carbon atom which, we wanted to modify either to attach —SO_3^- group or attach a polymerizable moiety covalently to it. Only functional groups on the α carbon that can be modified are halogens (I, Br, Cl) and $\text{—SO}_2\text{F}$. Sulfonyl fluoride ($\text{—SO}_2\text{F}$) group can be modified into —SO_3^- , whereas halogens can be substituted either to create —SO_3^- or polymerizable moiety. Because of strongly electronegative F atoms, the α carbon in $\text{R}_F\text{—X}$ is highly electron withdrawing, due to which; generation of carbocation is strongly disfavored (see Figure 2.2).⁴ Hence characteristic nucleophilic (S_N^2) substitution reactions on them are not possible. Further, repulsion due to α, α' difluorine atoms against approaching electron-rich nucleophile towards α carbon atom also plays a role in that respect.⁴

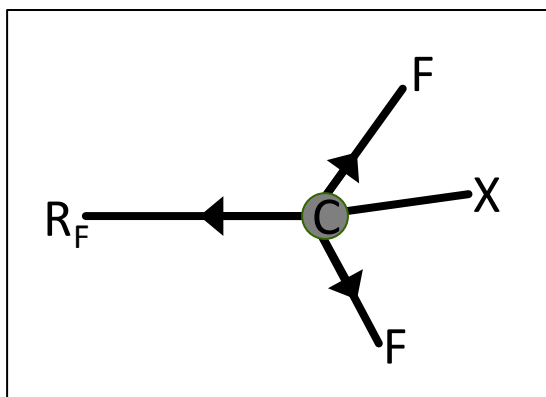


Figure 2.2. Electron withdrawing effect on α carbon due to $-R_F$ and α, α' difluorine atoms.

2.1.3 Choice of starting materials

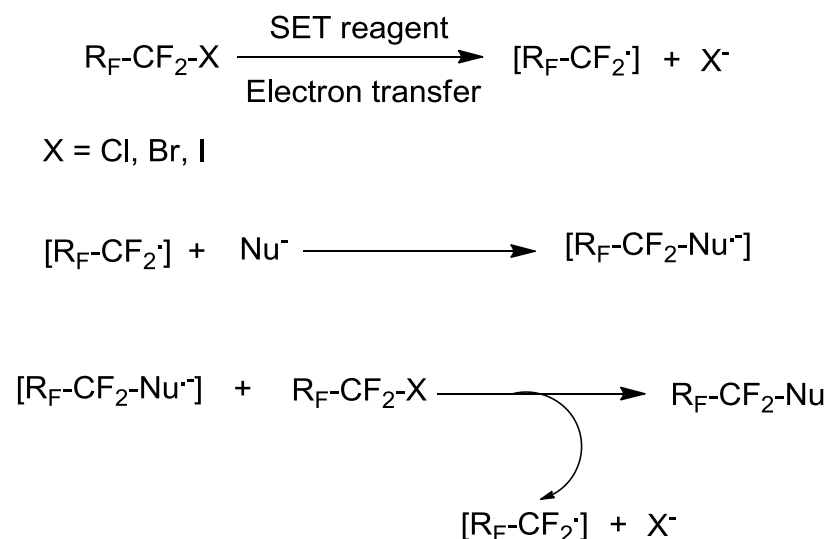
We first decided to study individual reactions to synthesize separately R_F -styryl and R_F - SO_3^- molecules. For this purpose, R_F -X and R_F - SO_2F were chosen as the starting compounds. To synthesize polymerizable fluorosurfactant, the fluoroorganic molecules with general formula $X-R_F-Y$ were chosen as the starting precursors. The molecules with $X = -Cl$ and $Y = -I$ and perfluoroalkanes $(-CF_2)_n$ with 6 or 8 carbon atoms as R_F , were chosen. We found another compound of type $X-R_F-Y$ with $X = -I$ and $Y = -SO_2F$ and $-(CF_2)_2O(CF_2)_2-$ fluoroalkoxy chain as the backbone. The general reaction pathway to prepare polymerizable surfactants is depicted in scheme 2.1.

The starting compounds of $X-R_F-Y$ type are not abundantly available in the market. Similarly, a state-of-the art laboratory facilities and special safety measures for handling volatile fluorinated molecules are required to synthesize these molecules. This situation constrained us to those compounds of type $X-R_F-Y$, which are available in the market.

2.1.4 Reactions on α carbon

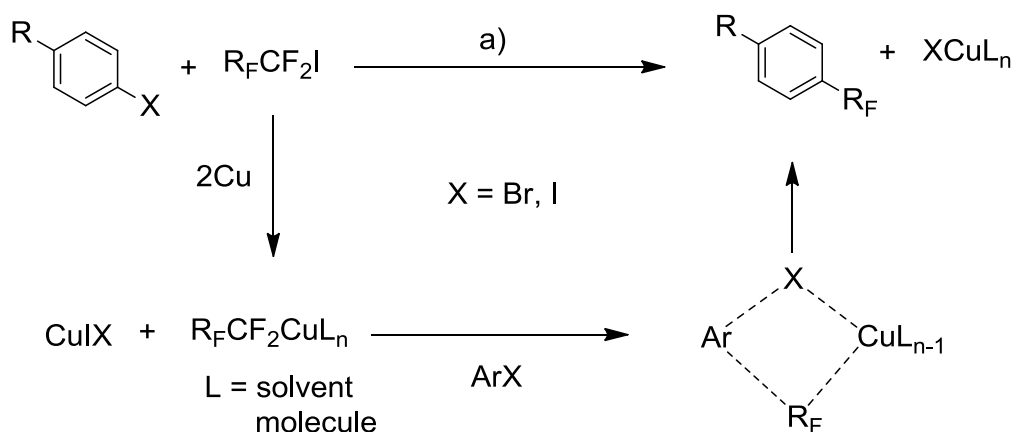
Two types of reactions are possible on α carbons to obtain the desired functionalities. The first is a single electron transfer (SET) reaction that occurs by electron transfer from SET reagents to electron deficient substituents X of R_FCF_2-X .⁴ This is depicted in Scheme 2.1. In a typical SET reaction, first, $R_FCF_2^\cdot$ active species are generated by a cleavage of the carbon-halogen bond that can react with nucleophile to generate anion radical $[R_FCF_2-Nu^\cdot]$. This anion radical then transfers electron again to X of R_FCF_2-X with or without undergoing structural modification

itself. The general mechanism of these reactions does involve formation of radical and radical anion species.⁴ The specific SET reactions we used in our study are “sulfinatodehalogenation” reactions and the reagents (sulfinating agents) used are sulphur-oxy-acid salts.



Scheme 2.1.^{3,4} Single electron transfer reaction. Nu⁻ can be organic or inorganic anions capable of transferring single electron to fluorocarbon chain.

The second type of reaction was metal insertion reaction between -CF₂ and -X of R_FCF₂-X. The particular reaction we studied was copper mediated cross-coupling between fluorocarbon iodides and aromatic bromides or iodides in aprotic polar solvents using metallic copper as reagent.^{3,5}



Scheme 2.2.^{3,6} Mechanism of copper mediated cross-coupling between aromatic halide and fluorocarbon iodide. a) DMSO or Pyridine-C₆F₆, Cu, 80 – 120 °.

A variety of aromatic substrates can be coupled to fluoroalkanes and other fluorocarbons in good to excellent yield.³ As shown in Scheme 2.2, the mechanism

of the reaction consists of formation of a solvated complex of fluoroalkyl copper along with cuprous halide. In the next step the fluoroalkyl copper makes a coordination intermediate with aromatic halide which is followed by exchange of ligand (solvent) molecules at Cu site.

2.2 Experimental Section

2.2.1 Instrumentation

TLC analysis was performed on silica gel, and ^1H and ^{19}F NMR spectra were measured in CDCl_3 or CD_3OD at 300/400 and 282.3 MHz, respectively. Chemical shifts for ^1H NMR and ^{19}F NMR are given in ppm (δ). Tetramethylsilane (TMS) for ^1H NMR whereas trifluoroacetic acid for ^{19}F NMR were used as internal standards.

2.2.2 Materials and synthesis

All reagents were used as purchased. All fluorocarbon starting materials were purchased from Apollo Scientific Ltd. Copper (99%), all aromatic molecules ($\geq 98\%$), absolute DMSO (99.5%), DMF (99%) and inorganic reagents were purchased from Aldrich chemical Co.

Sodium 1,1,2,2,3,3,4,4,5,5,6,6,7,7,8,8,8-heptadecafluorooctane-1-sulfonate (5).

1,1,2,2,3,3,4,4,5,5,6,6,7,7,8,8,8-heptadecafluorooctane-1-sulfonyl fluoride (**4**) (31.8 mmol, 10 g) was heated with NaOH (64 mmol, 2.56 g) in 17.5 mL deionized water to 95 °C overnight. The white colored material was recrystallized from water to give

9.88 g, (93%). ^{19}F NMR (282.3 MHz, CD_3OD), -80.71 (t, $J = 9.9$ Hz, 3F), -113.95 (t, $J = 14.1$ Hz, 2F), -119.97 (s, 2F), -121.04 (broad s, 6F), -122.05 (s, 2F), -125.57 (double d, $J = 6.8$ Hz and 7.6 Hz, 2F).

Potassium 1,1,2,2-tetrafluoro-2-(1,1,1,2,3,3-hexafluoro-3-

(perfluoroethoxy)propan-2-yloxy)ethanesulfonate (7).

1,1,2,2-tetrafluoro-2-(1,1,1,2,3,3-hexafluoro-3-(perfluoroethoxy)propan-2-yloxy)ethanesulfonyl fluoride (**6**) (22.1 mmol, 10 g) was stirred with 20% KOH (44 mmol, 2.5 g) for 4 days at 40 °C. The reaction mixture was filtered using buchner funnel and washed with deionized water and dried. The white waxy material was obtained in 10.1 g, (94%) after drying at 50 °C in vacuum. ^{19}F NMR (282.3 MHz, CD_3OD) -79.33 (broad s, 2F), -79.50 (double d, $J = 8.7$ Hz and 9.3 Hz, 3F), -82.39 (s, 2F), -86.71 (s, 3F), -88.15 (t, $J = 12.7$ Hz, 2F), -122.20 (s, 2F), 144.80 (t, $J = 22.3$ Hz, 1F).

sodium 1,1,2,2,3,3,4,4,5,5,6,6,7,7,8,8,8-heptadecafluorooctane-1-sulfinate (10). Perfluorooctyl iodide (**8**) (2.73 g, 5 mmol) was heated to 80 °C in DMF:water (10 mL:5 mL) mixture with Na₂S₂O₅ (1.9 g, 10 mmol) for two hours. The solvents were removed from yellow colored foamy reaction mixture by vacuo. The dry powder was extracted using hot ethylacetate. After removing ethylacetate, **10** was recrystallized from *i*-propanol solution to give white coloured solid, 1.34 g, 53%) product. ¹⁹F NMR (282.3 MHz, CD₃OD), -80.727 (t, *J* = 10.44 Hz, 3F), -121.31 (broad d, 6F), -121.88 (broad s, 2F), -122.09 (broad, s, 2F), -125.63 (s, 2F), -130.15 (ss, 2F).

sodium 8-chloro-1,1,2,2,3,3,4,4,5,5,6,6,7,7,8,8-hexadecafluorooctane-1-sulfinate (11). The reaction conditions were similar as described for the synthesis of **10**. Only washing the product with diethylether after removal of ethylacetate, was sufficient to give pure white solid, **11** (83%, 2.17 g). ¹⁹F NMR (282.3 MHz, CD₃OD), -68.15 (t, *J* = 13.55 Hz, 2F), -119.63 (s, 2F), -120.50 (s, 2F), -121.25 (broad s, 6F), -121.88 (s, 2F), -130.19 (s, 2F).

sodium 1,1,2,2,3,3,4,4,5,5,6,6,6-tridecafluorohexane-1-sulfinate (14). Perfluorohexyl chloride **13**, (2.8 mmol, 1 g) was added to 6 mL dry DMSO and stirred with 85% pure Na₂S₂O₄ (4.5 mmol, 0.78 g) and NaHC₃O (4.5 mmol, 0.279 g) at 75 °C for 6 hours under nitrogen flow. Yellowish solid (0.205 g, 18%). ¹⁹F NMR (282.3 MHz, CD₃OD), -80.71 (t, *J* = 10.4 Hz, 3F), -121.31 (broad d, 6F), -121.88 (broad, s, 2F), -122.09 (broad, s, 2F), -125.63 (s, 2F), -130.15 (s, 2F).

sodium 1,1,2,2,3,3,4,4,5,5,6,6,7,7,8,8,8-heptadecafluorooctane-1-sulfonate (5). Compound **10** (2.4 mmol, 1.2 g) and slight excess of 4% KMnO₄ (12 mL) solution in 2% NaOH (9 mL) was reacted at 60 °C for 24 h. Excess of KMnO₄ was destroyed using Na₂SO₃ and the hot reaction mixture was filtered using buchner funnel. The filtrate was later neutralized and solvent removed by vacuo. The residue was recrystallized from water solution to give crystalline white **5** (0.95 g, 76%). ¹⁹F NMR (282.3 MHz, CD₃OD), -80.71 (t, *J* = 9.9 Hz, 3F), -113.95 (t, *J* = 14.1 Hz, 2F), -119.97 (s, 2F), -121.04 (broad s, 6F), -122.05 (s, 2F), -125.57 (q, *J* = 6.8 Hz and 7.6 Hz, 2F).

sodium 8-chloro-1,1,2,2,3,3,4,4,5,5,6,6,7,7,8,8-hexadecafluorooctane-1-sulfonate (12). The reaction conditions are same as for **10** except temperature was maintained at 80 °C.⁷ Compound **12** was obtained as white crystalline solid in yield

(1.0 g, 80%). ^{19}F NMR (282.3 MHz, CD_3OD), -69.83 (t, $J = 13.0$ Hz, 2F), -115.62 (s, 2F), -121.29 (s, 2F), -121.64 (s, 2F), -122.15 (s, 2F), -122.70 (broad s, 8F).

Mixture of **1-methoxy-2-(perfluorohexyl)benzene**, **1-methoxy-3-(perfluorohexyl)benzene** and **1-methoxy-4-(perfluorohexyl)benzene (15)**.

Perfluorohexyl chloride **13** (2.8 mmol, 1 g) and anisole (4.5 mmol, 0.486 g) were heated in 6 mL DMSO to 75 °C with 85% pure $\text{Na}_2\text{S}_2\text{O}_4$ (4.5 mmol, 0.78 g) and NaHC_3O (4.5 mmol, 0.279 g) for 8 hours under nitrogen flow. The reaction mixture was extracted with ether (3 X 20mL). The collected ether layers were washed with brine (3 X 20 mL). Ether fraction was separated and dried by anhydrous MgSO_4 . Column chromatography with hexane as an eluent gave 55% product in ratio o:m:p = 50:27:13. ^1H NMR 400 MHz, CDCl_3), 7.69 to 7.12 (m, 4H), 3.92 (s, 3H). ^{19}F NMR (282.3 MHz, CD_3OD), -81.32 (m, 3F), -108.16 (t, $J = 14.1$ Hz, 2F (ortho)), -110.17 (t, $J = 15.0$ Hz, 2F (meta)), -111.03 (t, $J = 13.8$ Hz, 2F (para)), -121.63 (m, 2F), -122.38 (broad s, 2F), -123.25 (broad s, 2F), -120.62 (broad s, 2F).

2-(perfluorohexyl)-1H-pyrrole (16). The reaction conditions are similar to that of **15**. At the end of the reaction the mixture was poured into 8 mL ice-cold water. The aqueous layer was extracted with ether (3 X 20 mL), dried over MgSO_4 and evaporated to give solid residue. The residue was purified by column chromatography using dichloromethane as eluent. The yield was 0.100 g (~10%). ^1H NMR 300 MHz, CDCl_3), 8.29 (broad s, 1H), 6.95 (m, 1H), 6.62 (m, 1H), 6.31(m, 1H). ^{19}F NMR (282.3 MHz, CDCl_3), -81.36 (m, 3F), -107.66 (t, $J = 13.5$, 2F), -122.25 (t, $J = 6.8$, 2F), -122.99 (m, 2F), -123.32 (m, 2F), -126.64 (m, 2F).

1-(4-bromophenyl)ethyl acetate (18c). To Acetyl chloride (9.96 mmol, 0.782 g) in 25 mL dichloromethane, 1-(4-bromophenyl)ethanol (**18f**) (4.98 mmol, 1 g) was mixed. While continuous stirring the reaction mixture, pyridine (9 mmol, 0.711 g) was added in small portions for thirty minutes. After allowing the mixture to stir for 12 hours, it was washed with water (20 mL) two times and the DCM layer was separated and dried over MgSO_4 . It was evaporated and a column chromatography with DCM was made on the obtained crude material to give pure **18c**. Yield was 1.06 g (87%). ^1H NMR (300 MHz, CDCl_3), 7.47 (d, $J = 6.2$ Hz, 2H), 7.23 (d, $J = 6.1$ Hz, 2H), 5.82 (q, $J = 4.9$ Hz, 1H), 2.06 (s, 3H), 1.51 (d, $J = 4.9$ Hz, 3H).

1-(4-(perfluorohexyl)phenyl)ethanone (19b). A round bottom flask (25 mL) was charged with copper powder (51.7 mmol, 3.26 g) and heated under argon flow using a hot gun. The flask was cooled to ambient temperature and perfluorohexyliodide **17** (11.2 mmol, 5 g), 1-(4-bromophenyl)ethanone **18b** (11 mmol, 2.17 g) and DMSO (9.5 mL) were added to the flask and heated to 110 °C for 22 hours using an oil bath. The reaction mixture was cooled, 10 mL water was added and the mixture was filtered. Extraction with DCM (3 X 20 mL) was performed. The DCM layers were collected and dried over Na₂SO₄. The DCM was evaporated and column chromatography with DCM:ether (0.9:0.1) was carried out to give **19b** as a white solid, 3.6 g (70 %). ¹H NMR 300 MHz, CDCl₃, 7.80 (d, *J* = 6.4 Hz, 2H), 7.58 (d, *J* = 6.0 Hz, 2H), 2.57 (s, 3H). ¹⁹F NMR (282.3 MHz, CDCl₃), -81.30 (t, *J* = 9.3 Hz, 3F), -111.07 (t, *J* = 13.5 Hz, 2F), -121.94 (s, 2F), -122.24 (s, 2F), -123.28 (s, 2F), -126.60 (s, 2F).

1-(4-(perfluorohexyl)phenyl)ethyl acetate (19c). The reaction conditions and purification was similar to **19b**. The reaction was performed using copper powder (18 mmol, 1.13 g), perfluorohexyliodide **17** (1.78 g, 4 mmol) and **18c** (4.3 mmol, 1.05 g) in DMSO (4 mL). The column chromatography with DCM gave White solid, (1.1 g, 57%). ¹H NMR 300 MHz, CDCl₃, 7.59 (d, *J* = 8.4 Hz, 2H), 7.49 (d, *J* = 8.1 Hz, 2H), 5.93 (q, *J* = 6.6 Hz, 1H), 2.11 (s, 3H), 1.56 (d, *J* = 6.6 Hz, 3H). ¹⁹F NMR (282.3 MHz, CDCl₃), -81.30 (t, *J* = 9.3 Hz, 3F), -111.07 (t, *J* = 13.5 Hz, 2F), -121.94 (s, 2F), -122.24 (s, 2F), -123.28 (s, 2F), -126.60 (s, 2F).

1-Ethyl-4-(perfluorohexyl)benzene (19d). See the details on the synthesis in the Experimental section of Chapter 3.

4-(Perfluorohexyl)benzaldehyde (19e). See the details on the synthesis in the Experimental section of Chapter 3.

1-(4-(perfluorohexyl)phenyl)ethanol (19f). Compound **19c** (2.28 mmol, 1.1 g) and sodium hydroxide (3.42 mmol, 0.136 g) were reacted in EtOH:water (10 + 4 mL) overnight at 80 °C. A column chromatography (DCM:MeOH = 0.9:0.1) gave colorless liquid **19f** (0.8 g, 80 %). ¹H NMR 300 MHz, CDCl₃, 7.57 (d, *J* = 6.3 Hz, 2H), 7.51 (d, *J* = 6.3 Hz, 2H), 4.97 (q, *J* = 2.7 Hz, 1H), 1.52 (d, *J* = 4.8 Hz, 3H). ¹⁹F NMR (282.3 MHz, CDCl₃), -81.31 (t, *J* = 9.0 Hz, 3F), -110.98 (t, *J* = 13.3 Hz, 2F), -121.94 (s, 2F), -122.33 (s, 2F), -123.28 (s, 2F), -126.60 (s, 2F).

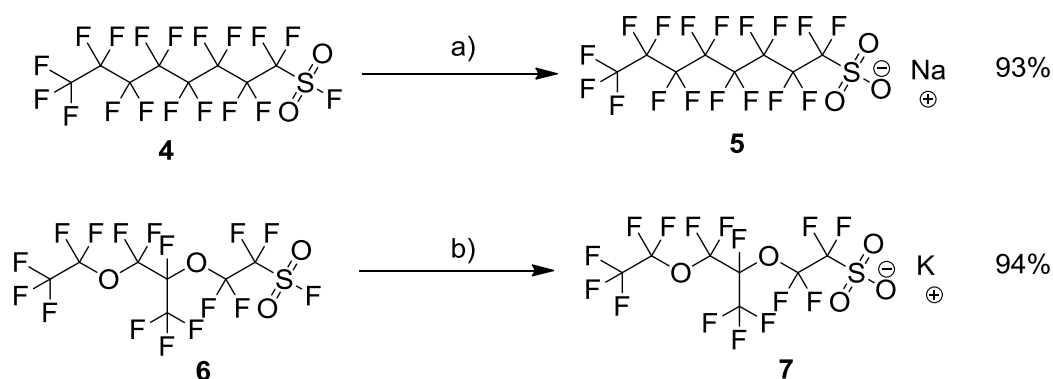
1-methoxy-4-(perfluorooctyl)benzene (20a) Reaction conditions were similar to **19b**. The reaction was performed with copper powder (11.6 mmol, 0.74 g), perfluorooctyliodide **8** (2.5 mmol, 1.36 g) and 4-bromoanisole, **18a** (2.31 mmol, 0.43 g) in DMSO (3 mL). Purification was done with hexane as eluent to give colorless liquid (0.74 g, 56%) ^1H NMR (300 MHz, CDCl_3) 7.43 (d, $J = 9.00$ Hz, 2H), 7.30 (d, $J = 8.47$ Hz, 2H), 3.78 (s, 3H). ^{19}F NMR (282.3 MHz, CDCl_3), -81.29 (m, 3F), -110.16 (s, 2F), -121.85 (s, 2F), -122.39 (broad s, 6F), -123.15 (s, 2F), -126.59 (s, 2F).

1-(4-(perfluorooctyl)phenyl)ethanone (20b) Reaction conditions were similar to **19b**. The reaction was performed with copper powder (11.6 mmol, 0.74 g), perfluorooctyliodide **8** (2.5 mmol, 1.36 g) and 1-(4-bromophenyl)ethanone **18b** (2.31 mmol, 0.47 g) in DMSO (3 mL). The column chromatography with DCM:ether (0.9:0.1) was carried out to give **20b** as a white solid, 0.82 g (60 %). ^1H NMR (300 MHz, CDCl_3) 8.08 (d, $J = 8.4$ Hz, 2H), 7.71 (d, $J = 8.1$ Hz, 2H), 2.66 (s, 3H). ^{19}F NMR (282.3 MHz, CDCl_3), -81.26 (m, 3F), -111.66 (t, $J = 13.8$ Hz, 2F), -121.64 (s, 2F), -122.24 (broad s, 6F), -123.17 (s, 2F), -126.59 (d, $J = 13.8$, 2F).

2.3 Results and discussion

2.3.1 Basic hydrolysis to synthesize model fluorosurfactants

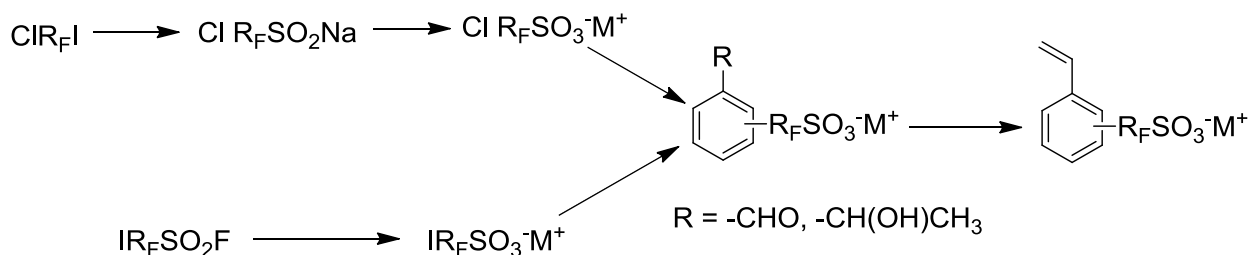
First, two model fluorosurfactants, **5** and **7** were prepared by hydrolysis of **4** and **6**, respectively as the model fluorocarbon sulfonated surfactants (see Scheme 2.3). These reactions have been reported previously.¹



Scheme 2.3. Synthesis of model fluorosurfactants by simple base hydrolysis. a) NaOH, water, 85 °C, 12 h. b) KOH, water, 85 °C, 12 h.

2.3.2 Sulfinatodehalogenation reaction

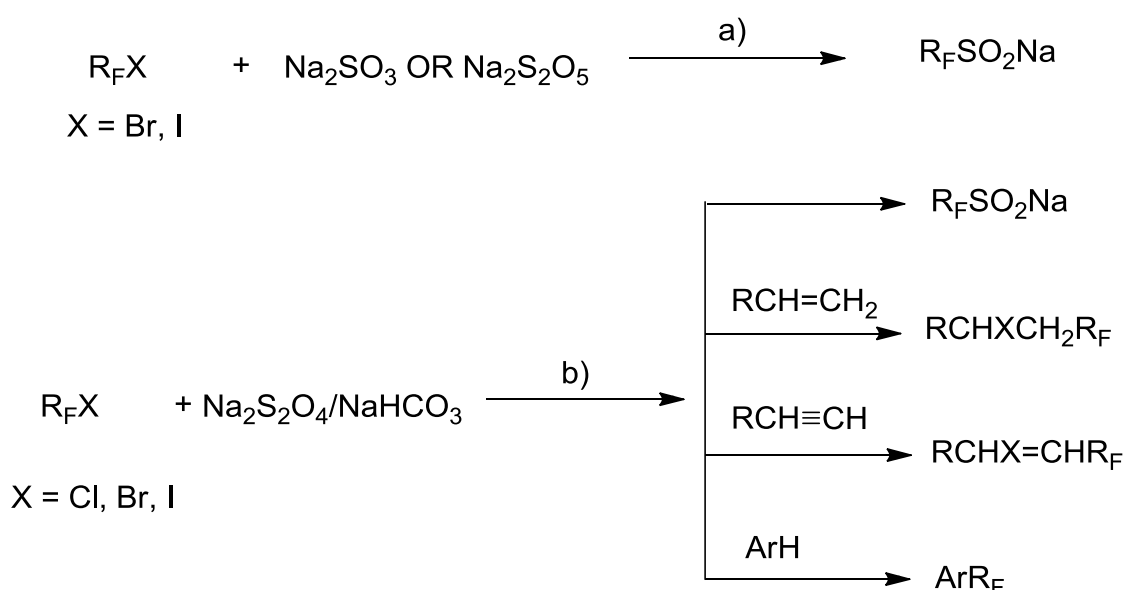
The general route to synthesize polymerizable fluorosurfactant using various reactions is shown in Scheme 2.4. These reactions will be further discussed hence forth. Sulfinatodehalogenation reactions were quite promising to create $-\text{SO}_3^-$ as well as to couple a polymerizable group on fluorocarbon chain. Scheme 2.5 gives a general idea about the reaction. It was discovered and later studied extensively by Huang *et al.*⁸



Scheme 2.4. General reaction pathway to make polymerizable fluorosurfactant.

It has been developed as an effective way to synthesize perfluoroalkyl sulfonates. These sulfonates further can be converted to respective sulfonyl halides and sulfonates.

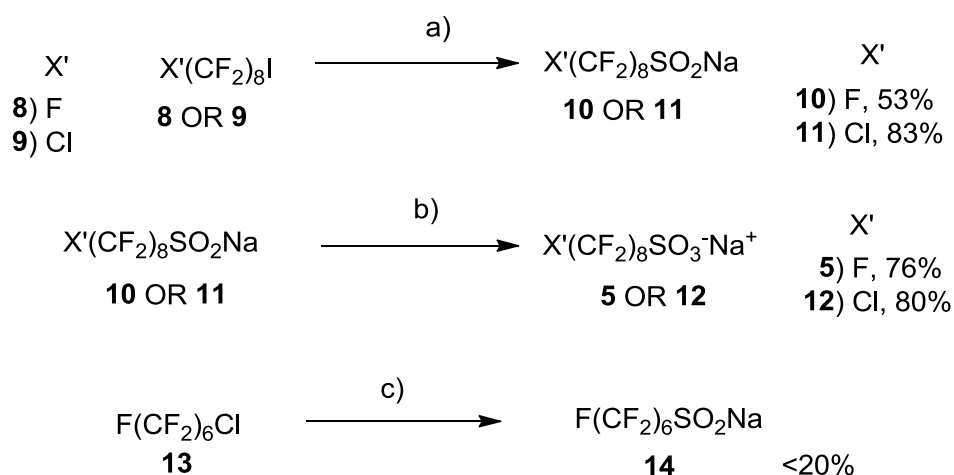
Similarly, the reaction has been applied for coupling perfluoroalkyl chains to various hydrocarbon based substrates and aromatic molecules by Huang's group as well as other researchers.⁹



Scheme 2.5.^{8,9,10} General sulfinatodehalogenation reaction to convert fluorocarbon halides into respective sulfinates and to couple with various hydrocarbon and aromatic substrates. a) DMF-H₂O, 80 °C. b) MeCN-H₂O or DMSO, 80 °C.

In a typical sulfinatodehalogenation reaction, perfluoroalkyl halide, generally iodides or bromides are converted efficiently to perfluoroalkyl sulfinates in polar aprotic solvents using various sulfur-oxy acid salts. The mechanism behind the sulfination reaction was revealed to be formation of the reactive species like sulfite anion radicals ($\text{SO}_3^{\cdot-}$), sulfinate anion radicals ($\text{SO}_2^{\cdot-}$), mixed system or sulfoxylate anions ($\text{HSO}_2^{\cdot-}$) and consequent process of single electron transfer from these species.⁸

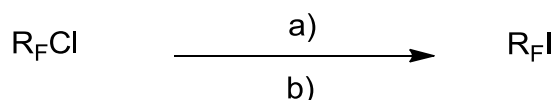
We carried out the test reactions as shown in Scheme 2.6 with various fluoroalkanes for hand-on-experience. We used various sulfinating agents like sodium dithionite ($\text{Na}_2\text{S}_2\text{O}_4$),¹⁰ sodium sulfite (Na_2SO_3) apart from sodium disulfite¹¹ ($\text{Na}_2\text{S}_2\text{O}_5$). The best results (yield and purity) were obtained from the reaction with $\text{Na}_2\text{S}_2\text{O}_5$.¹² The reaction was clean and fast. As shown in Schemes 2.5 and 2.6, $\text{R}_\text{F}\text{-I}$ gets transformed into $\text{R}_\text{F}\text{-SO}_2\text{Na}$.



Scheme 2.6. Sulfinatodehalogenation reaction to generate perfluoroalkyl sulfinates and coupling aromatic molecules with fluorocarbon chains. a) $\text{Na}_2\text{S}_2\text{O}_5$, DMF-H₂O, 80 °C, 2-3 h. b) 4% KMnO_4 , aq. 2% NaOH , 60-80 °C, 24h. c) $\text{Na}_2\text{S}_2\text{O}_4$, NaHCO_3 , DMSO, 75 °C. 8 h.

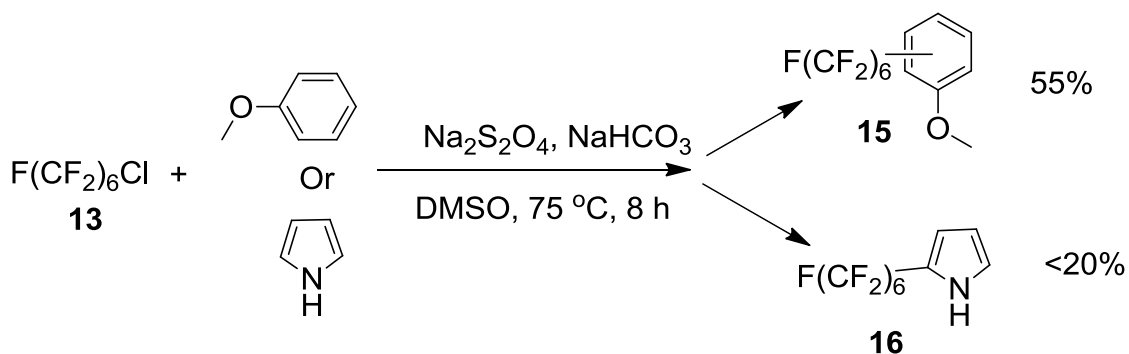
Further, perfluorooctyl sulfinate was efficiently oxidized to Perfluorooctyl sulfonate by heating it with KMnO_4 solution in basic conditions in very good yields (Scheme 2.6). Most of the sulfinating agents only react with fluoroalkyl iodides and bromides whereas $\text{R}_\text{F}\text{-Cl}$ bond remains unaffected.

One way to react perfluoroalkyl chlorides¹³ is to convert them into respective sulfinates by using combination of $\text{Na}_2\text{S}_2\text{O}_4$ and NaHCO_3 in DMSO. Our efforts to make sulfinates from perfluoroalkyl chlorides by this method, gave significantly lower yields than reported.¹³ Chen and coworkers¹⁴ have reported a reaction to convert perfluoroalkyl chlorides into perfluoroalkyl iodides through sulfinate intermediates as depicted in scheme 2.7. At the time of working on sulfinatodehalogenation, we were unaware of this reaction.



Scheme 2.7. Perfluoroalkyl iodides from perfluoroalkyl chlorides by sulfinatodehalogenation. a) $\text{Na}_2\text{S}_2\text{O}_4$, DMSO, rt to 100 °C, 15 min. b) $\text{Na}_2\text{S}_2\text{O}_8$, I_2 , H_2O -DMSO, rt, 1 h.

Sulfinatodehalogenation reactions using $\text{Na}_2\text{S}_2\text{O}_4/\text{NaHCO}_3$ in DMSO are quite versatile (scheme 2.7 and 2.8), since it can be used not only to create sulfinates but also to couple various aliphatic¹³ and aromatic¹⁵ substrates to fluorocarbon halides. We performed perfluoroalkylation reaction on aromatic molecules using perfluorohexyl chloride as described in the Scheme 2.9. In case of anisole, the yields were around 50% and the product (**15**) consists of mixture of ortho, meta and para-substituted molecules (o:m:p = 52:31:17). Reaction of perfluorohexyl chloride with pyrrole gave significantly lower yield of **16**.



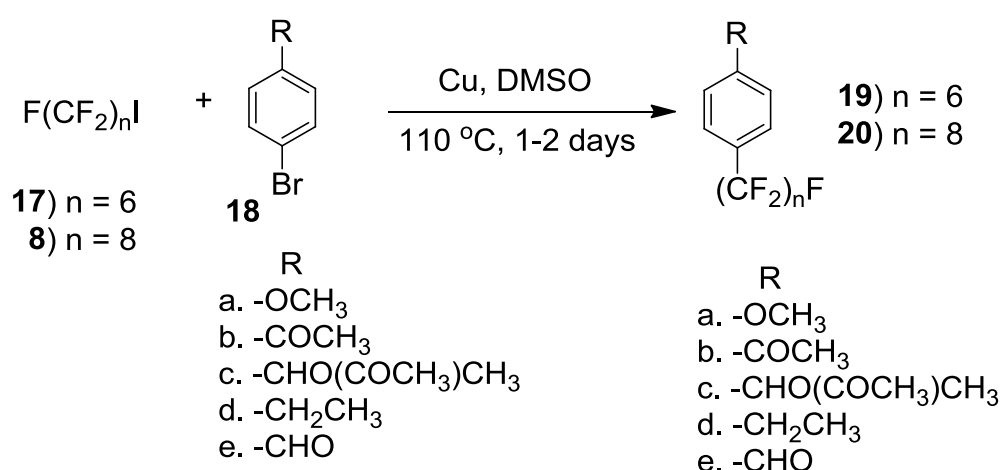
Scheme 2.8. Coupling aromatic molecules to perfluoroalkyl chlorides by sulfinatodehalogenation.

Black tar-like material was also observed apart from the main yellow colored compound **16**. Thus even though, it was possible to convert $\text{R}_\text{F}\text{I}$ and $\text{R}_\text{F}\text{Cl}$ into useful functionalities like sulfonates and aromatic moieties, the sulfinatodehalogenation based reactions with $\text{R}_\text{F}\text{Cl}$ were quite inefficient. Also, in the case of coupling of aromatic molecules to perfluoroalkanes, the mixture of ortho,

meta and para substituted products was obtained. Similarly, copper mediated cross-coupling discussed in Scheme 2.10 was not possible with $R_F\text{-Cl}$. Hence we found $I\text{-}R_F\text{-SO}_2F$ more suitable than $Cl\text{-}R_F\text{-I}$ to synthesize polymerizable surfactant.

2.3.3 Copper mediated cross-coupling

Because of the discussed limitations of sulfonatodehalogenation, we decided to focus on the copper mediated cross-coupling to attach aromatic moieties to fluorocarbons. Copper mediated cross-coupling reactions are an important class of reactions^{3,5} to couple fluorocarbon iodides to aromatic bromides and iodides with various functional groups like $-\text{COMe}$, $-\text{COOH}$, $-\text{OH}$, $-\text{NH}_2$, under mild conditions using copper bronze as reagent. We performed coupling reactions of various aromatic bromides with $R_F\text{-I}$ as illustrated in scheme 2.9.



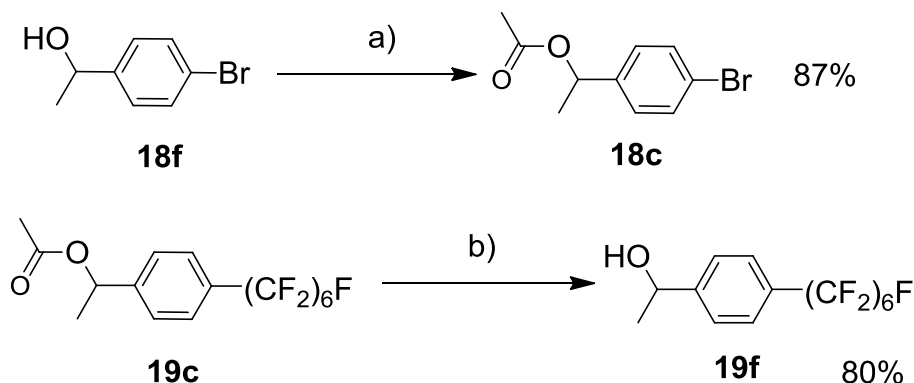
Scheme 2.9. Copper mediated cross-coupling between perfluoroiodides and aromatic bromides. Table shows the percentage yield for various products.

Perfluoroalkyl iodides having six or eight carbon atoms were reacted with various aromatic bromides. The copper mediated coupling reactions with aromatic bromides **18a** and **18c-e** have not been reported previously. In general, we found that an electron withdrawing group at the para position of an aromatic bromide enhances the yield of the reaction.³

Table 2.1. Fluoro-alkylated molecules and their yield.

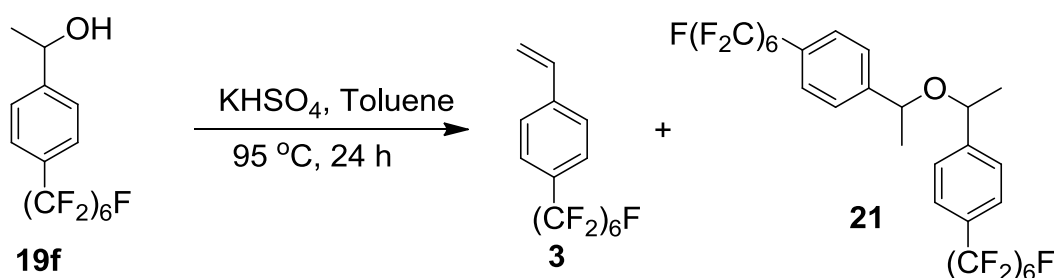
R _F Ar	% yield
20a	60
19b	70
20b	66
19c	62
19d	61
19e	94

Typically five equivalents of copper to perfluoroalkyl iodide (**17** or **8**) are used for the reaction. We observed that the –OH group of 4-bromophenyl methylcarbinol **18f** interferes during the cross-coupling with perfluoroalkyl iodide. Protecting –OH of carbinol group, using acetyl chloride gave very good yields of **18c**. After, the cross-coupling, compound **19c** was deprotected back to give perfluorohexyl carbinol **19f**, see Scheme 2.10.



Scheme 2.10. Protection and deprotection reactions for 4-bromophenyl methyl carbinol. a) CH₃COCl, Pyridine, DCM, rt, 12 h. b) NaOH, water, 80 °C, 24 h.

2.3.4 Creation of styryl functionality



Scheme 2.11. Dehydration of 4-perfluorohexyl phenylmethyl carbinol by potassium persulfate.

We will now discuss the synthesis of the fluorinated polymerizable model compound with styryl functionality. The introduction of a styryl functionality by various methods, like dehydration of alcohol,¹⁶ dehydrohalogenation,¹⁷ or a Wittig reaction with benzaldehydes,^{18,19} has been reported. To synthesize styryl group, initially, the dehydration reaction on **19f** using potassium persulfate as an acid catalyst was carried out (Scheme 2.11).

In a typical dehydration reaction, the reaction mixture in toluene is refluxed with or without free radical scavenger and the product is removed by distillation after the reaction is complete.²⁰ ¹H NMR of the reaction mixture after 24 hours, suggested the presence of product **3**, with large quantities of byproduct **21** and polymer.²¹ Thus due to the harsh reaction conditions and the formation of the byproduct **21**, we decided to use another milder reaction, the Wittig reaction.¹⁸ Another important reason to choose

milder reaction pathway was that while synthesizing polymerizable surfactant, it is not possible to distil the product out. Synthesis of the styryl based polymerizable fluorosurfactant using a milder form of Wittig reaction will be discussed in detail in Chapter 3.

2.4 Conclusions

The design of polymerizable fluorosurfactant, the choice of starting precursors and the synthetic routes are based on i) availability of the starting fluorocarbon precursor compounds ii) the reactivity of the α carbon bearing fluorine atoms of R_F chain, and iii) Stability and the reactivity of the polymerizable group.

Available starting compounds with general structure $X-R_F-Y$ were identified where X and Y are either halogen atoms or $-SO_2F$. Sulfinatodehalogenation reaction and copper mediated cross-coupling reactions were studied separately to generate $-SO_3^-$ group and create styryl group. Sulfinatodehalogenation was particularly useful to make fluorocarbon sulfinates from the respective fluorocarbon iodides or bromides with good conversion. These sulfinates further could be oxidized to sulfonate salts.

The sulfinatodehalogenation reactions were also useful to couple aromatic molecules to perfluoroalkyl halides. These reactions on perfluoroalkyl chlorides either did not give the desired product or gave lower yields. Similarly, coupling of aromatic molecules using sulfinatodehalogenation gives mixture of various substituted products. Copper mediated cross-coupling between perfluoroalkyl iodides and various aromatic bromides was found to be more suitable for the coupling aromatic moieties to fluorinated compounds. The reaction conditions are mild and the reactions gives higher yields.

2.5 References and Notes

- (1) Kissa, E. *Fluorinated Surfactants, Synthesis, Properties, Applications, Surfactant Science Series, Marcel Dekker*, New York 1994, 50, pp 1-21.
- (2) Mauritz, K. A.; Moore, R. B. *Chem. Rev.* **2004**, 104, 4535-4585.
- (3) McLoughlin, V. C. R.; Thrower, J. *Tetrahedron* **1969**, 25, 5921-5929.
- (4) Uneyama, K. *Organofluorine Chemistry*, (Wiley-Blackwell, Oxford), **2006**, ch. 2.
- (5) G.J. Chen, C. Tamborski, *J. Fluorine Chem.* **1989**, 43, 207-228.
- (6) We describe here all the reactions with aromatic bromides only.
- (7) Reaction at 60 °C would lead to presence of starting compound even after 24 h.
- (8) Huang, W.- Y.; Wu, F.- H. *Israel J. Chem.* **1999**, 39, 167-170.
- (9) Wu, K.; Chen, Q.- Y. *Chin. J. Chem.* **2004**, 22, 371-376.
- (10) Huang, B. N.; Wu, F. H. *Chin. Chem. Lett.* **1991**, 8, 605-611.
- (11) Huang, W.- Y.; Wu, F.- H.; Huang, B.- N. *Chin. J. Chem.* **1994**, 12, 549-551.
- (12) Reactions with Na₂SO₃ or Na₂S₂O₄ gave the product but purification led to low yield.
- (13) Long, Z.- Y.; Chen, Q.- Y. *J. Org. Chem.* **1999**, 64, 4775-4782.
- (14) Cao, H.- P.; Chen, Q.- Y. *J. Fluorine Chem.* **2007**, 128, 1187.
- (15) Huang, X.- T.; Long, Z.- Y.; Chen, Q.- Y. *J. Fluorine Chem.* **2001**, 111, 107.
- (16) Brooks, L. A. *J. Am. Chem. Soc.* **1944**, 66, 1295.
- (17) Halpern, M.; Zahalka, H. A.; Sasson, Y.; Rabinovitz, M. *J. Org. Chem.* **1985**, 50, 5088-5092.
- (18) Marsh, G. P.; Parsons, P. J.; McCarthy, C.; Corniquet, X. G. *Org. Lett.* **2007**, 9, 2613-2616.
- (19) K. Okuma, O. Sakai, K Shioji, *Bulletin of the Chemical Society of Japan*, **2003**, 76, 1675-1681.
- (20) Audic, N.; Dyer, P. W.; Hope, E. G.; Stuart, A. M.; Suharda, S. *Adv. Synth. Catal.* **2010**, 352, 2241-2250.
- (21) B. Das, M. Krishnaiah, B. Veeranjanyulu, Y. Srinivas, Y. Rao, *Journal of Chemical Research*, **2007**, 12, 717. ¹H NMR of the aromatic ethers (two similar doublets at 4.2 and 4.5 ppm) suggested that we obtained **X** as the byproduct.

Chapter 3

Syntheses of the polymerizable hybrid fluorosurfactant **1** and nonpolymerizable analogue **2***

The syntheses of a polymerizable fluorinated surfactant, sodium 1,1,2,2-tetrafluoro-2-(1,1,2,2-tetrafluoro-2-(4-vinylphenyl)ethoxy)ethanesulfonate (**1**), nonpolymerizable analogue, sodium 2-(2-(4-ethylphenyl)-1,1,2,2-tetrafluoroethoxy)-1,1,2,2-tetrafluoroethanesulfonate (**2**), and a number of related fluorocarbon compounds, are described in this chapter. Compound **2** is synthesized by copper-mediated cross coupling reaction of 4-bromoethyl benzene and sodium 5-iodooctafluoro-3-oxapentanesulfonate (**22**) whereas **1** by similar cross-coupling reaction of 4-bromobenzaldehyde and **22**. The resulting benzaldehyde is converted to a styrene unit, using a Wittig reaction with methyltriphenylphosphonium bromide in acetonitrile, using DBU as a base. This strategy for converting an iodo-functionalized fluorosurfactant to a styrene containing fluorosurfactant is highly efficient because both reactions are performed in polar solvents and are compatible with the sulfonate moiety. In addition, the copper-mediated cross-coupling reaction is most efficient with electron-poor arylbromides like 4-bromobenzaldehyde. We wish to employ **1** for the construction of nano-structured membranes by polymerization in a microemulsion or in lyotropic liquid crystalline phases.

*A modified version of this chapter was published in *J. Org. Chem.* **2010**, 75, 6814-6819. by Wadekar, M. N.; Jager, W. F.; Picken, S. J.

3.1 Introduction

In Chapter 2, we discussed various aspects required to synthesize polymerizable fluorosurfactant. In this chapter, the actual synthesis of polymerizable fluorosurfactants (**1**) and nonpolymerizable analogue of it (**2**) will be discussed. Nano-structured polymer membranes, composed of polymers with a well-defined morphology and consisting of at least two phases, find application in many areas.¹ Well known are membranes for filtration that are composed of cross-linked polymers, which contain mesoscale pores. We are interested in developing proton-conducting membranes for polymer electrolyte membrane fuel cells (PEMFC). For this application, apolar polymers decorated with anionic hydrophilic proton-conducting moieties, usually $-\text{SO}_3^-$, are employed.² The apolar polymer phase provides structural integrity and the anionic moieties form proton conducting hydrophilic channels in the membrane.² Ideally, the proton conducting polymer must possess long-term chemical stability, notably against negative pH, high temperatures and aggressive radicals like OH^\cdot and OOH^\cdot , which are present in operating fuel cells.³ In practice (partially) fluorinated and aromatic polymers have⁴ the appropriate properties and thus they are suitable for making proton conducting membranes. In the present generation PEMFCs, the sulfonated fluoropolymer Nafion[®], a statistical copolymer of tetrafluoroethylene and a sulfonate containing fluorinated comonomer is the most commonly used proton-conducting material.² From an emulsion of this polymer, proton-exchange membranes are produced by various pressing, stamping and ink deposition techniques. These membranes are co-continuous and highly proton conducting with channel sizes in the order of 1-4 nm.

For membranes prepared from the statistical copolymers like Nafion[®], little control over the microstructure is obtained, because of the low mobility of the polymer during membrane preparation. In addition, the statistical nature of the polymer does not facilitate a discrete phase separation and the formation of regular and well-developed morphologies. Another drawback associated with the use of polymers, is that the degree of sulfonation is limited to fairly low values, because highly sulfonated polymers are water-soluble. It is a known fact that the proton conductivity, water uptake and subsequent swelling are strongly influenced by chemical structure, morphology and the percentage of proton-carrying groups in the polymer.^{5,6} Thus, it

is a challenge to enhance the conductivity by increasing the degree of substitution with proton carrying groups without increasing the water uptake and swelling. This problem can partly be solved by synthesizing block or graft copolymers, in which one of the blocks is apolar in nature and the other is hydrophilic and carries anionic functionalities. These polymers can form phase-separated systems. For example, Chung and coworkers⁶ have shown that the conductivity of phase separated membranes of poly(vinylidene fluoride)-*g*-sulfonated polystyrene (PVDF-*g*-SPS) graft copolymers is better than that of Nafion[®] 112 due to a higher degree of sulfonation.⁷ In this polymer, the water swelling was controlled by the graft copolymer morphology. However, the rate of membrane manufacturing is still limited by the slow dynamics of polymer chains.

In an alternative approach, nano-structured membranes can be assembled by polymerizable surfactants or surfmers in microemulsions⁸ or lyotropic liquid crystalline (LLC) phases.⁹ Now the mobility of the surfactant molecules is no longer a limiting factor and equilibrium states with well-defined morphologies may be obtained quickly. Mechanically stable membranes are obtained by a subsequent polymerization of the polymerizable surfactants. By employing multifunctional monomers in these systems, cross-linked polymer membranes are obtained. For such membranes the degree of sulfonation, and thereby the conductivity, can be increased, since the cross-linking prevents the polymer from becoming water-soluble and will also control the degree of swelling.

The approach of using surfmers was pioneered by Luzzati and coworkers.¹⁰ The preparation of proton-conducting membranes by polymerization of a bicontinuous microemulsion of a zwitterionic surfmer, 3-((11-acryloyloxy-undecyl)imidazolyl)propyl sulfonate, has been reported.¹¹ However, the chemical stability of this polymer is expected to be low due to the presence of an easily hydrolyzable acrylate group.

Polymerizable surfactants with hydrocarbon backbones¹² and (semi)fluorinated backbones¹³ have been synthesized and studied for various objectives like micellar polymerization, drug delivery systems and applications in paints. Most polymerizable fluorosurfactants are cationic and nonionic in nature. In one report¹⁴ an anionic (-COO⁻-based) fluorinated surfmer, monofluoroalkyl maleate has been used by Pich

et al, as a stabilizer in the miniemulsion polymerization of styrene and *n*-butyl methacrylate.

In this chapter, we describe the synthesis of the polymerizable fluorosurfactant **1** and non-polymerizable analogue **2**. In the design of **1** and **2**, we chose the sulfonate group as the proton- conducting moiety because of its high stability and high proton conductivity. In addition, many fluorocarbons containing fluorosulfonyl groups, from which the sulfonate group is readily obtained by basic hydrolysis, are available.¹³ The styryl functionality was selected because aromatic moieties can directly be attached to fluorocarbon chains by a copper-mediated coupling reaction.^{15,16} In this fashion, hydrolyzable ester and amide functionalities, that are present in acrylates and acrylamides, are avoided. Although polymerizable surfactants have been synthesized by direct coupling of styryl moieties using methods like esterification¹⁷ or etherification,^{18,19} the harsh conditions of the copper-mediated coupling prevented such a direct approach. Therefore, 4-bromobenzaldehyde was coupled to the fluorosurfactant molecule and subsequently converted into a functional styrene group.

It is expected that the styrene moiety in **1**, in contrast to most fully fluorinated monomers,^{20,21} is readily polymerized with a wide variety of comonomers by anionic, cationic, coordination and controlled radical conditions.²² It is also expected that the partial fluorination of **1**, by the attachment of a fluorocarbon tail, increases the stability of Poly-**1**.²³ To the best of our knowledge, compound **1** is the only fluorinated surfactant, which contains a sulfonate and a readily polymerizable styrene that can be synthesized using standard synthetic tools. Special equipment for handling volatile and highly toxic halogenated compounds is not required. We wish to employ **1** for the construction of nano-structured membranes by polymerization of **1** in a microemulsion or in an LLC phase. Compound **2** is expected to be very similar to **1** regarding its physical properties but without ability of being polymerized. Therefore **2** is regarded as a nonpolymerizable model surfactant that is well suited for investigating the morphology formation in microemulsions and LLC phases.

The physical properties of **1** and **2**, with regard to their phase behavior in aqueous systems and the polymerization of **1** have been investigated. The aggregation properties and associated thermodynamics will be described in Chapter 4. Similarly, both surfactant display interesting LLC phases in water at high concentrations (>63 wt% surfactant). The LLC phase behaviour of **1** and **2** will be discussed in Chapter 5. Compound **1** is readily polymerized under standard free radical polymerization conditions²⁴ in polar solvents like water and DMF, and various properties of the resulting polymer will be discussed in Chapter 6. These investigations imply that compound **2** is capable of forming various nano-structured phases in water. Based on these observations it is reasonable to assume that the polymerizable fluorosurfactant **1** is well suited for the construction of nanostructured proton-conducting membranes.

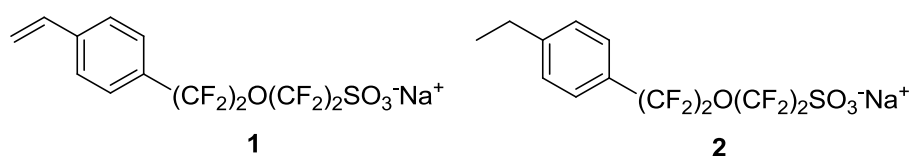


Figure 3.1. Polymerizable fluorosurfactant **1** and non-polymerizable fluorosurfactant **2**.

3.2 Experimental section

3.2.1 Instrumentation

TLC analysis was performed on silica gel, and ¹H, ¹⁹F and ¹³C NMR spectra were measured in CDCl₃ or CD₃OD at 300 or 400, MHz, 282.3 MHz and 75.4 MHz, respectively. Chemical shifts are given in ppm (δ). Tetramethylsilane (TMS) was used as internal standard for ¹H and ¹³C NMR whereas for ¹⁹F NMR we used trifluoroacetic acid as the standard. LC-MS data were collected with a Liquid Chromatograph Mass Spectrometer, with a diode-array detector. The column used was the Xbridge Shield RP 18.5 mm (4.6 X 150 mm) on MeOH. Fast Atom Bombardment (FAB) mass spectrometry was carried out with a four sector mass spectrometer, coupled to a system program. Samples were loaded in a matrix solution (3-nitrobenzyl alcohol) onto a stainless steel probe and bombarded with

Xenon atoms with energy of 3KeV. During the high-resolution FAB-MS measurements a resolving power of 10000 (10% valley definition) was used. IR spectra were from KBr pellets with an FTIR spectrophotometer.

3.2.2 Materials

4-(Perfluorohexyl)benzaldehyde (19b). A 25 mL round bottom flask was charged with copper powder (50 mmol, 3.15 g) and heated above 150 °C under an argon flow using a hot gun. The flask was cooled to ambient temperature and 1-iodofluorohexane (**17**) (11.2 mmol, 5.00 g), 4-bromobenzaldehyde (**18e**) (10.0 mmol, 2.07 g) in DMSO (9 mL) were added to it. The flask was heated to 110 °C for 22 hours using an oil bath. The reaction mixture was cooled, 20 mL water was added to it, and then filtered. The filtrate was further extracted with (3 X 20 mL) DCM. All the DCM layers were collected, washed with 20 mL water two times and dried over anhydrous Na₂SO₄. Column chromatography (pentane:DCM = 0.7:0.3) under argon atmosphere gave white solid **19b** (4.5 g, 94 %). ¹H NMR, ¹⁹F NMR and IR data were consistent with those reported in reference 26.

1-Ethyl-4-(perfluorohexyl)benzene (19d). Reaction conditions and purification procedure were similar to **19d**, The reaction was performed with copper powder (33 mmol, 3.07 g), **17** (6.73 mmol, 3.00 g), and 4-bromoethylbenzene (**18d**) (6.74 mmol, 1.27 g) in DMSO (6 mL). The reaction was performed for 2 days. Column chromatography with pentane gave **19d** as a colourless liquid (1.75 g, 61 %).

¹H NMR (400 MHz, CDCl₃), 7.49 (d, *J* = 8.2 Hz, 2H), 7.32 (d, *J* = 8.16 Hz, 2H), 2.72 (q, *J* = 7.56 Hz, 2H), 1.27 (t, *J* = 7.6 Hz, H). ¹⁹F NMR (282.3 MHz, CDCl₃), -81.12 (t, *J* = 9.03 Hz, 3F), -110.64 (t, *J* = 13.55 Hz, 2F), -121.76 (s, 2F), -122.173 (s, 2F), -123.08 (s, 2F), -126.41 (s, 2F). ¹³C NMR (75.4 MHz, CDCl₃), 148.73, 128.28, 127.02, 126.5, (Aromatic-C) 120.00-105.00, (CF₂ and CF₃), 28.90, 15.25, (Ethyl-C). IR ν cm⁻¹ 3045, 2974, 2941, 2881, 1517, 1464, 1420, 1363, 1239, 1091, 1040, 1015.

Elemental Analysis calcd. for C₁₄H₉F₁₃: C 39.64, H 2.14, F 58.22. Obtained: C 39.44, H 2.13, F 58.1.

1-(perfluorohexyl)-4-vinylbenzene (3). Methyltriphenylphosphonium bromide (18.7 mmol, 6.69 g) and DBU (19 mmol, 2.89 g) were dissolved in freshly distilled DCM

(65 mL). The solution was refluxed for 30 minutes, and **18g**, (6.25 mmol, 2.65 g) dissolved in 15 mL freshly distilled DCM, was added to the refluxing solution at once. The mixture was refluxed for 2 hours, and subsequently washed with water (3 x 20 mL) and dried over Na₂SO₄. The solvent was removed using vacuum at 40 °C and purification was done by column chromatography (pentane:DCM = 0.9:0.1). Compound **3** was obtained as a colourless liquid (2.05 g, 77 %). ¹H NMR, ¹⁹F NMR and IR data were consistent with those reported in reference 17.

Sodium 2-(2-(4-ethylphenyl)-1,1,2,2-tetrafluoroethoxy)-1,1,2,2-tetrafluoroethanesulfonate (2). Copper powder, (19.9 mmol, 1.25 g) was heated above 150 °C under flow of argon in a 25 mL round bottom flask. Sodium 5-iodooctafluoro-3-oxapentanesulfonate (**22**) (4.31 mmol, 2.00 g) and **18** (4.6 mmol, 0.85 g) were stirred in DMSO (3.6 mL) for 2 days at 110 °C under an argon atmosphere. The reaction mixture was cooled and *i*-propanol (10 mL) was added. The solution was filtered and *i*-propanol was removed by vacuum. The remaining mixture was extracted using ethyl acetate (3 X 20 mL) and all the ethyl acetate layers were washed using saturated brine to remove the DMSO and inorganic impurities. The ethyl acetate layer was dried using anhydrous Na₂SO₄. Around 50% DMSO (w/w) was added to the dry powder obtained after evaporation of ethyl acetate and column chromatography was performed (DCM:*i*-propanol = 0.85:0.15) to give white **2**, (1.09 g, 60 %). M.p. 241- 245 °C.

¹H NMR (300 MHz, DMSO-*d*₆) 1.26 (t, *J* = 7.8 Hz, 3H), 2.71 (q, *J* = 7.5 Hz, 2H), 7.36 (d, *J* = 6.9 Hz, 2H), 7.56 (d, *J* = 6.9 Hz, 2H). ¹⁹F NMR (282.3 MHz, DMSO-*d*₆), -82.09 (t, *J* = 14.1 Hz, 2F), -87.10 (t, *J* = 13.0 Hz, 2F), -113.37 (s, 2F), -117.53 (s, 2F). ¹³C NMR (75.4 MHz, DMSO-*d*₆), 148.83, 128.73, 127.15, 125.64, (Aromatic-C) 121.92-108.01. (CF₂) 28.43, 15.54, (Ethyl-C). IR ν cm⁻¹ 3044, 2968, 2929, 2874, 1517, 1421, 1254, 1027, 1155, 1093, 1078, 1008. HRMS calcd. for C₁₂H₉F₈Na₂O₄S⁺: [M + Na]⁺ 446.9889, found 446.9889. Elemental Analysis calcd. for C₁₂H₉F₈NaO₄S: C 33.97, H 2.14, F 35.83, Na 5.42, S 7.56. Obtained: C 33.92, H 2.27, F 35.20, Na 5.38, S 7.45.

Sodium 1,1,2,2-tetrafluoro-2-(1,1,2,2-tetrafluoro-2-(4-formylphenyl)ethoxy)ethanesulfonate (24). Copper powder (62.0 mmol, 3.84 g) was heated above 150 °C in argon atmosphere and cooled to room temperature. Added to it, were

compound **22**, (12.9 mmol, 6.00 g) and **18e** (13.0 mmol, 2.40 g). DMSO (11 mL) was added to it and the reaction mixture was stirred for 22 h at 110 °C in inert conditions. *i*-Propanol (20 mL) was added to the reaction mixture and it was filtered. The filtrate was evaporated to remove *i*-propanol and extracted with ethyl acetate (3 X 20 mL) and ethyl acetate layers were washed with brine. The ethyl acetate layer was dried over Na₂SO₄, under argon. The solvent was removed to give white solid **24** (4.77 g, 87%) and stored under an inert atmosphere.

¹H NMR (300MHz, DMSO-*d*₆) 7.95 (d, *J* = 8.1 Hz, 2H), 8.09 (d, *J* = 7.8 Hz, 2H), 10.12 (s, 1H). ¹⁹F NMR (282.3 MHz, DMSO-*d*₆), -81.86 (t, *J* = 12.98 Hz, 2F), -86.49 (broad s, 2F), -113.21 (s, 2F), -117.51 (s, 2F). ¹³C NMR (75.4 MHz, DMSO-*d*₆), 193.47, 139.38, 133.32, 130.32, 128.40, (Aromatic-C and -CHO), 122.09-108.18, (CF₂). IR ν cm⁻¹ 3063, 2865, 1710, 1587, 1513, 1400, 1287, 1178, 1024, 1005. HRMS calcd. for C₁₁H₅F₈Na₂O₅S⁺ [M + Na]⁺ 446.9525, found 446.9521.

Sodium 1,1,2,2-tetrafluoro-2-(1,1,2,2-tetrafluoro-2-(4-vinylphenyl)ethoxy)ethanesulfonate (1). Methyltriphenylphosphonium bromide (16.0 mmol, 5.71g) and DBU (16.5 mmol, 2.51 g) were dissolved in 75 mL freshly distilled acetonitrile. The solution was refluxed for 30 minutes. **24**, (8.0 mmol, 3.85 g), dissolved in acetonitrile (20 mL), was added to the refluxing solution at once and the reaction mixture was refluxed for 2 hours. After cooling to room temperature, 10 mL water was added and the mixture filtered. The solvent was removed using vacuum at 40 °C. The crude material was extracted with ethyl acetate (3 X 20 mL) and washed with 0.001 N HCl (3 X 20 mL) All the ethyl acetate layers were collected and dried over Na₂SO₄. The solvent was removed and the purification was done by column chromatography (DCM:*i*-propanol = 0.8:0.2) to give a waxy white solid **25**. The yield was 3.9 g (70%) with ~75% purity.²⁵

¹H NMR (400 MHz, CDCl₃) 2.92 (d, *J* = 13.6 Hz, 3H), 5.33 (d, *J* = 11.2 Hz, 1H), 5.81 (d, *J* = 17.6 Hz, 1H), 6.70 (double d, *J* = 11.1 Hz and 8.0 Hz, 1H), 7.43-7.68 (m, 19H). ¹⁹F NMR (282.3 MHz, CDCl₃), -82.62 (d, *J* = 12.70 Hz, 2F), -87.62 (s, 2F), -114.20 (s, 2F), -117.96 (s, 2F). LRMS calcd. for C₁₂H₇F₈O₄S⁻ P⁺Ph₃CH₃ : Neg. ion,

$\text{C}_{12}\text{H}_7\text{F}_8\text{O}_4\text{S}^-$: $[\text{M}]^-$ 398.99, Found 398.85; Pos. ion, $\text{P}^+\text{Ph}_3\text{CH}_3$: $[\text{M}']^+$ 277.11, found 276.95.

The solution of **25** in acetone:water mixture (1:1) was passed through a Dowex[®] cation exchange column loaded with Na^+ ions. Column chromatography (DCM:*i*-Propanol = 0.8:0.2) followed by recrystallization from toluene were performed to give **2**, a white crystalline solid 2 g (50%). M.p. 250 °C (dec.).

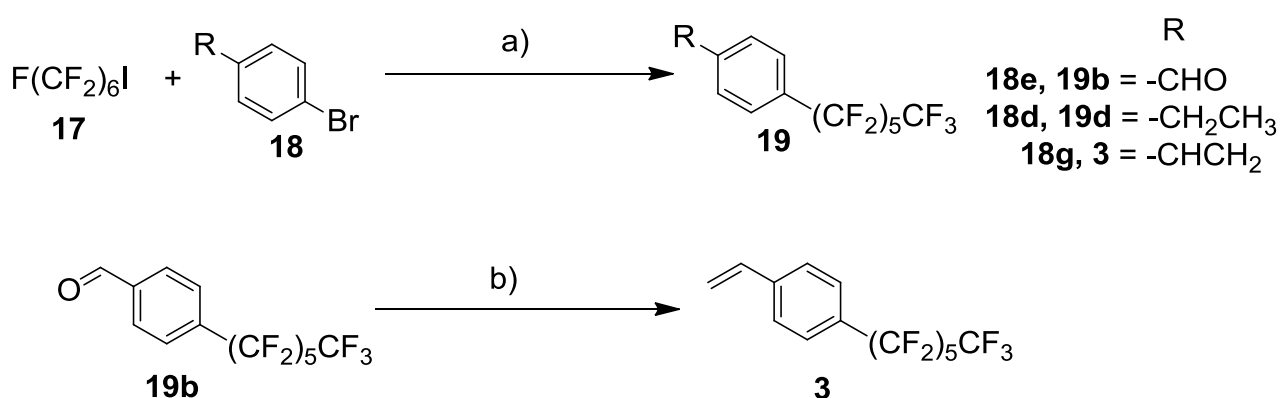
^1H NMR (300 MHz, MeOD) 5.3 (d, $J = 11.1$ Hz, 1H), 5.8 (d, $J = 16.8$ Hz, 1H), 6.67 (double d, $J = 11.1$ Hz and 6.6 Hz, 1H), 7.42 (d, $J = 8.9$ Hz, 2H), 7.51 (d, $J = 8.4$ Hz, 2H). ^{19}F NMR (282.3 MHz, MeOD), -83.12 (t, $J = 13.54$ Hz, 2F), -87.76 (t, $J = 12.98$ Hz, 2F), -114.80 (s, 2F), -118.20 (s, 2F). ^{13}C NMR (75.4 MHz, DMSO-*d*6), 141.49, 136.13, 127.71, 127.48, 127.13, 118.02, (Ar-C and vinyl-C), 127.00-113.00, (CF_2 -C). IR ν cm^{-1} 3087, 3007, 1651, 1571, 1515, 1407, 1293, 1255, 1220, 1170, 1100, 1080, 1008, 915, 841. HRMS calcd. for $\text{C}_{12}\text{H}_7\text{F}_8\text{Na}_2\text{O}_4\text{S}^+:[\text{M}.\text{Na}]^+$ 444.9727, found 444.9721. Elemental Analysis calcd. for $\text{C}_{12}\text{H}_7\text{F}_8\text{NaO}_4\text{S}$: C 34.14, H 1.67, F 36.00, Na 5.44, S 7.59 Obtained: C 33.87, H 1.67, F 35.00, Na 5.44, S 7.59.

3.3 Results and discussion

The syntheses of compounds **1** and **2** are based upon sodium 5-iodooctafluoro-3-oxapentanesulfonate (**22**), which contains an iodo and a sulfonate group at opposite ends of a fluorocarbon chain.¹³ For the substitution of the iodo moiety by an aromatic substituent, a copper-mediated cross-coupling is employed. In this reaction an iodine to copper exchange takes place that forms a copper(I) fluoroalkyl adduct, which subsequently reacts with an aromatic iodide or bromide.^{15,16} This reaction has been described using a wide range of aromatic iodides and bromides, and appears to be tolerant to the presence of functional groups like esters, carboxylic acids, nitro groups and amines.¹⁵

We decided to investigate the copper mediated cross-coupling reactions in the synthesis of model compounds **19**, which did not contain sulfonate groups (Scheme 3.1). In this manner, potential interference of the sulfonate with the reaction, and tedious surfactant purifications are avoided. The reaction of 1-iodofluorohexane (**17**)

with 4-bromoethylbenzene (**18d**) yielded 1-ethyl-4-(perfluorohexyl)-benzene (**19d**) in a moderate 60% yield. A direct coupling of 4-bromostyrene (**18g**) with **17** was attempted, but instead of the desired 1-(perfluorohexyl)-4-vinylbenzene (**3**), a highly viscous polymeric mass was obtained. Clearly the reaction conditions were too harsh for the styryl moiety and premature styrene polymerization had taken place. In order to obtain **19b**, we decided to couple 4-bromobenzaldehyde (**18e**) to the fluorocarboniodide **17**, and 4-(perfluorohexyl)benzaldehyde (**19b**)²⁶ was obtained in 88% yield. Compound **19b** appeared to be very sensitive to oxidation by air (even in the solid state) and had to be handled under an argon atmosphere to avoid oxidation to carboxylic acid. A subsequent Wittig reaction with methyl triphenylphosphonium bromide in DCM,^{27a} using 1,8-diazabicyclo[5.4.0]undec-7-ene (DBU) as a base, yielded the desired styrene compound **3** in 77% yield, see Scheme 3.1. The introduction of a styryl functionality by various methods, like dehydration of an alcohol,²⁸ dehydrohalogenation,²⁹ or a Wittig reaction with an aldehyde,^{27a,b} has been reported. We have chosen for the attachment of an aldehyde followed by a Wittig olefination, because this method is efficient, is performed under mild conditions, and can be employed in polar solvents in which fluorosulfonate compounds are soluble.^{27a}

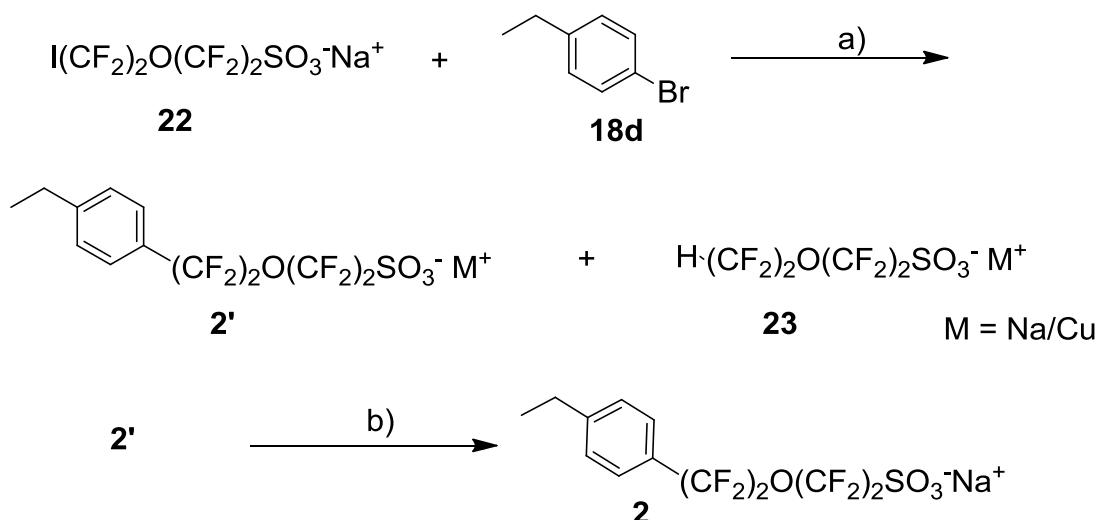


Scheme 3.1. Synthesis of compounds **5a-c**. a) Cu, DMSO, 110 °C, 22 h to 2 days. b) $\text{P}^+\text{Ph}_3\text{CH}_3\text{Br}^-$, DBU, DCM, reflux, 2 h.

The synthesis of the model surfactant **1** is outlined in Scheme 3.2. After the cross-coupling of sodium 5-iodooctafluoro-3-oxapentanesulfonate (**22**) and **19d**, a mixture of **2'**, which may contain Cu^+ or Na^+ as the counter ion, and the hydrogen substituted byproduct **23** was obtained.³⁰ The crude yield of this reaction, based on ^1H NMR spectra, was typically 70%. For standard reactions, in which the ratio between the reactants **22** and the **19d** was 1:1, the **2':23** ratio was typically 8:1. The substitution of iodide by hydrogen in this cross-coupling has been reported, and is ascribed to reaction of the Cu(I) -fluorocarbon adduct with water during work-up.¹⁵

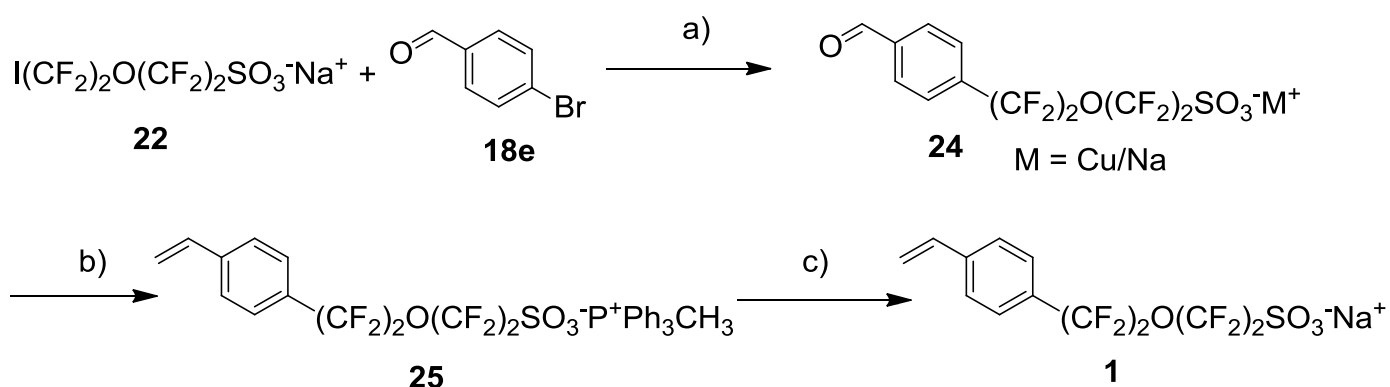
Isolation of **2** from this reaction mixture turned out to be difficult, and very sensitive to the exact work-up procedure. We found that only if the starting material contains DMSO, **2'** and **23** can be separated by column chromatography. Based on these findings, we performed the synthesis of **1** using two equivalents of **22**, which reduces the contents of **23** in the crude product to a mere 4%. For the removal of copper salts from the reaction, an ethyl acetate-brine extraction was used. After addition of DMSO to the mixture of **2'** and **23** a single column chromatography separation followed by cation exchange using an ion exchange column was sufficient to obtain **2** in pure form.³¹ The isolated yield after purification was 60%.³²

The synthesis of the polymerizable surfactant **1** is depicted in Scheme 3.3. The cross-coupling of **18e** and **22** produced compound **24**. After ethyl acetate and brine extraction, a procedure by which ionic contaminants and DMSO are removed and eventual Cu^+ ions are exchanged by Na^+ ions, the yield of **24** was 85%. Despite precautions to exclude air, traces of the carboxylic acid were observed in the NMR spectra of **24**.³³



Scheme 3.2. Synthesis of non-polymerizable fluorosurfactant **2**. a) Cu, DMSO, 110 °C, 2 days. b) Dowex cation exchange resin/Acetone-Water.

Remarkably, the hydrogenated product **23**, a compound that would be easily identified by ^1H and ^{19}F NMR was not detected. The subsequent Wittig reaction, performed with 2-3 equivalents of Wittig reagent, yielded the styrene **25**, in which the triphenylmethylphosphonium ion acts as the counter ion. After ion exchange using a sodium loaded Dowex[®] column, followed by chromatography on a silica column, **1** was obtained. Recrystallization from toluene gave crystalline **1** in 50% yield.



Scheme 3.3. Synthesis of the polymerizable fluorosurfactant **2**. a) Cu, DMSO, 110 °C, 22 h. b) $\text{P}^+\text{Ph}_3\text{CH}_3\text{Br}^-$, DBU, DCM, reflux, 2 h. c) Dowex cation exchange resin/Acetone-Water.

For the synthesis of compounds **1**, **2**, **19b** and **19d**, the cross-coupling reactions between an aromatic moiety ArBr **18** and the fluorocarbon iodides **17** and **22** were employed. We found that this reaction performed much better with 4-bromobenzaldehyde (**18e**) than with 1-bromo-4-ethylbenzene (**18d**). In case of **18e**, both the yields were higher and hydrogenated side-products were absent. These observations are best explained by assuming that the reactivity of the aromatic bromide in this reaction is enhanced by electron withdrawing substituents at the aromatic core. This conclusion is consistent with reported yields for this reaction.¹⁵ For the synthesis of fluoroalkyl-substituted styrenes a direct coupling of 4-bromostyrene was not possible. We have found that the coupling of benzaldehyde, followed by a Wittig reaction was an efficient method for the synthesis of these compounds. Both the copper mediated cross coupling and the Wittig reactions were not affected by the presence of a sulfonate moiety. The isolated yields of the sulfonate containing surfactants **1** and **2**, however, were markedly lower than those of **19b** and **19d**, but this was due to losses during purification of the surfactants. For the surfactant purification, ion-exchange and column chromatography were required. In particular the isolation of **1** from mixtures with the side-product **23** was very challenging. Attempts to avoid the formation of sulfonate containing surfactants by reversing the sequence of reaction steps, and making sulfonylfluorides instead, were not successful. We have found that sulfonylfluorides are not compatible with the copper-mediated cross-coupling conditions.

3.4 Conclusions

Compounds **1** and **2** were synthesized using the readily accessible sodium 5-iodooctafluoro-3-oxapentanesulfonate **22** as a starting compound. Coupling of aromatic molecules ArBr (**18**) to **22** was achieved by a copper mediated cross-coupling. The presence of a sulfonate moiety did not interfere with this reaction. The reaction of **22** with 1-bromo-4-ethylbenzene **18d** was slow and produced the hydrogenated side product **23**. The formation of **24** during the synthesis of **2** resulted in a challenging purification procedure. Attachment of a styryl functionality to **22** was achieved in two steps. The attachment of 4-bromobenzaldehyde (**18e**) to **22** was a

fast, efficient and clean reaction. The conversion of the aldehyde **24** to the polymerizable surfactant by a Wittig reaction proceeded smoothly. Extensive purification of this surfactant, including column chromatography and ion-exchange, however, seriously reduced the isolated yields. Along with fluorosurfactants **1** and **2**, the monomer **3** was synthesized by the cross-coupling of 4-bromobenzaldehyde and 1-iodo-fluorohexane followed by a Wittig reaction with methyltriphenylphosphonium bromide.

3.5 References and notes

- (1) Gin, D. L.; Bara, J. E.; Noble, R. D.; Elliott, B. J. *Macromol. Rapid Commun.* **2008**, 29, 367–389.
- (2) Mauritz, K. A.; Moore, R. B. *Chem. Rev.* **2004**, 104, 4535-4585.
- (3) LaConti, A. B.; Hamdan, M.; McDonald, R. C.; Vielstich, W.; Gasteiger, H.A.; Lamm (Eds.) A. *Handbook of Fuel Cells-Fundamentals, Technology and Applications*, Vol. 3, John Wiley and Sons, **2003**, Ch. 49.
- (4) Souzy, R.; Ameduri, B.; Boutevin, B.; Gebel, G.; Capron, P. *Solid State Ionics* **2005**, 176, 2839 –2848.
- (5) Ding, J.; Chuy, C.; Holdcroft, S. *Macromolecules* **2002**, 35, 1348-1355.
- (6) Zhang, Z.; Chalkova, E.; Fedkin, M.; Wang, C.; Lvov, S. N.; Komarneni, S.; Chung T. C. M. *Macromolecules* **2008**, 41, 9130-9139.
- (7) The degree of sulfonation is best represented by the equivalent weight (EW), which represents the mass of the polymer per SO₃⁻ unit. The equivalent weights for Nafion® 112 and the (PVDF-g-SPS) graft copolymer reported by Chung are 1100 and 454, respectively.
- (8) Gan, M. G.; Chow, P. Y.; Liu, Z.; Hana, M.; Queka, C. H. *Chem. Commun.* **2005**, 35, 4459–4461.
- (9) Gin, D. L.; Lu, X.; Nemade, P. R.; Pecinovsky, C. S.; Xu, Y.; Zhou, M. *Adv. Funct. Mater.* **2006**, 16, 865–878.
- (10) Herz, J.; Reiss-Husson, F.; Rempp, P.; Luzzati, V. *J. Polym. Sci. Part C Polym. Symp. Ed.* **1963**, 4, 1275-1290.
- (11) Lim, T. H.; Tham, M. P.; Liu, Z.; Hong, L.; Guo, B. *J. Membr. Sci.* **2007**, 290, 146–152.
- (12) Holmberg, K. *Novel Surfactants Preparation, Applications, and Biodegradability*, Marcel Dekker, New York **1998**, Ch.10.
- (13) Kissa, E. *Fluorinated Surfactants and Repellents*, Marcel Dekker, New York **2001**, Chapters 1-2.
- (14) Pich, A.; Datta, S.; Musyanovich, A.; Adler, H.-J. P.; Engelbrecht, L. *Polymer* **2005**, 46, 1323-1330.
- (15) McLoughlin, V. C. R.; Thrower, J. *Tetrahedron* **1969**, 25, 5921-5940.
- (16) Chen, G. J.; Tamborski, C. *J. Fluorine Chem.* **1989**, 43, 207-228.
- (17) Yamaguchi, K.; Watanabe S.; Nakahama, S. *Makromol. Chem.* **1989**, 190, 1195-1205.
- (18) Reppy, M. A.; Gray, D. H.; Pindzola, B. A.; Smithers, J. L.; Gin, D. L. *J. Am. Chem. Soc.* **2001**, 123, 363-371.
- (19) Soula, O.; Guyot, A. *Langmuir* **1999**, 15, 7956-7962.
- (20) Souzy, R.; Ameduri, B. *Prog. Polym. Sci.* **2005**, 30, 644–687.
- (21) Kirsh, Y. E.; Smirnov, S. A.; Popkov, Y. M.; Timashev, S. F. *Russ. Chem. Rev.* **1990**, 59, 560-574.

- (22) (a) Higginson, W. C. E.; Wooding, N. S. *J. Chem. Soc.* **1952**, 760-774. (b) Overberger, C. G.; Arnold, L. H.; Tanner, D.; Taylor, J. J.; Alfrey, T. Jr. *J. Am. Chem. Soc.* **1952**, 74, 4848-53. (c) Gao, H.; Pei, L.; Song, K.; Wu, Q. *Eur. Polym. J.* **2007**, 43, 908-914. (d) Chang, C. -C.; Studer, A. *Macromolecules* **2006**, 39, 4062-4068.
- (23) Tayouo, R.; David, G.; Ameduri, B. *Eur. Polym. J.* **2010**, 46, 1111-1118.
- (24) For an example, see the experimental section of: Jager, W. F.; Sarker, A. M.; Neckers, D. C. *Macromolecules* **1999**, 32, 8791-8799.
- (25) The remaining impurities were triphenylmethylphosphonium salts that were easily removed by the subsequent ion exchange.
- (26) The synthesis of **19d** via ethyl 4-bromobenzoate has been reported previously, but a reaction step using LiAlH₄ in this synthetic scheme, which may reduce the sulfonate group, made this procedure unsuited for our work, see: Reichardt, C.; Eschner, M.; Schafer, G. *J. Phys. Org. Chem.* **2001**, 14(11), 737-751.
- (27) (a) Okuma, K.; Sakai, O.; Shioji, K. *Bull. Chem. Soc. Jpn.* **2003**, 76, 1675-1676. (b) Marsh, G. P.; Parsons, P. J.; McCarthy, C.; Corniquet, X. G. *Org. Lett.* **2007**, 9, 2613-2616.
- (28) Overberger, C. G.; Saunders, J. H. *Organic Syntheses* **1948**, 28, 31-33.
- (29) Halpern, M.; Zahalka, H. A.; Sasson, Y.; Rabinovitz, M. *J. Org. Chem.* **1985**, 50, 5088-5092.
- (30) It is noteworthy that we did not find a similar hydrogenated product while preparing **19d**. Presumably this product has been formed, but since it is highly volatile, it has not been isolated.
- (31) After two columns, traces of **23** could be detected by ¹H and ¹⁹F NMR. The percentage of **23** in the product was below 1%.
- (32) Compound **1** can be recrystallized from toluene, but this procedure does not improve the purity of **1**.
- (33) The coupled product **19b** is very prone to oxidation. Fortunately, the carboxylic acid, that is formed, is removed in the ethyl acetate and brine extraction.

Chapter 4

Micellization properties and thermodynamics of micellization of hybrid fluorosurfactants **1** and **2***

Aggregation behaviour and thermodynamic properties of two novel homologous aromatic moiety bearing hybrid fluorocarbon surfactants, sodium 2-(1,1,2,2-tetrafluoro-2-(4-vinylphenyl)ethoxy)-1,1,2,2-tetrafluoroethanesulfonate (**1**) and sodium 2-(2-(4-ethylphenyl)-1,1,2,2-tetrafluoroethoxy)-1,1,2,2-tetrafluoroethanesulfonate (**2**) were studied using surface tension measurements and isothermal titration calorimetry (ITC) in dilute aqueous solutions at room temperature. Due to the aromatic group in the hydrophobic tail, both surfactants are soluble at room temperature unlike their starting precursor, 5-iodooctafluoro-3-oxapentanesulfonate as well as several other fluorocarbon sulfonic acid salts. Moreover, the surfactant **1** has the ability that it can be polymerized once microemulsions are formed with it. The ionic conductivity measurements of **2** at five different temperatures from 288 K to 313 K were carried out to study the effect of temperature on the micellization and its thermodynamics. The pseudo-phase separation model was applied to estimate thermodynamic quantities from conductivity data. The Gibbs energy of micellization versus temperature exhibited the characteristic U-shaped behaviour with a minimum at 306 K. The micellization process was found to be largely entropy driven. Due to its hybrid structure, the entropy change of micellization for **2** was larger than what is common for hydrocarbon surfactants like SDS but less than for fully fluorinated surfactants like NaPFO. The micellization process was found to be following entropy-enthalpy compensation phenomena.

*A modified version of this chapter was published in *Langmuir* **2012**, 28, 3397–3402, by Wadekar, M. N.; Boekhoven, J.; Jager, W. F.; Koper, G. J. M.; Picken, S. J.

4.1 Introduction

Fluorinated surfactants are molecules with fluorine atoms attached to the hydrophobic tail of the surfactants, which gives them very high chemical and thermal stability.¹ They differ from hydrocarbon surfactants mainly in three aspects. Firstly, they are much more hydrophobic than hydrogenated surfactants.² Secondly, they are bulkier and stiffer than hydrocarbon analogues due to the bigger size of fluorine atoms compared to hydrogen atoms. Further, due to the low polarizability of the fluorines, the van der Waals interactions between fluorinated molecules are weaker.³ Hence their physicochemical properties differ significantly from their hydrocarbon counterparts. For example, they show lower values for the critical micelle concentration (cmc) and lower surface tension at the cmc.³ By comparison, the cmc values of fluorinated surfactants are found to be similar to those of hydrocarbon surfactants with roughly 1.5 times longer chain length.⁴ The thermodynamics of micellization of the fluorinated surfactants is also different from that of hydrocarbon surfactants. For example, the Gibbs energy contribution to micellization per $-\text{CF}_2$ group in the fluorinated surfactant is -4.1 kJ/mol compared to -2.4 kJ/mol per $-\text{CH}_2$.² Due to the bulky nature of the fluorocarbon chains, the packing of the fluorinated surfactants is significantly different in the micelles. For instance, fluorine containing amphiphiles often tend to form oval shaped or rod-like micelles at higher concentrations.^{5,6}

The aggregation and thermodynamic properties in dilute solutions of various fully fluorinated surfactants have been well studied.^{1-7,8} Anionic fluorocarbon surfactants have been investigated more frequently than other types because they are easy to synthesize and useful for several applications. Amongst them, the perfluoroalkane carboxylic acid salts are the most often investigated systems. For instance, González-Pérez and coworkers have determined aggregation properties and associated thermodynamic quantities for sodium perfluoro alkanoates^{3,8} using various thermodynamic models. The relationships between cmc and temperature in these cases were found to be U-shaped. Also, they have shown the micellization process to follow the entropy-enthalpy compensation phenomena. In one example, Turro and coworkers have revealed that sodium perfluorooctanoate forms mini micelles with very low aggregation number (~ 7), by studying phosphorescence

hydrophobic tail is directly attached to polar head group $-\text{SO}_3^-$ on one side and aromatic groups on the other side.

The main objective of synthesizing **1** was to create nanostructured chemically robust membranes from bicontinuous microemulsions. . This will be done in a two step bottom-up approach. Initially, the behavior of **2** will be studied. Then, in the second step, the knowledge acquired from this study will be used to obtain bicontinuous microemulsions from the polymerizable fluorosurfactant **1**. These microemulsions are subsequently polymerized to form nanostructured polymer membranes. In a similar way, the bicontinuous microemulsion phase of another polymerizable surfactant has been (co)polymerized while preserving the phase morphology by Chew et al.¹⁸ Thus, **2** acts as a model system for phase behavior study without any risk of polymerization during the experiments.

We have used surface tension and isothermal titration calorimetry (ITC) for this study. Furthermore, the effect of temperature on associated thermodynamic properties of **2** is discussed. These temperature-dependent thermodynamic properties of **2** were studied by performing ionic conductivity measurements of its aqueous solutions at five different temperatures from 288 K to 313 K.

It is important to note that both surfactants, which are sodium salts of fluorocarbon sulfonate, are perfectly soluble in water due to the terminal ethyl phenyl moiety on **2** and vinyl phenyl group on **1**. Similarly, their micellar properties, notably the cmc values, aggregate shapes, and the aggregation numbers, are expected to be different from the usual perfluorocarbon sulfonate surfactants.

4.2 Experimental section

Syntheses of the surfactants **1** and **2** have been described in Chapter 3.¹³ All the solutions were prepared using deionized water (Milli Q, Millipore, the Netherlands) and allowed to equilibrate for a few hours to overnight before actual experiments. Surface tension measurements were conducted by the pendant drop method at 295 ± 2 K. The stock solutions of the appropriate concentration were prepared. The solutions were subsequently diluted to the desired concentration using deionized water.

ITC was performed using a VP-ITC microcalorimeter (MicroCal). It was carried out in two steps, in the first step; 150 mM surfactant solution was taken in the syringe and pure water in the sample cell. The titration was done with 7 μl per injection upto total 40 additions. In the second step, the syringe was loaded again with 150 mM surfactant solution and sample cell with 25 mM solution. The titration was done in the previous manner and the data points from the both measurements were combined to give a single graph as shown in Figure 4.4. The two step experiment was necessary for better resolution and better signal to noise ratio.

Conductivity measurements were carried out using a conductivity meter with a platinum electrode, having a cell constant of 0.798 cm^{-1} (model 712), from Metrohm AG. It was calibrated using a 0.1 M KCl solution. Equilibrated 150 mM stock solutions of **1** and **2** were used to make subsequent dilutions for ionic conductivity measurements. The measurements for **2** were carried out at five temperatures using a thermostated water bath. The temperature of the bath was kept within $\pm 0.05\text{ K}$.

4.3 Results and discussion

4.3.1 Surface tension experiments

The solubility of both surfactants in water was examined visually in the temperature range from 288 K to 313 K at the maximum concentration of 500 mM to be used in the experiments. Both surfactants were found to be perfectly soluble even at the lowest experimental temperature and did not precipitate, not even months after preparing the solutions. Thus all the experiments were done above the Krafft temperature.

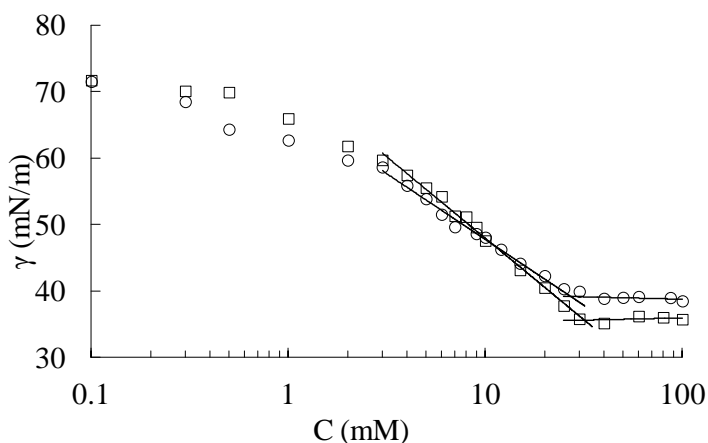


Figure 4.2. Surface tension (γ) for aqueous solutions of **1** (\square) and **2** (\circ) versus concentration at 295 ± 2 K. From the inflection points the cmc-values are determined at 31.8 mM for **1** and 27.1 mM for **2**. The slopes of the drawn lines were used to estimate $d\gamma/d\ln C$.

It is noteworthy that the room temperature solubility of the starting compound, sodium 5-iodooctafluoro-3-oxapentanesulfonate used to synthesize **1** and **2** is not very good in water. Typically, its purification is done by recrystallization from water solution.¹⁹

In Figure 4.2, the surface tension, γ is plotted versus the concentration of compounds **1** and **2** at 295 ± 2 K. The cmc values were determined using a linear regression on both sides of the intersection point as indicated in the graph. The adsorption of the surfactants Γ at the cmc was obtained using the Gibbs adsorption isotherm given by Eq. 4.1.

$$\Gamma = -\frac{1}{(2-\alpha)RT} \frac{d\gamma}{d\ln C} \quad (4.1)$$

where C is the surfactant solution concentration, T temperature and R the gas constant. The factor $2-\alpha$ has been added to account for the surface excess due to the counter ions in the absence of any other electrolyte; α is degree of ionization of the micelles^{3,20} of **1** and **2** obtained from ionic conductivity measurements and taken to be the same for the surface layer. The various parameters that have been obtained for both surfactants from the surface tension experiments are shown in Table 4.1.

The cmc values for both fluorosurfactants, being 31.8 and 27.1 for **1** and **2** respectively, are comparable to those of fully fluorinated anionic surfactants having around 7 to 8 carbon atoms. For instance, for $n\text{C}_7\text{F}_5\text{SO}_3\text{Na}$, $n\text{C}_7\text{F}_5\text{COONa}$, and $n\text{C}_7\text{F}_5\text{COOK}$ the values are found to be 17.5 mM at 329 K, 36 mM at 281 K, and 27 mM at 299 K respectively.⁴

Table 4.1. Critical micelle concentration (cmc), surface pressure π_{cmc} at cmc, surface excess concentration Γ , molecular surface area σ , Gibbs energy of micellization $\Delta G_{\text{mic}}^{\circ}$ and of adsorption $\Delta G_{\text{ads}}^{\circ}$ and, the aggregation number N as calculated from surface tension data in Figure 4.2. The degree of dissociation of counter ions, α , was taken for **1**, 0.60 and for **2**, 0.64 from electrical conductivity data (see Table 4.3).

Surfactant	cmc	γ_{cmc}	Γ	σ	$\Delta G_{\text{mic}}^{\circ}$	$\Delta G_{\text{ads}}^{\circ}$	N
	mM	(mN/m)	($\mu\text{mol}/\text{m}^2$)	($\text{\AA}^2/\text{molecule}$)	(kJ mol^{-1})	(kJ mol^{-1})	
1	27.1	38.4	2.5	66.2	-26.5	-41.8	22
2	31.8	34.2	3.2	51.9	-25.1	-35.8	29

It is important to note that the solubility of many of the fully fluorinated sulfonic acid salts at room temperature is poor, for which reason their cmc values have been determined at higher temperatures.⁴ The cmc values of **1** and **2**, however, have been determined around room temperature. The value of the surface tension γ_{cmc} at the cmc for both fluorosurfactants were quite similar, 38 mN/m (**1**) and 34 mN/m (**2**). These values are comparable to those of fully fluorinated sulfonic acid salt surfactants studied by Shinoda and coworkers.⁴ These authors have shown that the cmc values of fluorinated surfactants are similar to those of hydrocarbon surfactants with chain length roughly 1.5 times longer than the fluorinated surfactant. Although in the case of some semi fluorinated surfactants, due to the folded conformation of the hydrocarbon spacers, additional care has to be taken while following this rule.² In case of **1** and **2**, the comparison is difficult due to the presence of the aromatic moieties. The minimal interfacial area occupied by a single surfactant molecule (σ) has been calculated using Eq. 4.2.

$$\sigma = \frac{1}{N_A \Gamma} \quad (4.2)$$

where N_A is the Avogadro's number. Values of σ for **1** and **2**, 52 and 66 \AA^2 , respectively were found to be matching those of fully fluorinated carboxylate surfactants which have been reported in the range⁴ of $\sim 50 \text{ \AA}^2$.

The maximum excess surface pressure at the cmc, π_{cmc} is a measure of the cohesive force in the surfactant film or - in other words - the lateral interaction among the surfactant molecules. It is the difference between surface tension of pure water and the surface tension of surfactant solution at cmc, calculated by Eq. 4.3.

$$\pi_{\text{cmc}} = \gamma_{\text{water}} - \gamma_{\text{cmc}} \quad (4.3)$$

The values of π_{cmc} for **1** and **2** are 38.4 mN/m and 34.2 mN/m, respectively, suggesting a rather loose lateral packing of the hydrophobic tails of the surfactants.² The reason for this could be the presence of a bulky phenyl group on the hydrophobic tail.

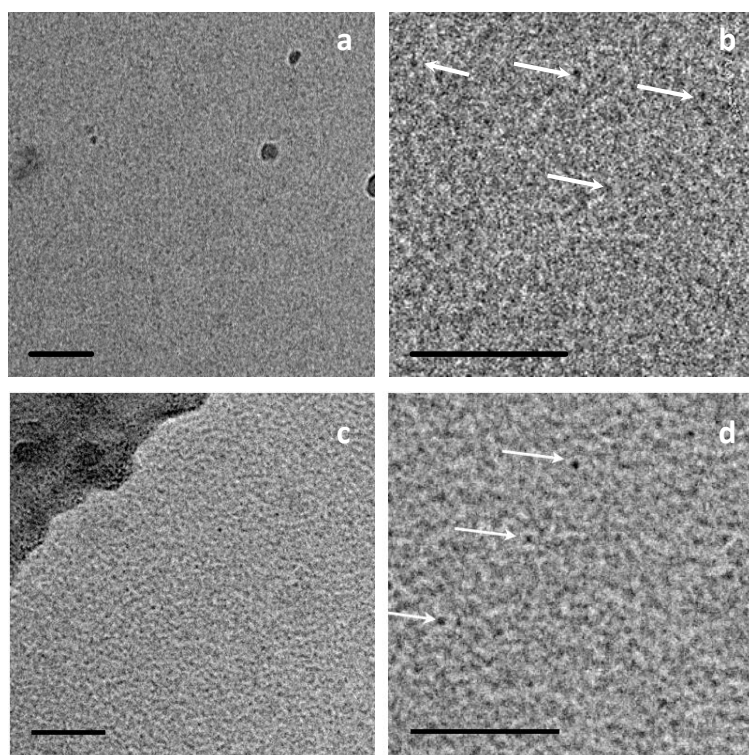


Figure 4.3(a), (b). CryoTEM of (100 mM) **1**-water solution. The scale bar is 60 nm. **(b), (c)** CryoTEM of (50 mM) **2**-water solution. The scale bar is 80 nm. The white arrows indicate micelles.

Cryo-TEM study on **1** and **2** shows that the surfactants form spherical micelles (see Figure 4.3). We estimated the number of surfactant molecules per micelle i.e. the aggregation number (N) using Eq. 4.4,²¹ using a value for the hydrophobic tail length $L = 11 \text{ \AA}$ that we derived from known values for other compounds.

$$N = \frac{4\pi L^2}{\sigma} \quad (4.4)$$

Aggregation numbers obtained are 32 and 29 for **1** and **2** respectively. These numbers are low which can be attributed to the presence of a fluorinated tail.^{22,23} These numbers are close to the value (36) observed for lithium perfluorooctane sulfonate.²³ Further, bulky phenyl groups when positioned at the end of the hydrophobic tails are known to affect packing of the surfactant molecules in micelles.²⁴

The standard Gibbs energy of micellization (ΔG_{mic}°) values for **1** and **2** have been obtained by using Eq. 4.5 that holds for ionic surfactants.

$$\Delta G_{mic}^\circ = (2 - \alpha) RT \ln x_{cmc} \quad (4.5)$$

where x is the surfactant mole fraction. ΔG_{mic}° values are 26.5 and 25.1 kJ/mol for **1** and **2** respectively. These values are similar to what was obtained for perfluorinated carboxylate surfactants.^{3,25} The Gibbs energy of adsorption (ΔG_{ads}°) values have subsequently been calculated using Eq. 4.6 and for **1** and **2** are found to be 41.8 and 35.8 kJ/mol.

$$\Delta G_{ads}^\circ = \Delta G_{mic}^\circ - \pi_{cmc} \sigma \quad (4.6)$$

4.3.2 Isothermal titration calorimetry

Isothermal titration calorimetry (ITC) is another technique that allows the determination of the critical micelle concentration and in addition the enthalpy of micellization, ΔH_{mic}° , in single experiments. Moreover, it is possible to obtain the aggregation number using the data of the same experiments and an appropriate model.^{26,27} The enthalpy of micellization has been plotted versus concentration in Figure 4.4. It clearly shows that the heat of dissolution of the surfactants in water is very high and hence, unfortunately, significantly contributes to the error in determining the enthalpy of micellization.

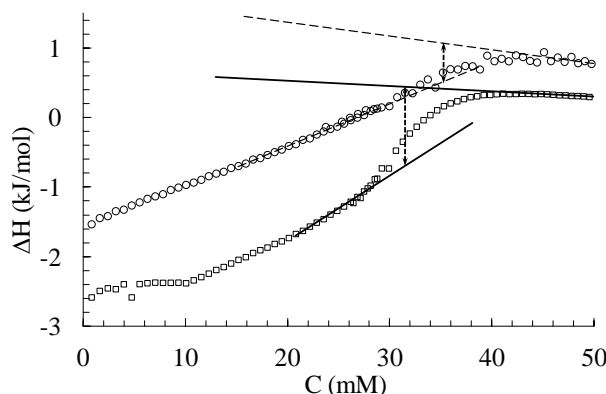


Figure 4.4. Enthalpy of demicellization for **1** (○) and **2** (□) vs concentration of the fluorosurfactants in water at 298 K. The cmc was estimated from the location of the midpoint of the inflection indicated in the plot by dotted arrow with two heads. The slopes of the data points around these inflections were used to calculate $d\Delta H/dC$.

Nevertheless the values for the enthalpy of micellization for both surfactants have been obtained by estimating the jump values around the cmc. The cmc was estimated from the location of the midpoint of the inflection in the plot and subsequently used to obtain the Gibbs energy of micellization.²⁶ The inflection was taken from the points with the highest slope value and with the best fit. From the slope of the data points of the inflection around cmc, $(d\Delta H/dC)$ the aggregation number, N was calculated using Eq. 4.7. The results are summarized in Table 4.2.

$$N = \frac{8C}{\Delta H_{mic}^o} \frac{d\Delta H}{dC} \quad (4.7)$$

Table 4.2. Critical micelle concentration (cmc), enthalpy of micellization ΔH_{mic}^o , Gibbs energy of micellization ΔG_{mic}^o , micellization entropy ΔS_{mic}^o and aggregation number obtained from ITC experiments (see Figure 4.4). Values of α were taken from electrical conductivity data as 0.60 for **1** and 0.64 for **2** (see Table 4.3).

Surfactant	cmc (mM)	ΔH_{mic}^o (kJ mol ⁻¹)	ΔG_{mic}^o (kJ mol ⁻¹)	ΔS_{mic}^o (J mol ⁻¹ K ⁻¹)	N
1	35 ± 3	0.6 ± 0.1	-26 ± 2	89 ± 8	29 ± 3
2	31 ± 3	1.2 ± 0.2	-25 ± 3	89 ± 9	35 ± 4

The cmc values, 35 ± 3 mM and 31 ± 3 mM for **1** and **2** respectively, thus obtained are comparable to the cmc values from surface tension measurements whereas the values for the aggregation numbers were found to be slightly larger than the numbers obtained from surface tension measurements.

4.3.3 Ionic conductivity experiments

Ionic conductivity measurements for aqueous solutions of **2** were performed at five temperatures in the range from 288 K to 313 K. It is important to note that such study is rather difficult in the case of **1** due to its ability to undergo polymerization.

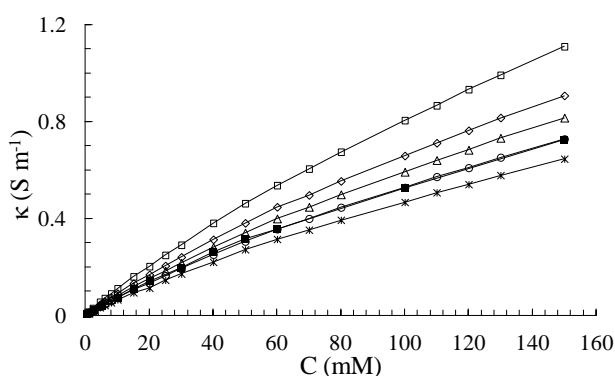


Figure 4.5. Specific conductivity for **1** at 295 ± 2 K (■) and for **1** at 288 K (x), 293 K (○), 298 K (□), 303 K (Δ) and 313 K (◇). The slopes of the data points above and below the narrow micellar transition region were used for the calculation of α .

Figure 4.5 shows the plot of specific ionic conductance (κ) of **2** versus concentration. At low concentrations, the specific ionic conductance varies more or less linearly with concentration. As micelles start forming, a break in this trend occurs within a narrow concentration regime after which the conductance again is linear with concentration, albeit with another slope. The change of slope is not the commonly observed sharp transition which is due to the fact that the micelles have low aggregation numbers, see Tables 4.1 and 4.2. By extrapolating the behavior of the specific ionic conductance versus concentration below and above the cmc, the value for the cmc could be determined from the intersection. Similarly, the degree of ionization (α) of micelles can be estimated from the ratio of their slopes.³ Thus obtained values are given in Table 4.3.

The degree of ionization, α does not change appreciably with temperature unlike for other surfactants. For example, perfluoroalkane carboxylate salts show a linear

behavior in α with change in temperature.²⁸ In the case of **2**, α changes little and was considered to be constant with a value 0.64 for all of our analyses.

The Gibbs energy of micellization, ΔG°_{mic} , was determined from the conductivity data using Eq. 4.5. The micellization enthalpy, ΔH°_{mic} , and subsequently the micellization entropy, ΔS°_{mic} were determined from the temperature dependence of the Gibbs energy using the van't Hoff equation (Eq. 4.8), and using the Gibbs-Helmholtz equation respectively (Eq. 4.9).⁸ The values of all the thermodynamic quantities and α are compiled in Table 4.3.

$$\Delta H^{\circ}_{mic} = -T^2 \frac{d(\Delta G^{\circ}_{mic} / T)}{dT} \quad (4.8)$$

$$\Delta S^{\circ}_{mic} = \frac{(\Delta H^{\circ}_{mic} - \Delta G^{\circ}_{mic})}{T} \quad (4.9)$$

Table 4.3. The values of the critical micelle concentration (cmc), degree of micellar ionization α , the standard thermodynamic properties, i.e. enthalpy of micellization ΔH°_{mic} , Gibbs energy of micellization ΔG°_{mic} and, micellization entropy ΔS°_{mic} estimated from ionic conductivity experiments.

Surfactant	Temp. (K)	cmc (mM)	α	ΔG°_{mic} (kJ mol ⁻¹)	ΔH°_{mic} (kJ mol ⁻¹)	ΔS°_{mic} (J mol ⁻¹ K ⁻¹)
2	288	47.4	0.66	-23.2	8.4	110
	293	44.5	0.64	-23.8	6.2	102
	298	42.4	0.63	-24.3	3.9	94
	303	43.4	0.63	-24.6	1.4	86
	313	43.2	0.65	-25.5	-4.1	68
1	293±2	35.7	0.60	-25.1		

The temperature dependence of the Gibbs energy of micellization was found to follow the characteristic U-shaped relationship,⁸ see Figure 4.6.

A parabolic curve fitted to the experimental data, goes through the minimum temperature $T^* = 306$ K with the associated minimum critical micelle concentration, $\text{cmc}^* = 42$ mM. The value determined for T^* is lower than the 316 K reported for a fully fluorinated surfactant like sodium perfluorooctanoate (NaPFO) and higher than the 298 K reported for sodium dodecyl sulfate, the classical hydrocarbon surfactant with similar chain length. It is generally accepted that two opposite processes control micellization, the first being the hydration of the polar head groups and the second being the generation of water structure surrounding the hydrophobic tail. With increase in temperature, hydration of polar head groups decreases disfavoring the micellization, whereas the water structure surrounding the hydrophobic tail breaks down favoring micellization. The U-shaped dependence of the free energy of micellization on temperature reflects the balance of these two processes.^{8,28}

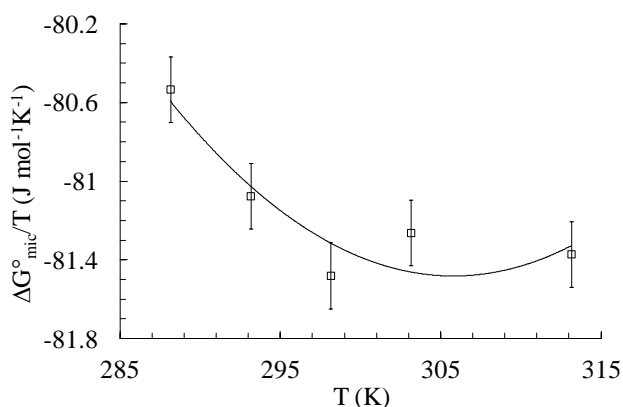


Figure 4.6. Gibbs energy of micellization versus temperature for surfactant **2**. The drawn line is the result of a fit to a polynomial equation.

The micellization process is largely entropy driven, at higher temperature the entropy is more dominant as expected; an entropy – enthalpy compensation plot is shown in Figure 4.7. Entropy-enthalpy compensation phenomena consist of two parts as described previously²⁹: a “desolvation” part due to the dehydration of the hydrophobic tail of the surfactant and a “chemical” part due to the aggregation of the surfactant tails to form micelles. This phenomenon has been summarized by Eq. 4.10,²⁹

$$\Delta H_{mic}^o = \Delta H_{mic}^A + T_c \Delta S_{mic}^o \quad (4.10)$$

where the compensation temperature (T_c) is a measure of the desolvation part, it was found to be 301.5 K, where the intercept ΔH_{mic}^A is considered as the enthalpy belonging to the chemical part which we found²⁸ to be 24.6 kJ mol⁻¹. The compensation temperature T_c in the case of **2** is smaller than what has been found for perfluoroalkane carboxylate salts with seven and more carbon atoms in the hydrophobic tail.²⁸

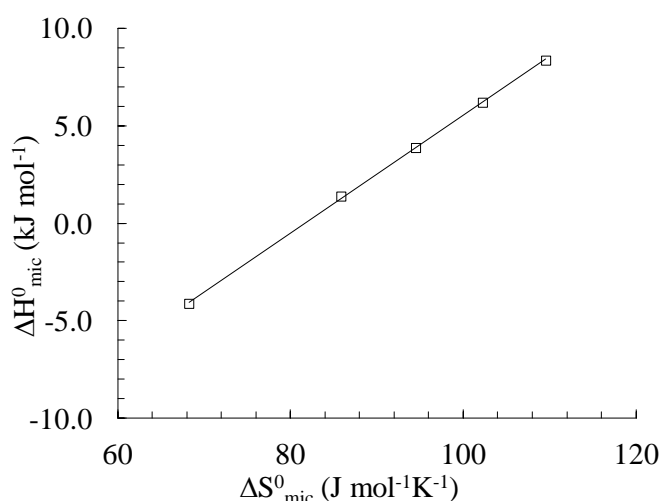


Figure 4.7. Enthalpy-entropy compensation for **1**-water solutions. The drawn line is the result of a linear regression of the data.

The ΔH_{mic}^o value for surfactant **2** at 298 K directly determined from ITC experiments to be $(1.2 \pm 0.2 \text{ kJ mol}^{-1})$ and the one obtained from the temperature dependence of the conductivity (3.9 kJ mol^{-1} ; reported in Table 4.3) are reasonably similar considering the variation of the obtained values with temperature as is obvious from Table 4.3. For ionic surfactants, such deviations have been observed before and are attributed to compensating effects of dilution and micellization that affect the two measurement techniques differently.^{30,31} It is noteworthy that ΔG_{mic}^o values obtained from surface tension, ITC, and specific conductivity measurements are also in the similar range (-22 and -28 kJ mol^{-1}).

The heat capacity of micellization, $\Delta C_{p, mic}^o$, was determined from the temperature dependence of the micellization enthalpy and found to be $-0.5 \text{ kJ mol}^{-1}\text{K}^{-1}$. This value

is comparable to $\Delta C_{p^{\circ}mic}$ values obtained for perfluorocarboxylic acid salts.²⁸ The negative value of $\Delta C_{p^{\circ}mic}$ signifies that the hydration shell, due to organized water molecules around the hydrophobic chain of surfactant, is lost during micellization process or in other words, more hydrophobic chains are exposed to water molecules upon demicellization.³¹ The $\Delta C_{p^{\circ}mic}$ value for **2** is larger than for the sodium salt of perfluoroalkane carboxylates and also for sodium octanoate, suggesting that the hydrophobic surface being exposed to water upon demicellization is larger for **2**.³² Figure 4.8 shows a comparison of the change with temperature of ΔS°_{mic} for **2**, NaPFO and SDS where the latter data are taken from reference 33. The ΔS°_{mic} values for **2** are somewhat smaller than those of NaPFO, but larger to the ΔS°_{mic} values of SDS. This can be attributed to the hybrid structure of **2**.

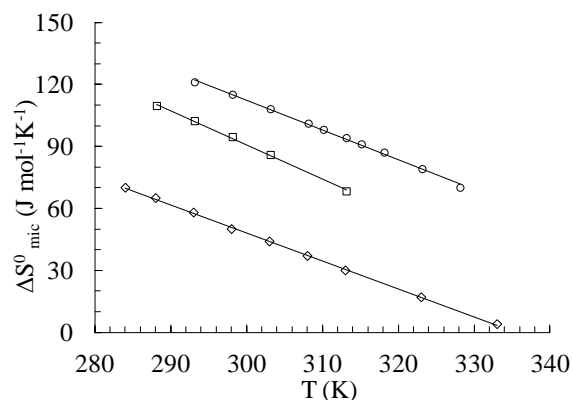


Figure 4.8. ΔS°_{mic} versus temperature for (□) **2**, (o) for sodium perfluorooctanoate and (◇) sodium dodecyl sulfate. The values for the latter two molecules are taken from ref. 3 and 33 respectively. The drawn lines are the linear fits.

4.4 Conclusion

The micellization properties of two novel hybrid fluorosurfactants **1** and **2**, obtained from three sets of experiments involving surface tension, calorimetry, and ionic conductivity show a coherent picture. These molecules are the first examples of fluorinated hybrid surfactants bearing $-\text{SO}_3^-$ directly attached to fluorocarbon on one side and the aromatic moieties on the other side. Both surfactants are perfectly soluble in water at room temperature unlike their starting precursor compound, sodium 5-iodooctafluoro-3-oxapentanesulfonate and several other fluorinated sulfonic acid salt surfactants. This enhanced solubility of **1** and **2** is due to the hybrid

character of, and the presence of bulky aromatic moieties in the surfactant tails. Both surfactants form spherical micelles in their water solutions. The cmc values, surface tension values at cmc are comparable, which can be attributed to their similar molecular structures. The Gibbs energy of micellization of **1** and **2** are in the range of -24 to -26 kJmol⁻¹. The aggregation numbers are low and in the range of 25 to 35. Micelle formation is largely driven by entropy changes where the dependence of the Gibbs energy of micellization on temperature follows a U-shaped relation. Entropy-enthalpy compensation plays an important role in the micellization process.

4.5 References and notes

- (1) Kissa, E. Fluorinated Surfactants, Synthesis, Properties, Applications, Surfactant Science Series, Marcel Dekker, New York, 1994, Vol. 50, pp 1-21.
- (2) Sadtler, V. M.; Giulieri, F.; Krafft, M. P.; Riess, J. G. *Chem. Eur. J.* **1998**, *4*, 1952-57.
- (3) González-Pérez, A.; Ruso, J. M.; Prieto, G.; Sarmiento, F. *J. Surf. Detergents* **2004**, *7*, 387-395.
- (4) Shinoda, K.; Hat, M.; Hayashi, T. *J. Phys. Chem.* **1972**, *76*, 909-914.
- (5) Szajdzinska-Pietek, E.; Wolszczak, M. *Langmuir* **2000**, *16*, 1675-1680.
- (6) Fung, B. M.; Mamrosh, D. L.; O'Rear, E. A.; Frech, C. B.; Afzal, J. *J. Phys. Chem.* **1988**, *92*, 4405-4411.
- (7) Matsuoka, K.; Moroi, Y. *Curr. Opin. Colloid Interface Sci.* **2003**, *8*, 227-235.
- (8) Gonza, A.; Rez, L.- P.; Prieto, G.; Ruso, J. M.; Sarmiento, F. *Mol. Phys.* **2003**, *101*, 3185-3195.
- (9) Turro, N. J.; Lee P. C. C. *J. Phys. Chem.* **1982**, *86*, 3371-3374.
- (10) Sulak, K.; Wolszczak, M.; Chittofrati, A.; Szajdzinska-Pietek, E. *J. Photochem. Photobiol. A: Chem.* **2007**, *191*, 1-5.
- (11) Kumar, K. S. *Research J. Chem. Environ.* **2005**, *9*, 50-79.
- (12) Mauritz, K. A. ; Moore R. B. *Chem. Rev.* **2004**, *104*, 4535-4585.
- (13) Wadekar, M. N.; Jager, W. F. Sudhölter, E. J. R.; Picken S. J. *J. Org. Chem.* **2010**, *75*, 6814-6819.
- (14) Hisatomi, M.; Abe, M.; Yoshino, N.; Lee, S.; Nagadome, S.; Sugihara, G. *Langmuir* **2000**, *16*, 1515-1521.
- (15) Matsuoka, K.; Moroi, Y. *Curr. Opin. Colloid Interface Sci.* **2003**, *8*, 227-235.
- (16) Xu, Z.; Li, P.; Qiao, W.; Li, Z.; Cheng, L. *J. Surf. Detergents* **2006**, *9*, 245-248.
- (17) Nave, S.; Paul, A.; Eastoe, J.; Pitt, A. R.; Heenan R. K. *Langmuir* **2005**, *21*, 10021-10027.
- (18) Chew, C. H. ;Li, T. D.; Gan, L. H.; Quek, C. H.; Gan, L. M. *Langmuir* **1998**, *14*, 6068-6076.
- (19) Zhang, L.; Jr. Dolbier, W. R.; Sheeller, B.; Ingold, K. U. *J. Am. Chem. Soc.* **2002**, *124*, 6362-6366.
- (20) The monograph *Physical Chemistry of Surfaces* by Adamson and Gast, 6th edition, section III-6-A.
- (21) Isrealachevili, J. N. Intermolecular and Surface Forces, Academic Press, *Ed. 2*, New York, 1998, pp 390-391.
- (22) Turro, N. J.; Lee, P. C. C. *J. Phys. Chem.* **1982**, *86*, 3367-3371.
- (23) Bossev, D. P.; Matsumoto, M.; Nakahara, M. *J. Phys. Chem. B* **1999**, *103*, 8251-8258.
- (24) De, S.; Aswal, V. K.; Ramakrishnan, S. *Langmuir* **2010**, *26*, 17882-17888.
- (25) Moroi, Y.; Take'uchi, M.; Yoshida, N.; Yamauchi, A. *J. Colloid Interface Sci.* **1998**, *197*, 221-229.

-
- (26) Koper, G. J. M.; Minkenberg, C. B.; Upton, I. S.; van Esch, J. H.; Sudhölter, E. J. R. *J. Phys. Chem. B* **2009**, *113*, 15597–15601.
- (27) Ohta, A.; Toda, K.; Morimoto, Y.; Asakawa, T.; Miyagishi, S. *Colloids Surf. A.: Physicochem. Eng. Aspects* **2008**, *317*, 316–322.
- (28) González-Pérez, A.; Rez, L.-P.; Ruso, J. M.; Romero, M. J.; Blanco, E.; Prieto, G.; Sarmiento, F. *Chem. Phys.* **2005**, *313*, 245–259.
- (29) Chen, L.-J.; Lin, S. -Y.; Huang, C. -C. *J. Phys. Chem. B* **1998**, *102*, 4350–4356.
- (30) Chatterjee, A.; Moulik, S. P.; Sanyal, S. K.; Mishra, B. K.; Puri, P. M. *J. Phys. Chem. B* **2001**, *105*, 12823–12831.
- (31) Bouchemala, K.; Agnelya, F.; Koffib, A.; Djabourov, M.; Ponchela, G. *J. Mol. Recognit.* **2010**, *23*, 335–342.
- (32) Garidel, P.; Hildebrand, A.; Neubert, R.; Blume, A. *Langmuir* **2000**, *16*, 5267–5275.
- (33) Marcolongo, J. P.; Mirenda, M. *J. Chem. Educ.* **2011**, *88*, 629–633.

Chapter 5

Supramolecular “Leeks” of the fluorinated hybrid amphiphile, **2** that self-assemble into a supramolecular columnar phase*

We report on the formation of unprecedented “Leek” shaped aggregates of the anionic fluoroalkyl sulfonate surfactant (**2**), and their assembly into a supramolecular columnar phase (C_s). The leeks form by wrapping of 2 to 3 water-**2** bilayers of thickness 26-28 Å into 10-20 nm thick and >100 nm long structures, in a concentration regime of 63 to 70 wt% of **2**. A lamellar (L_a) lyotropic liquid crystalline (LLC) forms at higher concentration, between 70 to 84 wt%. In the two LLC phases the **2** molecules were organized in either an interdigitated or tilted fashion, or combination of the two. Such a unique supramolecular self-assembly of amphiphiles has not been predicted nor observed before.

*An article is in preparation on the modified version of this chapter by Wadekar, M. N.; Abezgaus L.; Djanashvili, K.; Mendes, E.; Danino, D.; Jager, W. F.; Picken, S. J.

5.1 Introduction

Amphiphilic molecules like surfactants and lipids are well known to form micellar and lyotropic liquid crystalline (LLC) mesophases in strongly polar solvents like water. In general, LLC phase behavior is controlled by the hydrophobicity of amphiphiles, their packing characteristics, that are defined by the architecture, and global packing constraints imposed by their volume fraction.¹ The packing characteristics are described in terms of the local curvature at the hydrophobic-hydrophilic layer interface, which is expressed in terms of the critical packing parameter (CPP).^{1,2}

Fluorinated surfactants are amphiphiles with fluorine instead of hydrogen atoms attached to the hydrophobic tails. The insertion of strongly electronegative fluorine atoms considerably affects their physical and chemical properties. For example, fluorinated surfactants are thermally and chemically more stable than hydrocarbon surfactants. Since fluorine atoms are bigger than hydrogen atoms, fluorinated surfactants are bulkier and stiffer compared to hydrogenated ones. This fact induces all-trans conformations in fully fluorinated tails.³ Thus fluorinated surfactants display quite different packing behavior from their hydrogenated counterparts.⁴ Furthermore, fluorocarbons display weak Van der Waals interactions that lead to weaker intermolecular cohesive forces and enhanced hydrophobicity compared to the hydrogenated analogs.^{2,5,6} Because of these reasons, their physical properties like phase behavior, lyotropic LC phase morphology and rheology, are drastically modified.²

The LLC phase behavior of fluorinated surfactants and hybrid surfactants with fluorocarbon and hydrocarbon tails has not been studied as extensively as that of hydrocarbon based surfactants. From a fundamental point of view it is interesting to study the differences in phase behavior between fluorinated and hydrogenated surfactants with similar molecular structures, and to investigate the effect of fluorinated structure in the hydrophobic tail on the LLC phase behavior and morphology.

The LLC phase behaviour of ionic^{2,7,8,9,10}, nonionic^{11,12} fluorinated surfactants, and hybrid fluorocarbon-hydrocarbon surfactants,^{13,14,15} have been investigated.

Tetraalkyl ammonium as well as inorganic metal salts of perfluorinated carboxylic acids have been studied in detail,⁷ and generally phase diagrams of these compounds exhibit lamellar (L_α), normal hexagonal (H_1) and reverse hexagonal (H_2) mesophases. An additional complex hexagonal (H_C) phase in the binary lithium perfluorooctanoate-water system,⁹ was reported by Tiddy and coworkers. This phase was made of surfactant bilayers arranged into hollow pipes that assembled in hexagonal symmetry. For the tetramethyl ammonium perfluorodecanoate-water system,³ a novel rhombohedral intermediate mesh (Mh_1) phase¹⁶ was reported by Holmes and coworkers. Similarly, cubic bicontinuous (V) mesophases, which are rarely found in hydrogenated systems,¹⁰ have been reported for sodium and ammonium salts of homologous perfluoroether carboxylic acid surfactants.

The phase behavior of fluoroalkyl sulfonate surfactants is not extensively reported upon, which may be due to their poor solubility in water at ambient temperature.¹⁷ One of the few explored systems is lithium perfluorooctane sulfonate (LiFOS)-water.¹⁸ This system exhibits lamellar (L_α), hexagonal (H_1) and bicontinuous (V) phases, and a phase diagram that is qualitatively similar to that of lithium dodecyl sulfate (LiDS).

Hybrid surfactants, containing a hydrophilic, a hydrocarbon and a fluorocarbon segment generally exhibit a more complex phase behavior. This is due to the fact that the three phases have a tendency to separate. Surfactant systems like the star polyphile, reported by Hyde et al,¹⁴ display a tilted hexagonal phase, in which the fluorocarbon and hydrocarbon chains are phase separated within the hydrophobic domains. Interestingly, a hybrid phospholipid¹⁹ and a zwitterionic hybrid surfactant²⁰ have been reported to form nano- and microtubules by wrapping up of 2-3 bilayers. However these multilayer assemblies are formed at low concentrations, 3 and 6wt % respectively.²¹

Here we report on the phase behavior of sodium 1,1,2,2-tetrafluoro-2-(1,1,2,2-tetrafluoro-2-(4-ethylphenyl)ethoxy)ethanesulfonate (Figure 5.1), a sulfonated hybrid fluorosurfactant (**2**) designed in our laboratory.²² This compound has an unusual topology, with the sulfonate head group attached to a short perfluoroether group, which is attached to an ethylbenzene moiety at the other side.

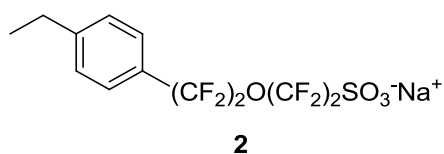


Figure 5.1. Molecular structures of **2**, sodium [1,1,2,2-tetrafluoro-2-(1,1,2,2-tetrafluoro-2-(4-ethylphenyl)ethoxy)ethanesulfonate].

Compound **2** is highly water-soluble at room temperature and forms an unprecedented columnar LLC phase composed of “leek” like supramolecular aggregates, which are composed of multiple bilayers of **2**. To the best of our knowledge this is the first LLC phase composed of multi lamellar supramolecular entities. Apart from this supramolecular phase composed of multi-walled leeks, we have also identified a conventional lamellar (L_a) phase at higher surfactant concentrations. The phase behavior of **2** in water has been investigated using optical polarized light microscopy (OPM), small angle X-ray scattering (SAXS), ^2H NMR and freeze-fracture transmission electron microscopy (FF-TEM) and cryogenic scanning electron microscopy (cryo-SEM).

5.2 Experimental

5.2.1 Materials and Methods

The synthesis of sodium 1,1,2,2-tetrafluoro-2-(1,1,2,2-tetrafluoro-2-(4-ethylphenyl)ethoxy)ethanesulfonate (**2**) has been described elsewhere.²² The density of **2**, which is required to estimate various parameters from X-ray diffraction data, was determined by taking a known mass of the dry powder in dichloromethane (a nonsolvent) into a five ml measuring cylinder and by measuring the increase in the dichloromethane volume. It was found to be 1.66 g/cm³. All the samples were prepared in deionized (miliQ) water and airtight screw cap vials. They were heated, vortexed several times and visually inspected to be homogenous before thermal equilibration from three hours to three days. The vials were weighed before and after the heat treatment as well as after storage to ensure there is no mass loss due to water evaporation.

A Nikon Eclipse E600 optical polarized microscope equipped with a Leica tilting compensator was used to observe the thermally equilibrated **2**-water mixtures. ²H NMR spectra were recorded on Varian INOVA-300 spectrometer operating at 46.06 MHz with a typical spectral width of 100 kHz, acquisition time of 525 ms and a pulse width of 10 μ s. Samples were prepared by weighing desired quantities of **2** and D₂O directly in 5 mm NMR tubes, which were tightly closed and homogenized by several heating and vortexing cycles. The weights of the NMR tubes were verified before and after homogenization to monitor a possible loss of D₂O (typically below 0.001%). The samples were allowed to equilibrate at room temperature for at least three days. Measurements were done at 25 °C.

For SAXS, equilibrated **2**-water mixtures in 0.7 mm flame sealed capillaries were examined in a Bruker AXS D8 Discover X-ray diffractometer with a Hi-Star 2D detector using Cu K α source wavelength (1.54 Å). The incident beam was filtered by cross-coupled Göbel mirrors at 40 kV and 40 mA. The sample to detector distance was set at 30 cm. For freeze fracture electron microscopy (FFEM), a small sample drop was placed between two copper grids and inserted into gold planchettes. The “sandwich” was equilibrated in the controlled-environment vitrification system (CEVS) at 25 °C, then vitrified in liquid ethane and transferred into the BAF-060 replication system (BAL-TEC AG, Liechtenstein). In the BAF the sandwich was opened and the

fractured surfaces were coated with a platinum and carbon. The planchettes were thawed outside the BAF and the replicas were cleaned, then examined in a Tecnai 12 G² TEM at room temperature. Images were recorded on an Ultrascan 1000 2k x 2k sensitive CCD camera at nominal magnifications of up to 50k.²³

5.3 Results and discussion

The aggregation behavior of **2** at low concentration has been described elsewhere.²⁴ It is worth mentioning that **2** is highly soluble in water at room temperature, and spherical micelles of around 3 nm size start forming at 4 wt% **2**.

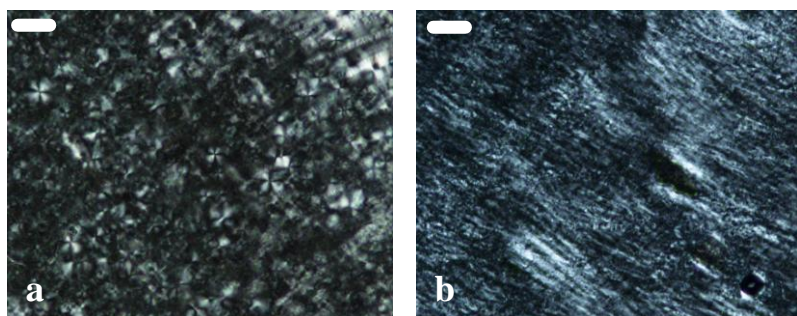


Figure 5.2. Representative OPM pictures of the lyotropic mesophases, at 25 °C. a) 66 wt% **2** (Phase I) and b) 76 wt% **2** (Phase II). Scale bar is 50 μ .

The **2**-water phase diagram was explored by first examining the optical texture of a range of samples by OPM. This was useful to identify lyotropic phases by their characteristic optical textures, and determine the phase boundaries. Samples at [**2**] below 63 wt% did not show birefringence implying that they exhibit an isotropic micellar phase (L_1). A mosaic texture with the presence of a few maltese-crosses was observed at [**2**] between 63 and 70 wt% (**Phase I**, Figure 5.2a). This optical texture is similar to the pattern observed by Monduzzi and coworkers for a lyotropic phase with multilamellar vesicles.¹⁰ The small features in the micrograph suggest that this LLC phase is composed of small domains. Above 70 wt% **2**, a tightly packed streaky pattern, which is characteristic for lamellar phase, was observed, (**Phase II**, Figure 5.2b).^{10,25} Also, the viscosity of **Phase II** was higher compared to that of **Phase I** samples. Thus, two LLC phases were identified by OPM, **Phase I**

between 63 and 70 wt% **2**, and **Phase II** at [**2**] between 70 to 84 wt%. Beyond 84 wt%, solid particles of surfactant and birefringent structures were observed. Contact samples, in which a concentration gradient is present within the sample, were taken in order to check for additional mesophases. In particular we were interested in bicontinuous mesophases, which may exist in narrow concentration windows and are isotropic. None were found, so we are quite confident that only two LLC phases exist for the system.

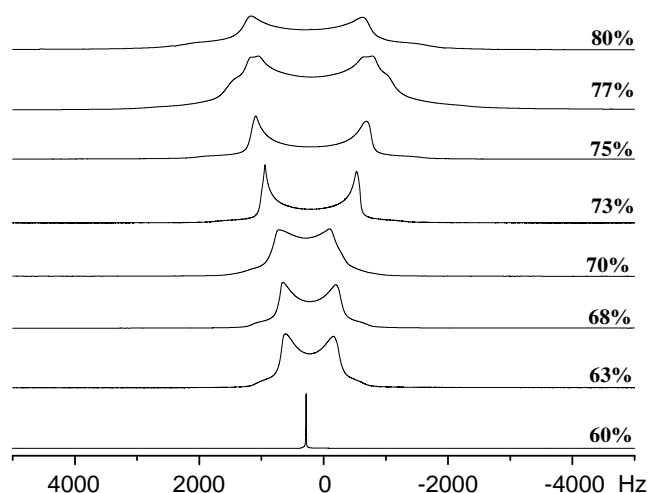


Figure 5.3. ^2H NMR spectra of aqueous **2** samples at surfactant concentrations ranging from 60 wt% to 80 wt%, at 30 °C.

^2H NMR measurements were performed to identify LLC phases and provide additional information regarding their structures. The shape of the ^2H NMR spectra is indicative of the alignment of water molecules embedded inside the LLC phases whereas the quadrupole splitting of the deuterium signal ($\Delta\nu_q$) from the D_2O in them quantifies the extent of the anisotropy present. In anisotropic liquid crystalline samples, the deuterium signal splits into $2I$ lines (where I is nuclear spin quantum number) separated by the splitting $\Delta\nu_q$, as given by Equation 5.1.^{26,27}

$$\Delta\nu_q = \frac{3}{4} C_q (3\cos^2\theta - 1) \quad 5.1$$

In Eq. 5.1, θ is the angle between the external magnetic field and the averaged electric field gradient, which is parallel to the director of the phase, and C_q is the averaged quadrupole coupling constant equal to e^2qQ/\hbar (e is the absolute value of the electron charge, q is the electric field gradient, Q is the nuclear quadrupole moment, and \hbar is the Planck constant). In isotropic liquids such as micellar solutions

or bicontinuous cubic phases, θ changes very fast due to molecular motion. As a result, quadrupolar interactions are averaged to zero and a single peak is observed.²⁸

^2H NMR spectra of **2**-water mixtures, with [**2**] between 60 and 80 wt%, are shown in Figure 5.3.²⁹ At surfactant concentrations <60 wt% no splitting is observed, which implies the presence of isotropic micellar (L_1) phase (Figure 5.3). In contrast, at higher surfactant concentrations a symmetric doublet with a quadrupolar splitting $\Delta\nu_q$ is observed, indicative for the presence of liquid crystalline phases. The shapes of the peaks are typical to a powder or “Pake” pattern⁷ and the line broadening can be ascribed to the presence of small-sized domains in **phase I**,³⁰ which have been observed by optical microscopy and presence of non aligned samples for the whole LLC regime.

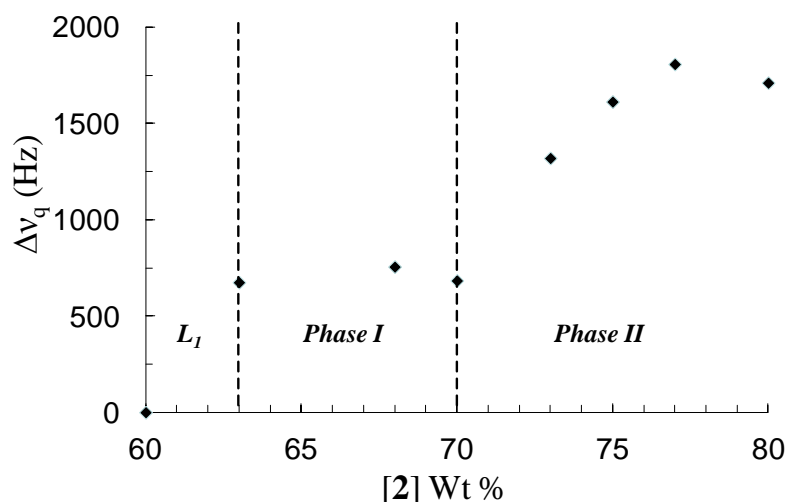


Figure 5.4. Quadruple splitting vs. **2** content (in wt%). Dotted line represents the **Phase I** to **Phase II** transition.

In Figure 5.4, $\Delta\nu_q$ values are plotted against [**2**]. $\Delta\nu_q$ values of **Phase I** samples remain constant at around 700 Hz. Upon the formation of **Phase II**, $\Delta\nu_q$ values double (around 1300 Hz at [**2**] 73 wt%) and increase linearly up to ~1800 Hz at [**2**], 77 wt% and slightly decreases to ~1700 Hz at [**2**] 80 wt%.³¹ Thus, $\Delta\nu_q$ values in **Phase II** increase more than two times from the values in **Phase I** samples, which may indicate that the water molecules in **Phase I** are confined in cylindrical geometry (See part B of Appendix) whereas **Phase II** has planar geometry.

Thus, ^2H NMR confirms that surfactant solutions are isotropic micellar below a concentration of 63% and form two anisotropic phases, **Phase I** and **II** from 63 to 70 wt% and from 70 to 80 wt%, respectively. The values from both phases suggest that **Phase I** has cylindrical geometry while **Phase II** has planar morphology.

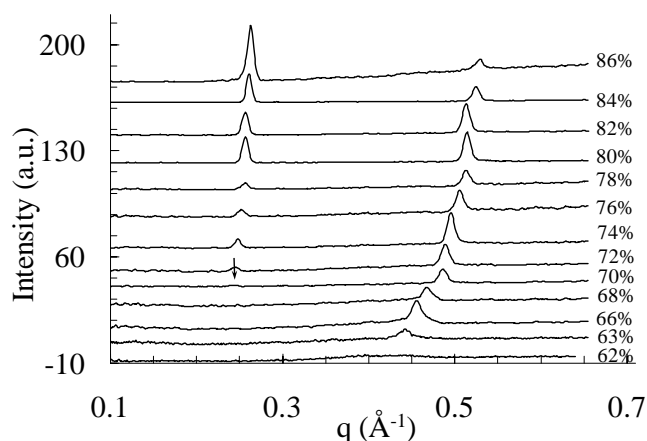


Figure 5.5. SAXS patterns for different aqueous **2** solutions at 30 °C. Intensity is shown in arbitrary units. q is the wave vector. The arrow at 0.24 \AA^{-1} for the 70 wt% **2** sample indicates the weak first order reflection.

X-ray data provides geometrical parameters of the mesophases, originating from repeating layers composed of water and surfactant molecules. Diffraction patterns of **2**-water mixtures measured by SAXS are shown in Figure 5.5. No significant diffraction peaks were observed below 60 wt%.

In **Phase I**, between 63 and 70 wt% [**2**], a single Bragg reflection was observed at q -values between 0.44 and 0.48 \AA^{-1} . The q -value increases with [**2**], which indicates a decrease of characteristic distances.

In **Phase II**, at [**2**] larger than 70 wt%, a weak reflection at a q -value of $\sim 0.24 \text{ \AA}^{-1}$ started appearing along-with the reflection at $\sim 0.48 \text{ \AA}^{-1}$ that was already detected in **phase I**. The Bragg peak at 0.24 \AA^{-1} steadily shifted towards higher q values (from 0.24 \AA^{-1} to 0.26 \AA^{-1}) with increase in [**2**]. Under all conditions the high q -value was exactly twice that of the low q -value. Further, the intensity of the weak reflection at $\sim 0.24 \text{ \AA}^{-1}$ steadily increased whereas that of the $\sim 0.48 \text{ \AA}^{-1}$ reflection decreased with increase in [**2**]. The intensity of both reflections became similar at 80 wt% [**2**].

The change in the SAXS diffraction in **Phase II**, notable with the appearance of an additional reflection at 0.24 \AA^{-1} , coincides with the change in the optical texture in OPM and change in Δv_q values from the ^2H NMR measurements.

The characteristic SAXS diffraction pattern with 1:1/2 reflections is indicative for the presence of a L_α phase between 70 and 84 wt.% [2]. The typical streaky OPM patterns and Δv_q values higher than those from the samples in **Phase I**, further support this assignment. The absence of Bragg reflections at lower q , in **Phase I**, and modulation in the relative intensities of both peaks in **Phase II** are attributed to the disappearing form factor at q^* due to infinitely long oriented bilayers.^{32,33} Similar effects were observed in AOT-water lyotropic phases.³³

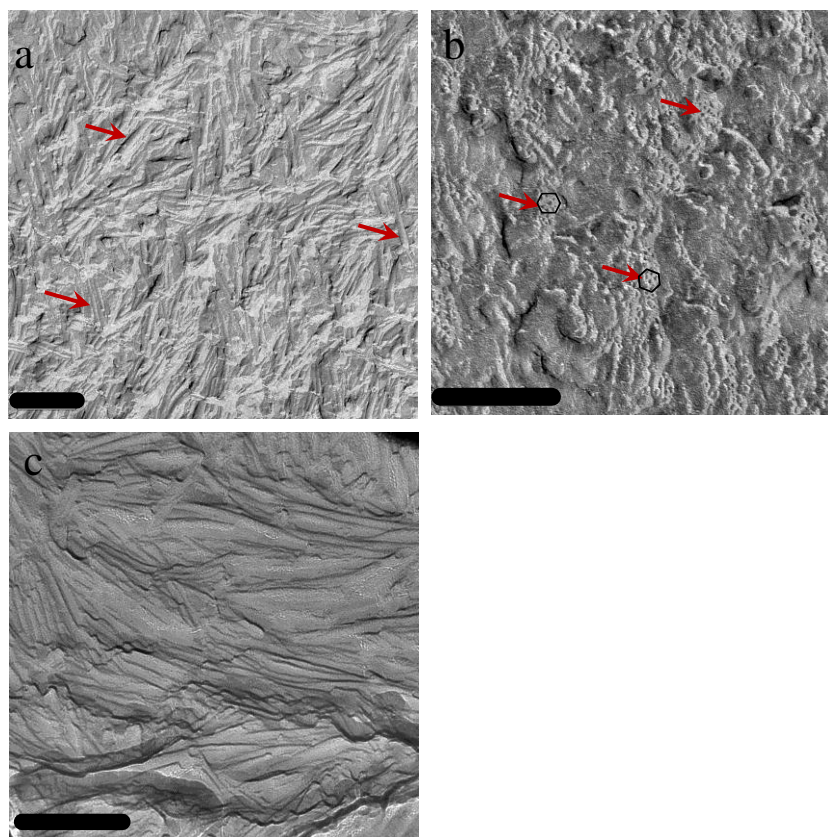


Figure 5.6. FFEM pictures of (a) and (b) 70 wt%, and (c) 77 wt% **2** showing the morphology of LLC phases. Scale bars 200 nm. Arrows indicate the “Leek” shaped aggregates.

LLC morphologies of **2**-water mixtures were also investigated by FF-TEM. This complementary technique is useful to obtain direct information on the 3-D structure, and the dimensions of the aggregates building up the LLC phases. The freeze fracture image in Figure 5.6a reveals a complex morphology of rod-like structures, with diameters between 10-20 nm and lengths exceeding 100 nm (**Phase I** sample, 70 wt% **2**). On a local scale the rods are clearly oriented. A top view of these aggregates is shown in Figure 5.6b. The rod-like aggregates seems to be clustered

in stacks of 8 to 10 rods and organized into domains with hexagonal symmetry (Figure 5.6b, marked by arrows and hexagons). However, the domains are small and long-range positional order among individual rods is absent.

Figure 5.6c shows a distinct morphology with flat layers in the **Phase II** sample at 77 wt % **[2]**. The layered morphology clearly points to the presence of a lamellar L_α phase, which is in accordance with the data provided by the other techniques.

At this stage it is clear that **Phase II** is a lamellar phase and that **Phase I** is a columnar phase in which the columnar aggregates are heterogeneous in diameter and larger than the expected worm-like micelles.

The efforts to do ultra low-angle X-ray scattering did not reveal scattering originating from the lateral ordering of the columnar aggregates in the relevant size domain of 10-50 nm. This implies the absence of long-range order in the lateral direction. Presumably the variations in the thickness of the rods,³⁴ which are observed in Figure 5.6a and 5.6b, prevents long-range positional ordering in the lateral direction. The lateral dimensions of the columnar aggregates indicate that these must be multi-walled, leek-like aggregates. As these aggregates are heterogeneous in size, the number of surfactant layers must be different for the individual aggregates. The X-ray scattering that was observed for **Phase I** originates from the internal structure of the multi-walled aggregates and not from their positional ordering.

Here, it is noteworthy that the Δv_q values obtained from ^2H NMR of **Phase I** samples are slightly less than half to those from **Phase II** (lamellar phase) samples which suggest that the surrounding of the D_2O molecules has cylindrical geometry⁷ in **Phase I** (Please see the part B in Appendix). Typically such a change in Δv_q values occurs during hexagonal to lamellar phase transitions. In our case, from SAXS and FFEM, it is clear that **Phase I** is not a hexagonal phase but a phase with leek-like supramolecular cylindrical aggregates whereas, **phase II** is lamellar (L_α) phase.

A detailed analysis of the surfactant layer thickness (L_s) and the water layer thickness (L_w) with increasing water fraction was conducted for **Phase I** and **Phase II**, based on the SAXS data, as described by Equations 5.2 and 5.3.^{35,36} In Equation 5.2, Φ_2 is the weight fraction of **2**, ρ_w and ρ_2 are water and **2** densities, and d_{001} is the first order reflection representing the bilayer thickness, respectively.

$$L_s = \frac{\Phi_2 d_{001} \rho_W}{\rho_2 (1 - \Phi_2) + \rho_W \Phi_2} \quad 5.2$$

$$L_w = d_{001} - L_s \quad 5.3$$

Similarly, the effective interfacial area per head group (A_2) can be calculated using Equation 5.4.

$$A_2 = \frac{2(V_2 + \alpha V_W)}{d_{001} N_A} \quad 5.4$$

In Equation 5.4, V_2 and V_W are molar volumes of the **2** and water molecules, α is the molar ratio of water molecules to **2** molecules, and N_A is Avogadro's number.

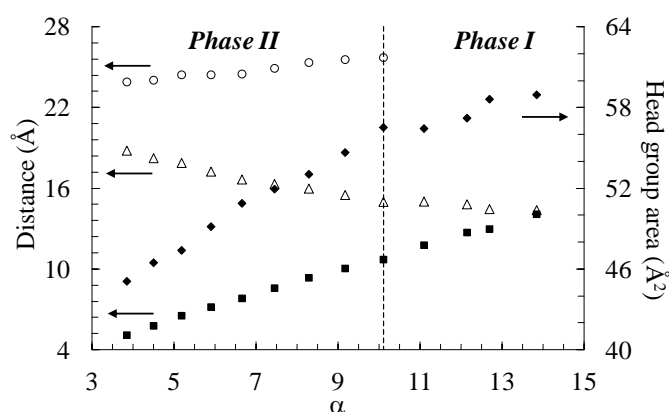


Figure 5.7. Plot of the first order Bragg's reflection (o), hydrophobic layer thickness, L_s (Δ), water layer thickness, L_w (\blacksquare), and area per head group of **2**, A_2 (\blacklozenge), normalized to the number of water molecules per surfactant molecule (α). The dotted line represents the boundary between supramolecular columnar (C_s) and lamellar (L_a) phases. Values of L_s , L_w and A_2 above $\alpha = 10$ were calculated by assuming that the invisible first order reflection (d_{001}) is exactly at half the second order reflection (d_{002}).

The results are compiled in Figures 5.7 and 5.8. Plots of d , L_s and L_w (the primary Y axis) against α are shown in Figure 5.7. On the right Y axis, A_2 has been plotted against α .

The values of d_{001} throughout the whole phase diagram range from 23.9 to 28.5 Å. These values are close to twice the length of an extended **2** molecule (~ 29 Å), which

is indicative of bilayer structures in both phases. In **Phase II**, d_{001} lies between 23.6 and 25.7 Å, and in **Phase I** between 26.8 and 28.5 Å.³⁷

The data in Figure 5.8 clearly shows that the bilayer structure does not change significantly upon the transition from **phase I** to **Phase II**. The values of L_s are lower than twice the length of the extended hydrophobic tails of **2** (~22.0 Å), which suggest that the hydrophobic tails are partially interdigitated (Figure 5.8c) or tilted (Figure 5.8b), or both (Figure 5.8d). Interdigitation of the surfactant tails is expected if we assume that the hydrocarbon and fluorocarbon phase separate, *vide infra*.

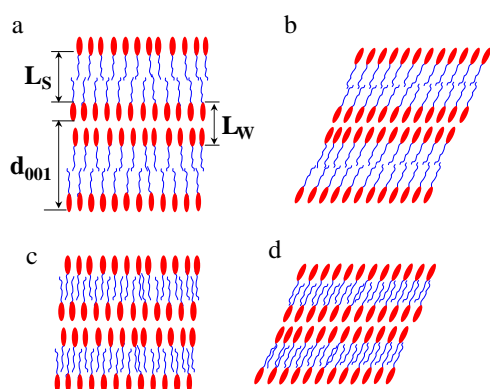


Figure 5.8. Possible arrangements for the surfactant bilayers. a) normal arrangement, b) tilted bilayers, c) interdigitated assembly of the surfactant molecules, and d) tilted + interdigitated self-assembly. L_s represents the hydrophobic layer thickness, L_w the water layer thickness (including the **2** head groups) and d_{001} is the first order Bragg reflection from the phase.

Throughout the phase diagram, L_s decreases (from 18.8 to 15.0 Å) with increasing α , whereas, L_w increases (from 5.1 to 14.0 Å). The effective interfacial area per head group, A_2 increases (from 45.1 to 59.0 Å²) with α . A larger interdigitation and/or tilting of the hydrophobic chains were observed in **Phase I** than in **Phase II**. With increase in the water concentration, a significant increase in A_2 is seen with α , unlike in nonionic surfactants.¹¹ This can be attributed to the increased electrostatic repulsion felt by the polar head groups of neighbouring **2** molecules with decreasing water concentration. The values of A_2 are closer to those reported for LLC phases of ammonium perfluorooctanoate.³⁵ The increase in d_{001} with α is not linear (not shown here). This suggests reorganization of the **2** molecules with increasing the water content.³⁸

To the best of our knowledge, columnar lyotropic phases that are composed of multi-walled leek-like aggregates have not been previously reported. Interestingly, a hybrid phospholipid¹⁹ has been reported to form micro and nanotubules with cigar like arrangements of bilayers with thickness of three bilayers. Interdigitation or tilting were observed within submicron sized tubules that were formed in 3 wt% perfluoroalkylated glucophospholipid-water mixtures. Similar nanotubules have been observed in water solutions of a zwitterionic hybrid surfactant at 6 wt%.²⁰ These multilayer assemblies, however, are formed at low concentrations. Another hybrid surfactant, the star polyphile, reported by Hyde et al,¹⁴ displays a tilted hexagonal phase, in which the fluorocarbon and hydrocarbon chains are phase separated within the hydrophobic domains.

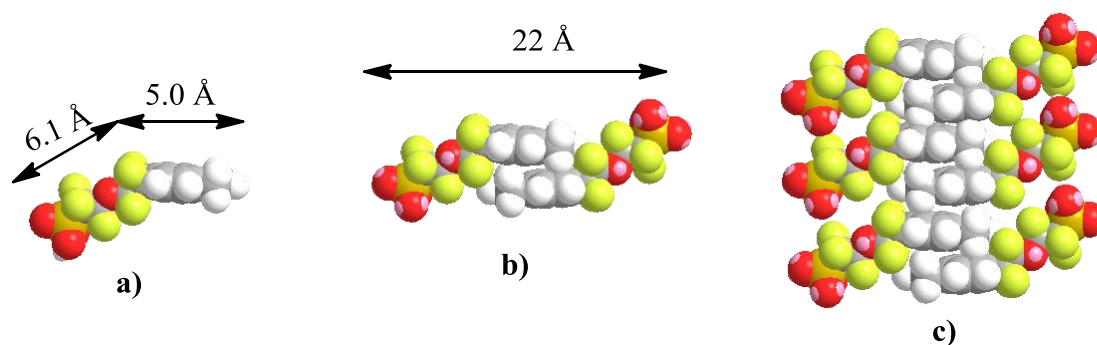


Figure 5.9. Molecular structures of **a)** individual **2** molecule in 3D. **9b)** interdigitated and tilted arrangements of two **2** molecules and **c)** **2** molecules in a bilayer. (Yellow and red balls represent fluorocarbon part with sulfonate group)

Based on these observations, we postulate that phase separation within the hydrophobic domains of **2** induces interdigitation and thereby reduces the layer thickness. The molecular structure of fully extended **2**, which consists of an extensive and rigid fluorocarbon part and a slim hydrocarbon part, is depicted in Figure 5.9a. The length of the fluorocarbon and the hydrocarbon blocks are 6.1 and 5.0 Å, respectively, and the angle between them is $\sim 120^\circ$.

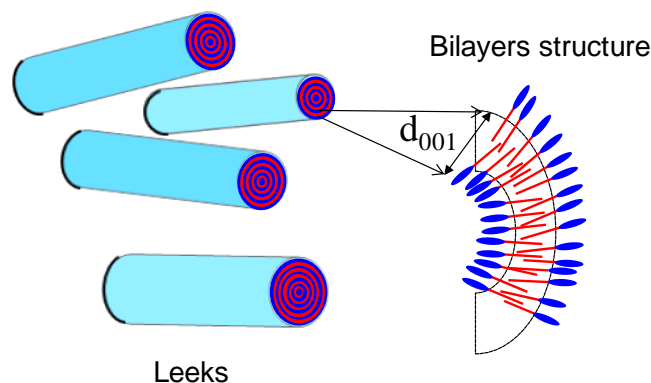


Figure 5.10. Schematic representation of the Leeks. The Leeks are made up wrapping up of 3-4 bilayers with the bilayers structure as depicted in the figure.

The fluorocarbon and the hydrocarbon blocks like to phase separate and the resulting interdigitated bilayer structure is presented in Figure 5.9b. The bilayer thickness is around 22 Å, but this thickness may be reduced further, by increasing the angle between the hydrocarbon and the fluorocarbon chains.

Leek-like aggregates are formed by wrapping these bilayers around each-other, as shown schematically in Figure 5.10. Assuming that the interior of the leeks are worm-like micelles of 3 nm diameter and that the thickness of the bilayers are 28 Å, leeks with 3, 4 and 5 bilayers, with diameters of 11.5, 17 and 23 nm, respectively, may be present.³⁹ Because the leeks are rigid and have decent persistence lengths, it is likely that the self-assembly of surfactant molecules into leek-like aggregates has induced the formation of an LLC phase state.

Thus, the “Leeks” self-organize in a supramolecular columnar phase (C_S) as seen in FFEM pictures (Figure 5.6b). The supramolecular self-assembly has rarely been observed in surfactants in the lyotropic phase regime.

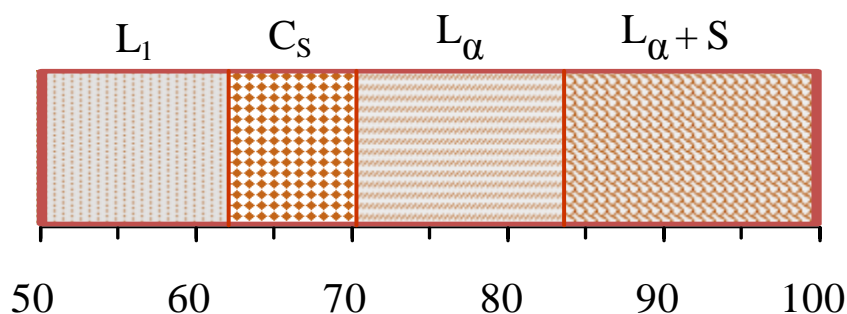


Figure 5.11. Schematic phase diagram of aqueous **2** samples at 30 °C. The marked phases are micellar (L_1), supramolecular columnar (C_S), lamellar (L_α) and lamellar + solid particles ($L_\alpha + S$).

A schematic phase diagram for the **2**-water binary system at 30 °C is shown in Figure 5.11. Above the critical micelle concentration, at around 4 wt%, the **2**-water mixture displays an isotropic micellar phase (L_1) up to a concentration of 60-63 wt%. Between 63 and 70 wt% (**Phase I**), a supramolecular columnar C_S phase is formed and from 70 up to 84 wt% (**Phase II**) a lamellar L_α phase was observed. Above this composition, a biphasic region with **2** crystals along with the L_α phase was present. The C_S phase is characterized by a mosaic texture with maltese crosses in OPM, and lower Δv_q values than in the L_α phase from ^2H NMR results. Similarly it shows the presence of only a second order reflection peak in SAXS study and “Leek” shaped aggregates in FFEM experiments. The L_α phase is characterized by a tight streaky pattern in OPM and more than twice the Δv_q values of the C_S phase. Also it shows the characteristic 1:1/2 SAXS peak pattern and a distinct layered morphology in FFEM investigations.

The phase behaviour study of polymerizable fluorosurfactant **1** at in lyotropic regime could not be carried out because it has somewhat lower solubility at room temperature compared to compound **2**. Although it shows the lyotropic characteristics at elevated temperatures (>50 °C), at such high concentration it undergoes polymerization which could rapidly change the phase properties. For example, it was not possible to make homogenous mixtures of fluorosurfactant **1** and water in X-ray capillaries. Similarly, ^2H NMR results for **1**-water mixtures were not reproducible.

5.4 Conclusions

This chapter reports on the phase behavior of **2**-water mixture at high **2** concentrations. Below 63 wt% **2** isotropic micellar solutions exist. Between 63 to 84 wt% [**2**] two phases are found. An unusual supramolecular columnar (C_S) phase made up by self-assembly of “Leek” shaped aggregates was observed between 63 and 70 wt% [**2**]. Those “Leeks” were shown to be formed by wrapping up of the **2**-water bilayers. Surprisingly, **2** molecules were arranged into partially interdigitated or

tilted or both fashions, and not organized in the ‘usual’ tail-to-tail and head-to-head manner. A lamellar (L_α) phase was observed from 70 to 84 wt% [2], with somewhat decreased interdigitation or tilting of the hydrophobic chains of **2** molecules. Above 84 wt%, a biphasic region with surfactant crystals dispersed in a lamellar phase was observed.

5.5 Appendix

A) Calculation of geometrical parameter from X-ray diffraction data.

From Figure 5.8 and Equation 5.3,

$$d_{001} = L_s + L_w \quad (5A.1)$$

To calculate hydrophobic layer thickness L_s and hydrophilic thickness layer L_w , for bilayers in the Leeks and lamellar phase, **2** molecules are assumed to attain cylindrical shape. Thus, the weight fraction of **2**, (Φ_2) can be given as,

$$\Phi_2 = \frac{L_s \cdot \rho_2}{L_s \cdot \rho_2 + L_w \cdot \rho_w} \quad (5A.2)$$

Where, ρ_2 and ρ_{H_2O} are the densities of **2** and water molecules respectively.

Further, L_s can be rewritten as described by equation 5.2 and the head group area of **2** simply can be determined by dividing the volume occupied by a cylindrical unit of the bilayers by the length of the cylinder i.e. d_{001} as described by equation 5.4.

B) Calculation of maximum and minimum $\Delta\nu_q$ values from *Phase I* with leeks and *Phase II* with the lamellar sheets.

The quadruple spin spin splitting $\Delta\nu_q$ is given by,⁴⁰

$$\Delta\nu_q = p \cdot C_q \cdot \langle S \rangle \quad (5A.3)$$

Where p is the fraction of water molecules bound to polar head group of **2**, C_q is averaged quadruple coupling constant and $\langle S \rangle$ is averaged orientational order parameter of water molecules. p does not change a lot within the LLC regime.

a) For *Phase I* with Leeks,

The averaged orientational order parameter $\langle S \rangle$ of water molecules of LLC phases arranged at an angle θ to the director of the applied magnetic field (generated by NMR machine) H_o is given by,

$$\langle S \rangle = \frac{1}{2}(3\cos^2 \theta - 1) \quad (5A.4)$$

For the Leeks that are arranged \perp to H_o , the averaged orientation of individual water molecules is isotropic over the circular cross section of the Leeks. $\langle S \rangle$ can be given by

$$\langle S \rangle = \pm \frac{1}{2\pi} \int_0^{2\pi} S d\theta = \pm \frac{1}{2\pi} \left[\frac{1}{2}(3\cos^2 \theta - 1) \right]_0^{2\pi} = \pm \frac{1}{4} \quad (5A.5)$$

For Leeks arranged in \parallel to the magnetic field, $\langle S \rangle$ is \perp to H_o .

$$\langle S \rangle = \pm \frac{1}{2}(3\cos^2 \frac{\pi}{2} - 1) = \pm \frac{1}{2} \quad (5A.6)$$

Thus, the maximum value of quadruple splitting for ***Phase I*** is $\pm \frac{1}{2}.C_q$ and minimum of $\pm \frac{1}{4}.C_q$.

b) For *Phase II* with Lamellar sheets

For the lamellar sheets arranged \perp to H_o , the orientation of individual water molecules with H_o is \parallel .

$$\text{Thus, } \langle S \rangle = \pm \frac{1}{2}(3\cos^2 \pi - 1) = \pm 1 \quad (5A.7)$$

For the lamellar sheets arranged \parallel to H_0 , the orientation of individual water molecules is \perp .

So we can write

$$\langle S \rangle = \pm \frac{1}{2} (3 \cos^2 \frac{\pi}{2} - 1) = \pm \frac{1}{2} \quad (5A.8)$$

The maximum value of quadruple splitting for **Phase II** is $\pm 1.C_q$ and minimum is

$$\pm \frac{1}{2}.C_q.$$

5.6 References and notes

- (1) Isrealachevili, J. N. *Intermolecular and Surface Forces*, Academic Press, Ed. 2, New York, 1998, pp 390-391.
- (2) Monduzzi, M. *Curr. Opin. Colloid Interface Sci.* **1998**, 3, 467-477.
- (3) Puntambekar, S.; Holmes, M. C.; Leaver, M. S. *Liquid Crystals* **2000**, 27(6), 743-747.
- (4) V. Percec, M. Glodde, G. Johansson, V. S. K. Balagurusamy, P. A. Heiney, *Angew. Chem. Int. Ed.* 2003, 42, 4338 - 4342.
- (5) Alfredo, G.-P.; Juan M. R.; Gerardo P.; Félix S. J. *Surf. & Det.* 2004, 7 (4), 387-395.
- (6) Kissa, E. *Fluorinated Surfactants and Repellents*, Marcel Dekker, New York **2001**, Chapters 1-2.
- (7) Wang, K.; Orädd, G.; Almgren, M.; Asakawa, T.; Bergenståhl B. *Langmuir* **2000**, 16, 1042-1049.
- (8) Fontell, K.; Lndman B. *J. Phys. Chem.* **1983**, 87, 3289-3297.
- (9) Everiss, E.; Tiddy, G. J. T.; Wheeler, B. A. *J. Chem. Soc., Faraday Trans. 1* **1976**, 72, 1747-1758.
- (10) Mele, S.; Barry, W. N.; Monduzzi, M. *J. Phys. Chem. B* **2004**, 108, 17751-17759.
- (11) Ropers, M.- H.; Stebe, M.- J. *Phys. Chem. Chem. Phys.* **2001**, 3, 4029-4036.
- (12) Ropers, M.- H.; Stebe, M.- J.; Schmitt, V. *J. Phys. Chem. B* **1999**, 103, 3468-3475.
- (13) Sagisaka, M.; Fujita, Y.; Shimizu, Y.; Osanai, C.; Yoshizawa, A. *J. Colloid Interf. Sci.* 2011, 357, 400–406.
- (14) de Campo, L.; Varslot, T.; Moghaddam, M. J.; Kirkensgaard, J. J. K.; Mortensen, K.; Hyde S.T. *Phys. Chem. Chem. Phys.* **2011**, 13, 3139–3152.
- (15) Maybe insert Oda, R. et al *Langmuir* **2000**, 16, 9759-9769. Not in low C regime. Does however form multi-walled structures Regev, O. et al *Langmuir* **2001**, 17, 5141-5149. May be interesting, includes LLC phases
- (16) Additional phases found between hexagonal and lamellar phases in two component surfactant-water systems have been termed as “intermediate” phases. Leigh, I. D.; McDonald, M. P.; W d , R. M.; Tiddy, G. J. T.; Trevethan, M. A . *J. Chem. Soc., Faraday Trans. 1* **1981**, 77, 2867-2876.
- (17) Shinoda, K.; Hat, M.; Hayashi, T. *J. Phys. Chem. B* **1972**, (76)6, 909-914.
- (18) Tamori, K.; Esumi, K.; Meguro, K. *J. Colloid Interf. Sci.*, **1991**, 142(1), 236-243.
- (19) Imae, T.; Funayama, K.; Krafft, M. P.; Giulieri, F.; Tada, T.; Matsumoto, T. *J. Colloid Interf. Sci.* **1999**, 212, 330–337.
- (20) Giulieri, F.G.; Krafft, M.- P. Riess, J. G. *Angew. Chem. Int. Ed.* **1994**, 33(14), 1514-1515.
- (21) The LLC phases of this fluorinated glycolipid have not been reported as of now.

- (22) Wadekar, M. N. ; Jager, W. F.; Sudhölter, E. J. R.; Picken S. J. *J. Org. Chem.* **2010**, 75, 6814–6819. FS serves as a model fluorosurfactant which is similar in molecular structure to that of a polymerizable fluorinated surfactant (**1**) depicted in previous chapters. **1** can be polymerized to generate a membrane used for proton transportation in fuel cells. So by a two step bottom-up approach, we first intend to investigate various mesophases of **2**-water system and then exploit the know-how obtained from the phase behavior and morphologies of it to create self-assembled nanostructured membranes by polymerizing the desired mesophases of PFS-water system.
- (23) Danino, D.; Bernheim-Groswasser, A.; Talmon, Y. *Coll. Surf. A-Physicochem. Eng. Aspects*, **2001**, 183, 113–122.
- (24) Wadekar, M. N.; Boekhoven, J.; Jager, W. F.; Koper, G. J. M.; Picken S. J. *Langmuir* **2012**, 28, 3397–3402.
- (25) Kunieda, H.; Shigeta, K.; Ozaw, K. *J. Phys. Chem. B* **1997**, 101(40), 7952–7957.
- (26) Blackburn, J. C. ; Kilpatrick P. K. *J. Colloid Interf. Sci.* 1992 149(2), 450–471.
- (27) Ghosh, S. K.; Rathee, V.; Krishnaswamy, R.; Raghunathan, V. A. Sood, A. K. *Langmuir* **2009**, 25, 8497–8506.
- (28) Sjöbom, M. B.; Edlund, H.; Lindström, B. *Langmuir* **1999**, 15, 2654–2660.
- (29) It was difficult to prepare homogenous samples inside the NMR tubes above 80 wt%.
- (30) Smith, A. M.; Holmes, M. C.; Pitt, A.; Harrison, W.; Tiddy, G. J. T. *Langmuir* **1995**, 11, 4202–4204.
- (31) Usually, Δv_q values increase with increase in surfactant concentration through anisotropic-anisotropic LLC phase transition, within the whole phase diagram.
- (32) Ropers, M. -H.; Stèbè M. -J.; Schmitt, V. *J. Phys. Chem. B* **1999**, 103(17), 3468–3475.
- (33) Nallet, F.; Laversanne, R.; Roux, D. *J. Phys. II Fr.* **1993**, 3, 487–502.
- (34) Estimated rod thickness from Figure 5.6a is ~10 nm whereas from 5.6b, it is around rods look 20 – 30 nm thick.
- (35) Luzzati, V.; Mustacchi, H.; Skoulios, A.; Husson, F. *Acta Cryst.* **1960**, 13, 660–667.
- (36) Ropers, M.- H.; Stebe, M.- J. *Phys. Chem. Chem. Phys.* **2001**, 3, 4029–4036.
- (37) L_s and L_w for $\alpha > 10$ (Phase I) were calculated assuming that the position of the undetected first order Bragg peak was located at twice the q-value of the observed second order reflection.
- (38) Fontell, K. *J. Colloid Interf. Sci.* **1973**, 44, 318–329.
- (39) Splitting of the leek-like aggregates has not been observed in the FFEM images and therefore a direct count of the number of bilayers in one “leek” shaped aggregate could not be made.
- (40) Khan, A.; Fontell, K.; Lindblom, G.; Lindman, B. *J. Phys. Chem.* **1982**, 86, 4266–4271.

Chapter 6

Syntheses and characterization of (co)polymers from **1**

In this chapter, the syntheses and characterization of homopolymers from polymerizable fluorosurfactant (**1**) and model comonomer (**3**), as well as copolymers from **1** with **3** and styrene, are discussed. The polymers were synthesized by free radical polymerization in DMF solutions and characterized using FTIR, NMR and thermal analytical techniques like DSC and TGA. Attempts were made to study molecular weight of homopolymer of **1** using GPC. FTIR provides the clues that water is present within the ionic clusters of all polymers except the homopolymer of **3**. The ^{19}F NMR results show that large compositional drifts occur during the copolymerizations of **1** with **3**. Thermal stability of the homopolymer of **3** and copolymers containing **3** was observed to be somewhat lower to that of homopolymer of **1** and copolymers of **1** with styrene. Homopolymer of **1** forms long worm-like micelles in aqueous solution that were studied by Cryo-TEM. It is proposed that these micelles are formed by lateral assembly of 2-4 extended polymer chains of the homopolymer.

6.1 Introduction

A range of proton conducting polymers with aromatic and fluorocarbon backbone has been reported in the literature, as discussed in Chapter 1. Typically these polymers contain sulfonic acid ($-\text{SO}_3^-$) groups for proton transportation. These polymers have been characterized by investigating properties like, morphology,^{1,2} thermomechanical behavior,^{3,4} water desorption⁵ and proton conductivity.² These properties are highly relevant for the utility of these polymers as proton conducting membranes, and heavily depend upon the nature, percentage and distribution of ionic functionalities on their polymer chains.

This chapter is focused on the synthesis of homopolymers from polymerizable fluorosurfactants (**1**), (which provides the proton conducting $-\text{SO}_3^-$ groups) and model comonomer (**3**), and copolymers from **1** with **3** and styrene (**26**). These polymers are characterized and structure-property relationships are discussed.

6.2 Experimental Section

All the organic reagents and solvents were purchased from Aldrich and used without further purifications. Syntheses of **1** and **3** have been described in Chapter 3. Compound **3** is liquid and it was stored in the fridge at 2 °C without adding free radical inhibitor. Styrene, **26** was purified by washing three times with 10% NaOH solution and three times with deionized water. It was dried over MgSO_4 and stored in fridge at 2 °C until used. Dry DMF (99%) was used as the solvent for polymerization.

6.2.1 Polymer Synthesis

For homopolymerization of **1**, 300 mg (0.71 mmol) of monomer, and 1.5 mg (0.009 mmol) AIBN (98%) was dissolved in 3 ml DMF in a pyrex polymerization tube. (see Scheme 6.1 and Table 6.1). The solution was given three freeze-thaw cycles using argon as the inert atmosphere. The polymerization tube was flame-sealed under vacuum and heated at 55 °C for 48 hours (Figure 6.1).

After the reaction was completed, DMF was removed from viscous solution of **P1** using vacuum. Then the polymer was dissolved in minimum amount of acetone and precipitated using THF as the nonsolvent. The obtained polymer was dried under vacuum at 50 °C overnight. The yield was 230 mg, (78%), see Table 6.1.

All other polymers were synthesized under identical conditions in DMF with the molar quantities of monomers and AIBN as illustrated in Table 6.1. **P2** precipitated out of solution during the polymerization process. At the end of polymerization, DMF was removed from the precipitated **P2** and the polymer was washed with acetone. From **P3** and **P4**, DMF was removed under reduced pressure and the polymers were purified by dissolution in minimum amount of acetone and precipitation using THF as nonsolvent. The copolymers **P5** and **P6** were purified in similar manner but using diethyl ether as nonsolvent in the precipitation step. All polymers were dried at 50 °C overnight under vacuum. The yields of all polymers are depicted in Table 6.1.



Figure 6.1. A typical setup for free radical polymerization with flame sealed polymerization tube.

6.2.2 Polymer characterization

FTIR of the polymer samples were performed on Nicolet 6700 FT-IR Spectrometer in attenuated reflectance mode using diamond window. ^1H and ^{19}F spectra were measured in d_6 -DMSO solution, at 282.3 MHz and 75.4 MHz, respectively. For NMR experiments **P1**, **P5** and **P6** were dissolved in the appropriate amounts of d_6 -DMSO whereas **P3** and **P4** were sonicated with the solvent in NMR tubes. GPC was performed on the filtered solution of polymer **P1** in NMP at a concentration of 1 mg ml^{-1} . Polystyrene standards with narrow molecular weight distribution were used for molecular weight calibrations. A mixture of NMP/LiBr was used as the eluent at a flow rate of 0.5 ml/min at 40 °C. DSC and TGA were performed on PerkinElmer

instruments at $20\text{ }^{\circ}\text{C min}^{-1}$ under the flow of nitrogen. DSC was performed on >10 mg polymer samples kept in nonhermetic (unsealed) aluminium crucibles. The samples were heated at $20\text{ }^{\circ}\text{C min}^{-1}$ in the temperature range 25 to $250\text{ }^{\circ}\text{C}$. Thermal data was processed using Universal Analysis™ software by TA instruments. Cryo-Transmission Electron Microscopy images were obtained on a Philips CM120 electron microscope operating at 120 KV. Samples were prepared by depositing a few microliters of **P1**-water solution of appropriate concentration on a holey carbon coated grid (Quantifoil 3.5/1, Quantifoil micro tools GmbH, Jena, Germany). After blotting away the excess of liquid, the grids were plunged quickly in liquid ethane. Frozen-hydrated specimens were mounted in a cryo-holder (Gatan, model 626). Micrographs were recorded under low-dose conditions on a slow-scan CCD camera (Gatan, model 794).

6.3 Results and Discussion

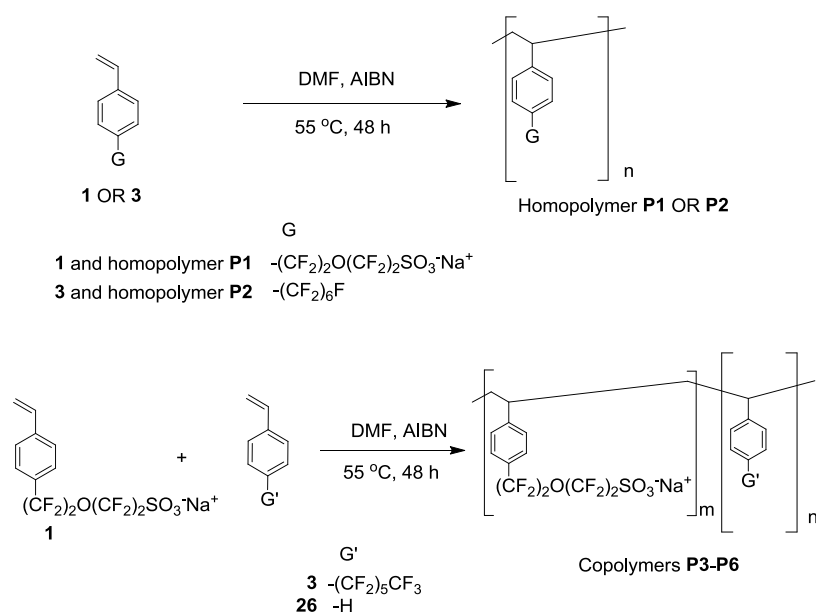
6.3.1 Synthesis of polymers

Homopolymers **P1**, **P2** and copolymers **P3-P6** were synthesized by free radical polymerization in DMF solutions as shown in Scheme 6.1. Homopolymer **P1** is soluble in polar solvents like water, DMSO, and DMF. In fact we did a test run of polymerization of **1** in water and obtained viscous solution of **P1** as in the case of polymerization in DMF.

During the polymerization of **3** in DMF, the polymer precipitated. Once the polymer chains come out of the solution, further chain propagation was not possible. Thus, most likely the precipitation restricted the growth of the polymer chains of **P2** to a threshold molecular weight. Polymer **P2**, was found to be insoluble in all the polar (like DMF, DMSO, DMAc) as well as nonpolar (DCM, toluene, chlorobenzene, etc.) solvents investigated. It was washed with acetone after removal of DMF by decantation and additional purification by precipitation was not possible.

All other polymers were purified by first dissolving them in minimum amount of acetone and precipitation using THF (for **P1**, **P3** and **P4**) or diethyl ether (for copolymers **P5** and **P6**) as nonsolvents. In the cases of **P3** and **P4**, at the end of polymerizations, the solutions became highly turbid. As the polymerization starts monomer **1** and **3** start to incorporate into the polymer chains with rates that are

characteristic to their relative reactivities. As in the case of **P2**, polymer molecules precipitated after sufficient percentage of **3** was incorporated into them. The turbid solutions suggested that the solubility of the polymer chains containing a threshold percentage of **3** was poor in DMF which resulted in precipitation. Due to the presence of ionic moieties (from **1**) on the polymer chains, most of the precipitated mass remains dispersed or forms an emulsion. The precipitated mass at the bottom of the tubes could be due to slow sedimentation of some of the precipitated fraction or from the polymer chains essentially made up of **3**. Since the precipitation restricted the growth of polymer chains further, **P3** and **P4** are expected to have largely restricted molecular weight polymer chains, similar to **P2**. The polymer solutions of **P1**, **P5** and **P6** became little hazy as the polymerization progressed. This could be due to sufficiently large micellar aggregates formed in DMF due to the presence of polymerizable fluorosurfactant (**1**) repeating unit in **P1**, **P5** and **P6**.⁶



Scheme 6.1. Syntheses of homopolymers **P1** and **P2** and copolymers **P3-P6** by free radical polymerization in DMF, using AIBN as the initiator.

Table 6.1 shows the molar quantities of monomers and the obtained yields of polymers **P1-P6**. Somewhat higher yields were observed for **P2**, **P3** and **P4**; it can be attributed to the fact that purification procedure is not effective to remove low molecular weight polymer chains from the polymer samples.⁷ We tried to determine molecular weight of **P1** by GPC. A broad peak with bimodal distribution was observed as shown in Figure 6.2. Not all the polymer chains came in the first elution

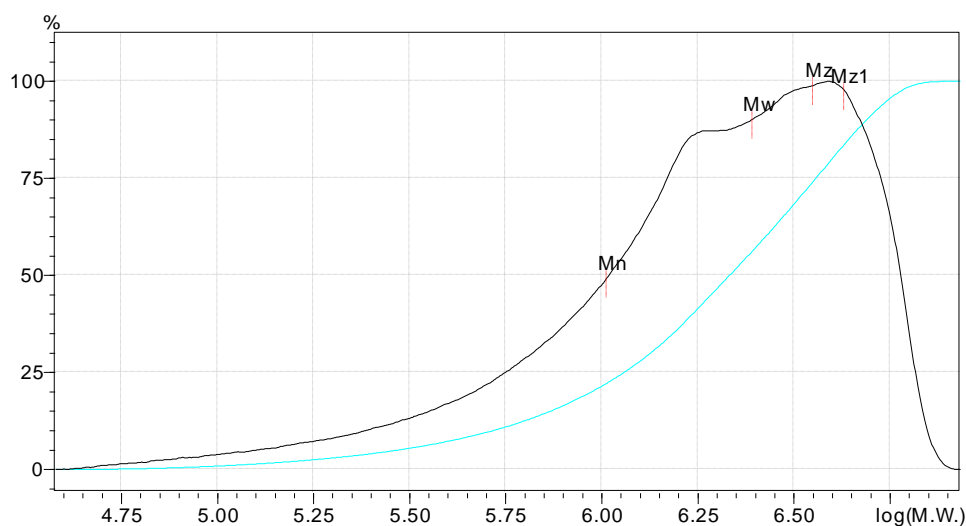
and in fact majority of them were observed to be coming in the second blank “only solvent” run.

Table 6.1. Monomers and initiator in mmol, polymer yield in percentage and in grams is shown. Also the comonomer ratio in feed and in actual polymer is depicted.

Polymer	Monomers/(mmol)			AIBN/ (mmol)	Yield/ g (%)	1: comonomer molar ratio	
	1	3	26			in feed	in copolymers
P1	0.71			0.009	0.20 (67)		
P2		1.18		0.015	0.43 (85)		
P3	1.30	1.18		0.032	0.84 (80)	1.1	^a 8.2
P4	0.92	1.54		0.032	0.85 (82)	0.6	^a 3.8
P5	1.25		4.54	0.030	0.73 (73)	0.3	
P6	0.91		5.92	0.030	0.70 (70)	0.2	

^a. Estimated from ^{19}F NMR of the soluble fractions of **P3** and **P4** in d_6 -DMSO.

This might be because some of the polymer chains of **P1** remain adsorbed inside the column which causes them to elute out in the second elution run.



Mn	Mw	Mw/Mn
1030000	2470000	2.5

Figure 6.2. GPC run on **P1** and estimated molecular weights are shown in accompanying table.

The calculated M_n is 1.03 million Daltons and M_w is 2.5 million Daltons respectively. Such high molecular weights have been obtained in the case of styrene polymerization by free radical method in microemulsions.⁸ It is important to note that **1** forms stable microemulsion in water up to 60 wt% of [**1**] that could facilitate growth of high molecular weight polymer chains. Although, usually it is not easy to investigate molecular weights of strongly aggregating fluorinated ionic polymers since they do not form true solutions. For instance, Nafion[®] forms aggregates in water at room temperature which break irreversibly to form molecular solution after heating the Nafion-water dispersion at >250 °C and GPC has been performed on these solutions at 40 °C.⁹ It is likely that **P1** might have formed aggregates in NMP/LiBr which could be the reason also for bimodal shape of the molecular weight distribution curve.⁹ No further attempts were made to do GPC on **P1** as well as other polymers with modified procedure.

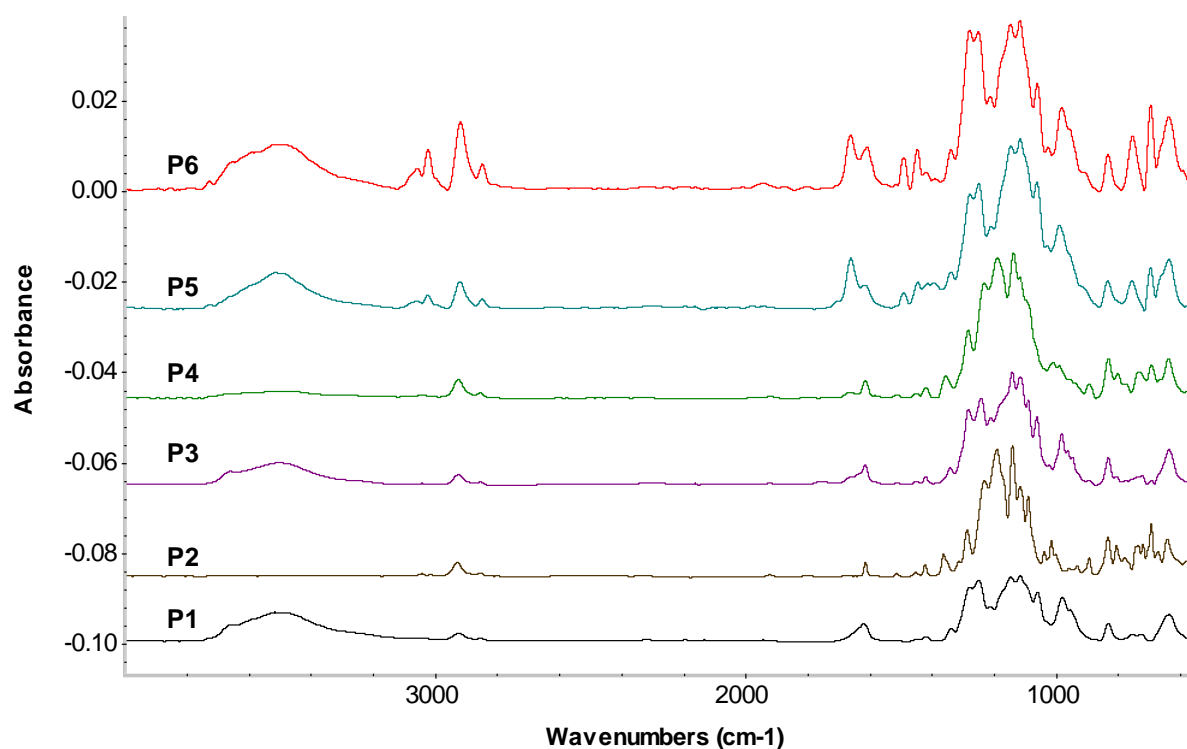


Figure 6.3. FTIR spectra of polymers **P1** and **P3-P6**. Spectra are recorded in the reflectance mode from the polymer particles.

6.3.2 FTIR spectra

Figure 6.3 illustrates FTIR spectra for **P1-P6**. Analysis of the spectra is challenging due to the presence of aromatic and fluoroalkoxy structure which give rise to several overlapping stretching and bending absorption peaks between 1500 and 400 cm^{-1} .

All polymers except **P2**, show a broad peak at $\sim 3520\text{ cm}^{-1}$ which is due to the H-O-H stretching⁵ of water molecules that are present in ionic clusters as well as those are directly coordinated with SO_3^- groups of the polymer. Typically drying these polymers at lower temperature $<150\text{ }^\circ\text{C}$, removes the adsorbed water molecules inside the ionic clusters. The coordinated water molecules can only be released above $150\text{ }^\circ\text{C}$.⁵ It is worth to note that all the polymers were dried using vacuum at $50\text{ }^\circ\text{C}$ overnight and stored in screw capped bottles. It is possible that 24 hours drying at $50\text{ }^\circ\text{C}$ might not be enough and due to atmospheric moisture, these polymers might have absorbed some water during storage. Aromatic C-H stretching bands between $3000\text{ to }3070\text{ cm}^{-1}$ from monosubstituted aromatic carbons of all polymers except **P5** and **P6** are either very weak or absent.¹⁰ Thus only for **P5** and **P6**, C-H stretching modes from sp^2 hybridized carbons of unsubstituted styrenic (**26**) segments of the polymer chains show up in FTIR. The aliphatic C-H stretching band between $2850 - 2960\text{ cm}^{-1}$ from -CH and CH_2 groups of polymer backbone is strong in all polymers.

Table 6.2. Some important IR absorption frequencies from polymers **P1-P6**.

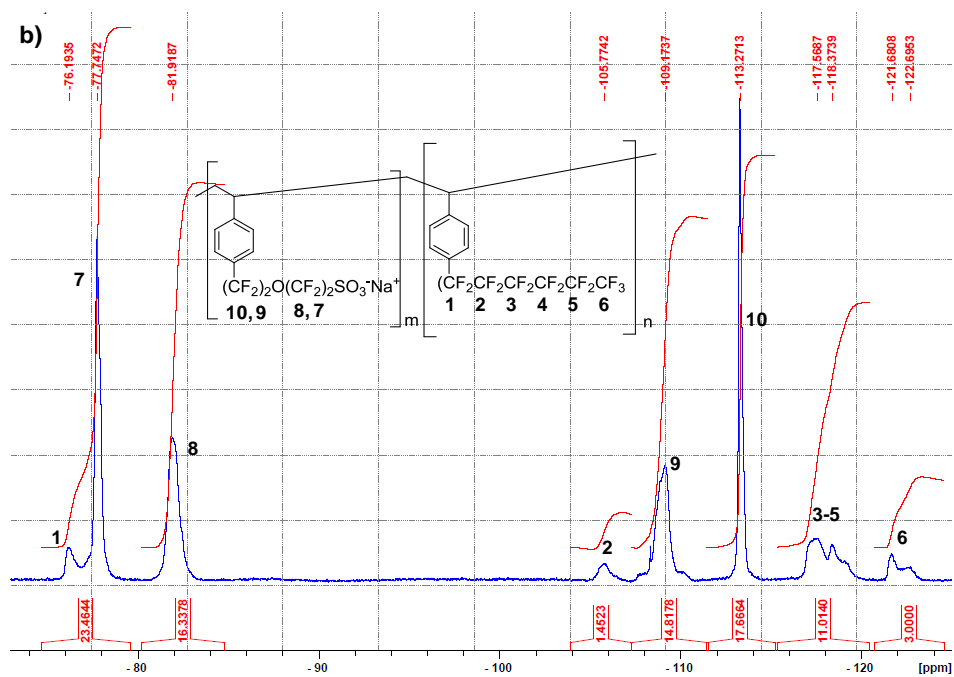
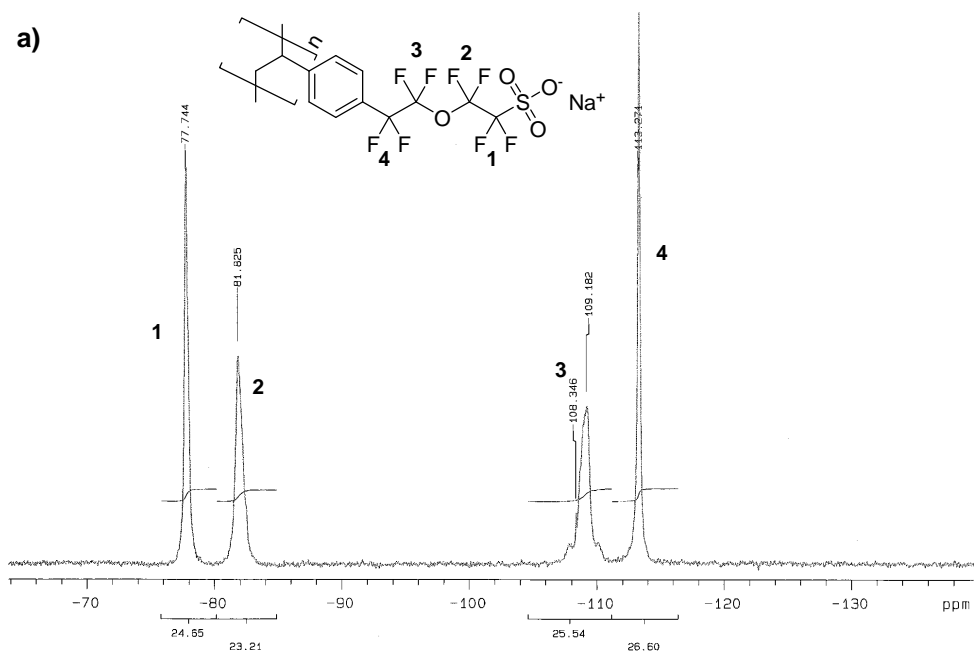
Type of absorption	IR Absorption (cm^{-1})
Aromatic CH str.	3000-3070
Aliphatic CH/ CH_2 str.	2850-2960
C=C from aromatic & HOH bend.	1620 to 1660
Phenyl	755
S=O str.	1420
C-F str.	1340
SO_3^- str.	1061
-S-OH str.	980
Aromatic CH bend.	600-900

Some other important absorption frequencies and their assignment are shown in Table 6.2. FTIR spectra thus reveal that water molecules are present inside the ionic functionalities.

6.3.3 NMR study

P1, **P5** and **P6** formed slightly hazy solution in d_6 -DMSO whereas **P3** and **P4** showed quite turbid solution with small amounts of precipitate at the bottom of the NMR tubes. Sonication of these solutions did not improve their visibility further. The NMR spectra for **P3** and **P4** were taken without further filtration.

^1H (not shown here) and ^{19}F NMR spectra of **P1** showed broad peaks indicative of polymeric structure. Also the characteristic signals for the monomers were mostly absent in the ^1H NMR spectra of all polymers. However it is not possible to comment on molecular weight, since we could not identify and integrate the peaks from the initiator fragments, which could have served as a reference peak for molecular weight calculation of the polymers. Further it is important to note that molecular weight determination by end group analysis technique like NMR is only accurate up to 30,000 Daltons.¹¹ ^1H NMR of all samples display three broad signals, respectively centered at ~ 1.45 ppm (protons from polymer backbone), ~ 6.5 ppm and 7.1 ppm (both for aromatic protons). **P5** and **P6** showed two extra shoulders, one at ~ 1.69 ppm overlapping the signal at 1.45 ppm and another at 7.27 ppm overlapping the signal at 7.1 ppm. Both shoulder peaks could have originated from styrenic (**26**) segments or the segments containing **1** due to some steric or other molecular interactions.¹² ^{19}F NMR of **P1** (Figure 6.3a) shows four signals (1-4) assigned to fluorine atoms on each $-\text{CF}_2$ and ^{19}F NMR of **P3** and **P4** (Figure 6.3b and c) display 8 signals assigned by numbers 1-10. Fluorine atoms in $-\text{CF}_3$ on perfluorohexyl chain are depicted by number 6. All other signals belong to fluorine atoms on each $-\text{CF}_2$.



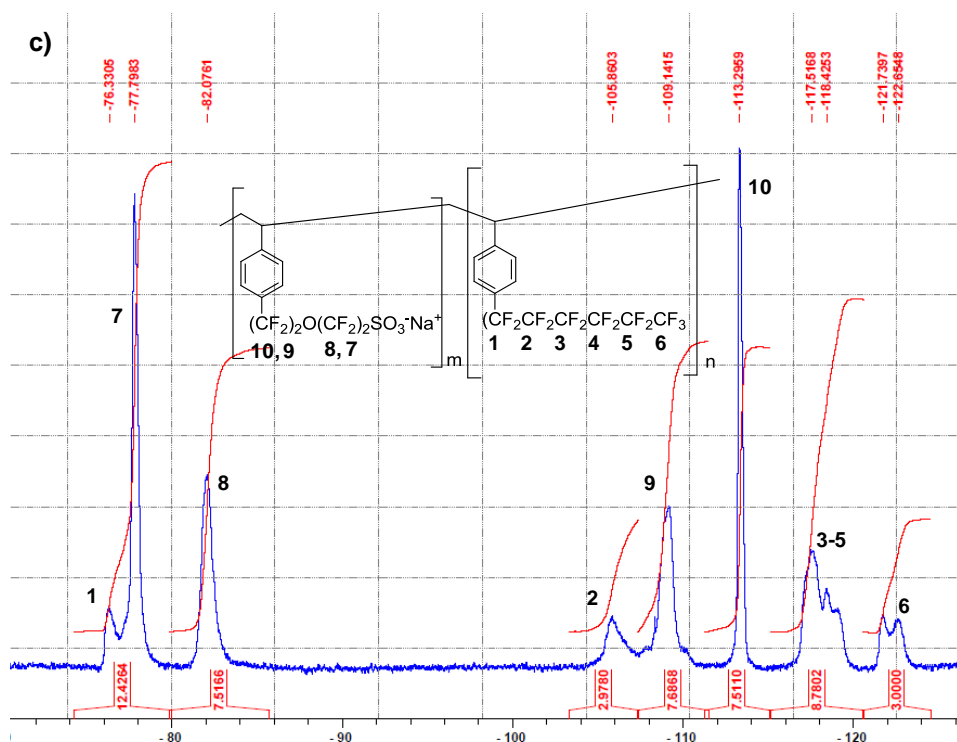


Figure 6.4a) ^{19}F NMR of **P1**, b) **P3**, and c) **P4** in d^6 -DMSO.

6.3.4 Comonomer ratio

Attempts were made to investigate the actual percentage of comonomers incorporated into copolymers **P3** – **P6** by studying ^1H and ^{19}F NMR as well as FTIR spectra of these copolymers. No separate distinguishable peaks were observed for **1** and **3** in ^1H NMR of the soluble fractions of **P3** and **P4**. Fortunately from ^{19}F NMR of the soluble fractions (Figure 6.4b) and c)), we could calculate the comonomer fraction of **1** and **3** incorporated into soluble fractions of **P3** and **P4** (by taking the ratios of the area of signal numbers 8:6).¹³ The comonomer ratio **1:3** in feed and that of actually incorporated into the soluble fraction of copolymers **P3** and **P4** are reported in Table 6.1. A big difference is observed between the comonomer feed ratio and comonomer ratio in the soluble fractions. Monomer **1** was found to be six to eight times more incorporated into the soluble fractions of **P3** and **P4** than the actual feed ratios. Comonomer **1:3** ratio in the soluble fraction of **P3** is 8.2, whereas that for **P4** is 3.8. These results suggest that *i*) a large compositional drifts occur during the polymerization with respect to the actual comonomer feed ratios for both polymers and thus *ii*) there is a big inhomogeneity of comonomers within the soluble and insoluble fractions.

In case of **P5** and **P6**, no resolvable signals were observed for two comonomer residues, of **1** and styrene (**26**) in ^1H NMR (two extra shoulders one at 1.69 ppm overlapping with signal at 1.45 ppm and another at 7.27 ppm overlapping the signal at 7.1 ppm).¹² Thus it was not possible to estimate **1:26** ratio in **P5** and **P6** by ^1H NMR.

It has been shown that styrene molecules with electron withdrawing moieties attached to the aromatic ring, polymerize faster than unsubstituted styrenes in controlled radical polymerization.¹⁴ Similar effects have been observed by Okamoto *et al* for the free radical polymerization of fluorine and fluorocarbon substituted styrenes.¹⁵

It is possible to study the comonomer ratio in the polymer by studying FTIR, if the individual signals from the comonomers are identified and ratio of the areas under the well resolved bands can be extracted. For **P5** and **P6**, signals between ~ 3000 and 3080 cm^{-1} (C-H stretching for aromatic SP^2 hybridized carbons) come from the unsubstituted styrenic (**26**) segments of the polymer chains. As discussed in FTIR subsection, in all other polymer samples, this band is either absent or has very weak intensity. This band along-with the C-H stretching signals coming from aliphatic SP^3 hybridized carbons of the polymer backbone is present in all polymers as well as normal polystyrene.¹⁰ It was not possible to normalize the area under these bands to respective molar ratio of aliphatic and aromatic carbons present in the polymer. Thus **1:26** ratio in **P5** and **P6** could not be estimated by FTIR as well.

6.3.5 Thermal characterization

Thermal properties of polymers **P1-P6** were studied using TGA and DSC. Figure 6.5a and b show the weight loss and the first derivative of the weight loss plotted against temperature for all polymers. Initial weight loss from polymer samples **P1** and **P3-P6** up to $\sim 150\text{ }^\circ\text{C}$ are due to the loss of water molecules adsorbed inside the ionic phases of the polymer samples (also see Table 6.3).⁵ **P1** shows maximum weight loss of $\sim 10\%$ at $150\text{ }^\circ\text{C}$. Copolymers **P3** and **P4** show weight loss of $\sim 6\%$, whereas **P5** and **P6** show lower weight loss (around 4%) at $150\text{ }^\circ\text{C}$. Thus the amount of water inside the ionic domains seems to be dependent on the percentage of **1** in the polymer samples (see comonomer molar ratios in the feed in Table 6.1). The

water molecules that are directly coordinated with the $-\text{SO}_3^-$ groups are lost during further heating up to $\sim 400^\circ\text{C}$.⁵ However, it is difficult to differentiate between water loss and weight loss due to other reasons above $\sim 200^\circ\text{C}$. Above this temperature, all polymers decompose rapidly. The presence of water within the ionic domains is in accordance with FTIR results.⁵

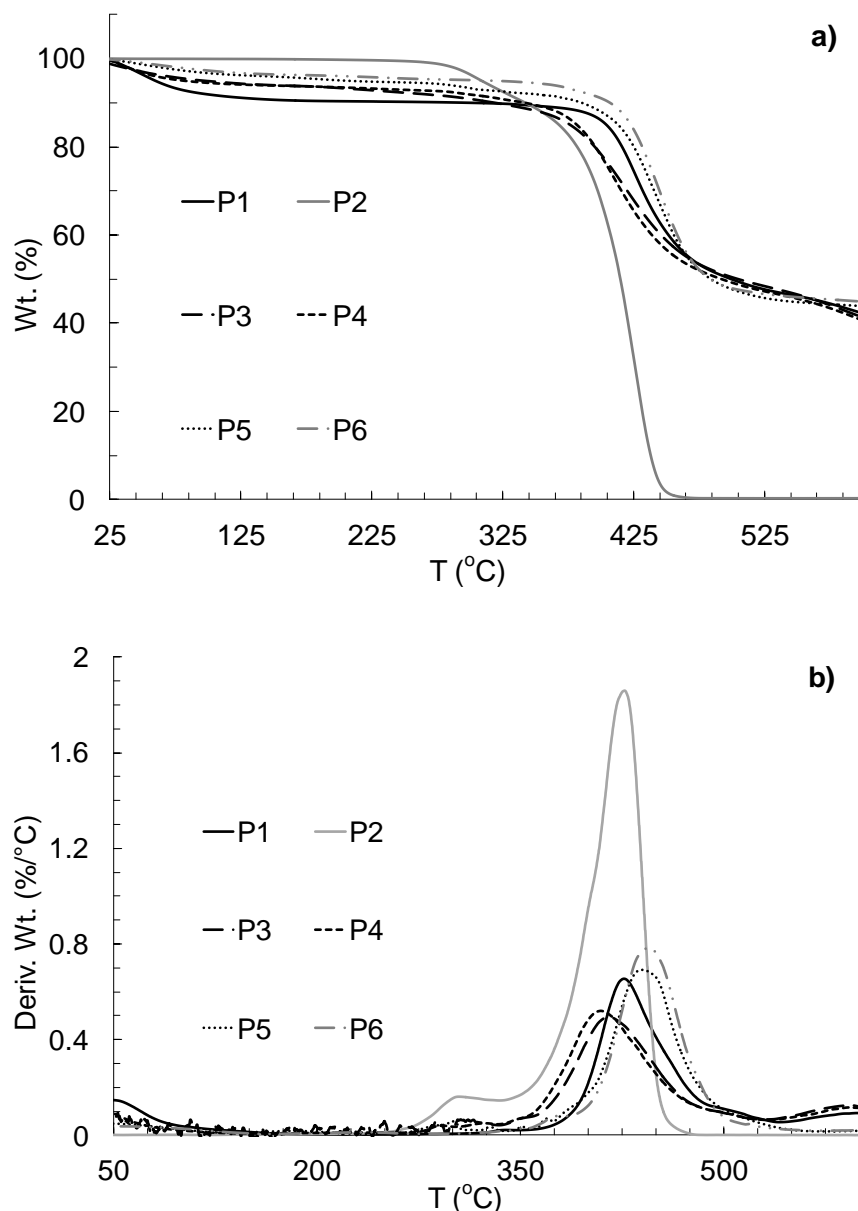


Figure 6.5a) TGA curves and **b)** derivative of weight loss with temperature of **P1-P6**. The heating rate was $20^\circ\text{C min}^{-1}$

As reported in Table 6.3, the temperatures with maximum decomposition rates (T_{md}) for **P1-P6** were found to be in the range of $410\text{--}450^\circ\text{C}$. They are higher compared to pure polystyrene ($\sim 400^\circ\text{C}$),¹⁶ similar to sulfonated polystyrene (variable from 420 to

450 °C)¹⁷ and somewhat lower than nafion[®] 117 with Na⁺ ions (>450 °C).⁵ In general, **P3** and **P4** display lower T_{md} whereas **P5** and **P6** have higher T_{md} values. **P2** shows a two step weight loss. Except **P2**, all polymer samples do not show 100% weight loss after 600 °C, owing to the inorganic residues that are left after heating them up to 600 °C. Thus TGA experiments demonstrate that the thermal stability of homopolymers is moderate whereas the copolymers containing **3** is the lowest and the thermal stability of those containing unsubstituted styrene is better than the homopolymers.

Table 6.3. Weight loss at 150 °C and maximum decomposition temperature for the synthesized polymers determined from TGA curves of **P1** to **P6**.

Polymers	(Wt. loss) _{150 °C} (%)	T_{md} (°C)
P1	90.6	425.6
P2	99.9	426.7
P3	94.0	415.0
P4	93.8	409.7
P5	95.9	440.8
P6	96.4	445.1

DSC experiments were carried out on all polymers to study their phase transitions. The glass transition temperature of ionic polymers depend upon the factors like type of backbone, nature of ionic interactions between their ionic groups, the percentage and distribution of ionic groups throughout polymer chains, the extent of phase separation and the distance of the ionic groups from the polymeric chains.^{4,16} Nafion[®] for example has two separate glass transitions one for the ionic microphase separated domain and another for the fluorinated polymer matrix. During these transitions, two endothermic peaks (one at around 160 °C and another at ~250 °C) were observed in DSC heating scans.⁴ Depending upon the thermal history of Nafion[®], one more peak above 300 °C was observed, attributed to the melting of the crystalline domain of polytetrafluoroethylene domain of the polymer. Only styrene **26** containing copolymers viz. **P5** and **P6** show glass transitions at 124 °C and 141 °C respectively. These values are comparable to T_g values of sulfonated polystyrene.¹⁶ Ionic polymers typically show higher T_g values compared to their parent polymers due to physical cross-linking created by ionic clusters. The relaxation time of the

polymeric chains increases due to formation of ionic clusters.⁴ This may have led to diminish the signals in DSC for other polymers.

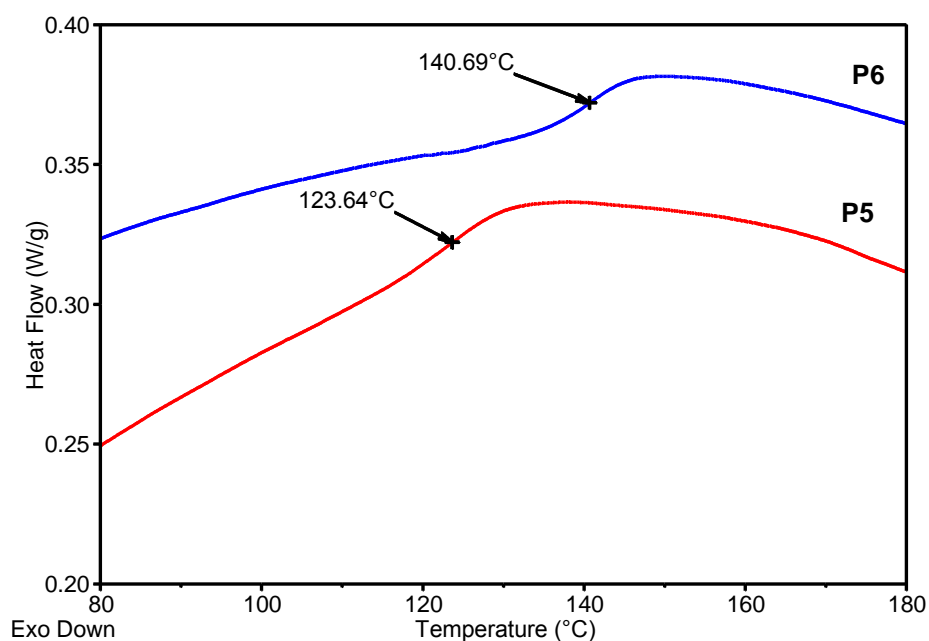


Figure 6.6. DSC, second heating scans for **P5** and **P6**. Heating rate was 20 °C min⁻¹

6.3.6 Cryo-TEM study on the micelles of P1

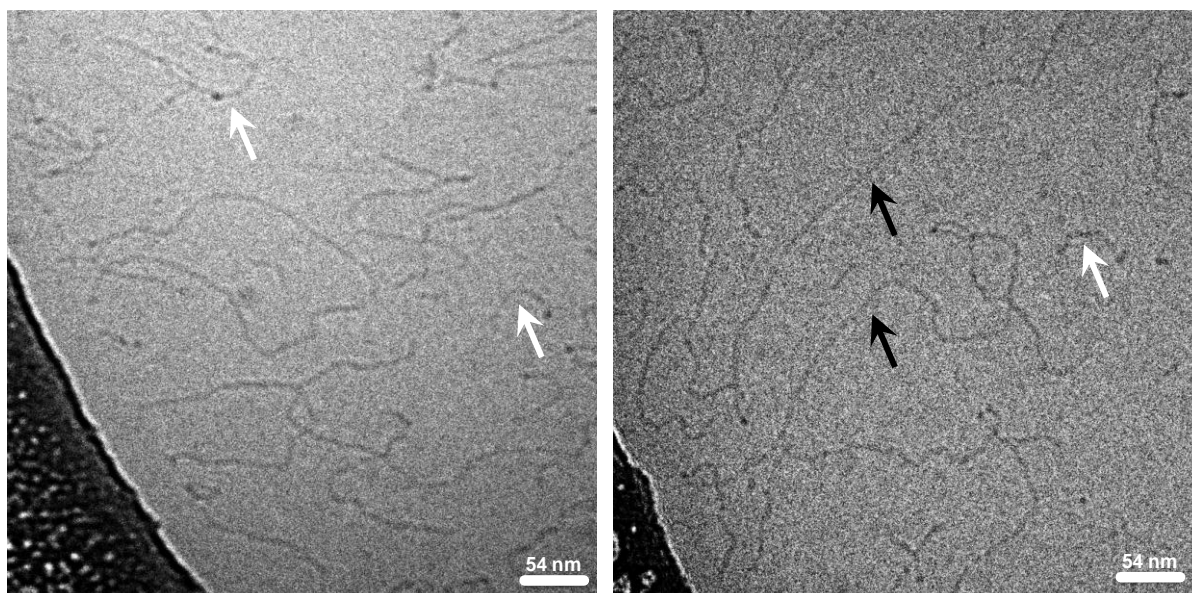


Figure 6.7. Cryo-TEM images of 0.1% **P1**-water solution. White arrows represent smaller micelles and black arrows represent longer micelles.

The phase behavior of **P1** in water by doing cryo-TEM of very dilute (0.1%) solution has been investigated. As shown in Figure 6.7, **P1** forms worm-like or thread-like micelles at such low concentration. Smaller micelles (shown by white arrows) are around 50-100 nm long whereas longer micelles (represented by black arrows) range from 200-400 nm roughly. Their diameter is around 5 nm for all the micelles consistently, which is roughly 2.5 times the diameter of a single stretched polymer chain.

Long worm-like micelles and super structures formed by assembly of these micelles have been observed for rod shaped poly(*p*-phenylene)sulfonates in water with diameter around 5 nm.¹⁸ Due to the peculiar molecular structure of **P1** (with hydrocarbon backbone, fluorocarbon spacer and $-\text{SO}_3^-$ group at the spacer end), the polymer chains can be expected to have extended conformation (also typically polyelectrolyte chains in dilute solutions attain such extended conformation due to electrostatic repulsion among the ionic moieties on them) in water. Thus, two to four polymer chains can be assumed to self-assemble to form worm-like micelles with their molecular axes oriented in the direction of micellar length as depicted in Figure 6.8.

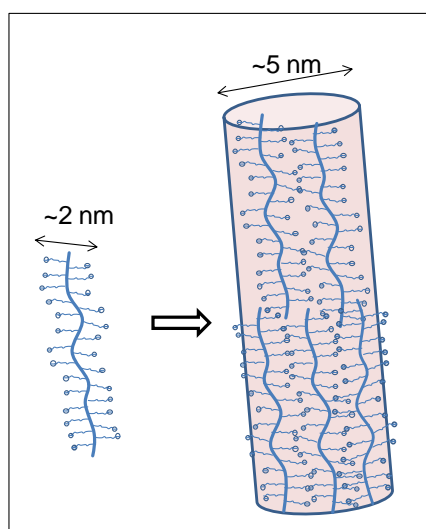


Figure 6.8. Pictorial representation of formation of worm-like aggregates from extended polymer chain of **P1** in water.

6.4 Conclusions

Polymers **P1-P6** were synthesized by free radical initiated polymerization in DMF. Due to strong interactions of ionic groups and fluorocarbon moieties, the molecular weights of **P1** could not be determined as suggested by the GPC results and the signals in the second “only solvent” elution run. Polymer **P2** was found to be insoluble in most of the polar as well as nonpolar solvents. FTIR study shows strong evidence of the adsorbed and coordinated water molecules inside the ionic clusters of the polymers **P1** and **P3-P6**. ^{19}F NMR of **P3** and **P4** revealed inhomogeneity within the soluble fractions of the polymer molecules due to large compositional drifts occurred during polymerization with respect to the comonomer feed ratios. Thermal stability of **P1**, **P5** and **P6** was found to be better than **P2**, **P3** and **P4**. Only **P5** and **P6** show weak signals at 124 and 141 °C respectively, in DSC measurements, owing to their glass transitions. Cryo-TEM on **P1**-water solution reveals that the polymer forms elongated worm-like aggregates with ~5 nm diameter and length of up to 400 nm. These self assembled structures are proposed to be formed by the lateral self-assembly of 2-4 extended polymer chains of **P1**.

6.5 References and notes

- (1) Mauritz, K. A.; Moore, R. B. *Chem. Rev.* **2004**, 104, 4535-4585.
- (2) Tsang, E. M. W.; Zhang, Z.; Yang, A. C. C.; Shi, Z.; Peckham, T. J.; Narimani, R.; Frisken, B. J.; Holdcroft, S. *Macromolecules* **2009**, 42, 9467-9480.
- (3) R. A. Weiss[†], S. R. Turner[‡], R. D. Lundberg *J. Polym. Sci. Polym. Chem. Ed.* **1985**, 23, 525-533.
- (4) Page, K. A.; Cable, K. M.; Moore, R. B. *Macromolecules* **2005**, 38, 6472-6484.
- (5) Wang, Y.; Kawano, Y.; Aubuchon, S. R.; Palmer, R. A. *Macromolecules* **2003**, 36, 1138-1146
- (6) For example, Nafion[®] also forms big micellar aggregates in the mixture of water and certain alcohols. Lee, S. -J.; Yu, T. L.; Lin, H. -L.; Liu, W. -H.; Lai, C.-L. *Polymer* **2004**, 45, 2853-2862
- (7) Due to poor solubility of **P3** and **P4**, purification was not efficient enough to remove low molecular weight polymer chains.
- (8) Gan, L. M.; Chew, C. H.; Lye, I.; Imae, T. *Polym. Bulletin* **1991**, 25, 193-198.
- (9) Curtin, D. E.; Lousenberg, R. D.; Henry, T. J.; Tangeman, P. C.; Tisack, M. E. *J. Power Sources* **2004**, 131, 41-48.
- (10) Pei, Z.; Busenlehner, L.; Worley, S. D.; Tang, Y.; Curtis, C. W. *J. Phys. Chem. B* **1997**, 101, 10450-10454.
- (11) Odian, G. *Principles of Polymerization*, 4th Ed., Wiley, New Jersey, 2004; pp 21.
- (12) ¹H nmr of pure polystyrene (in CDCl₃ solution) shows four peaks. Two are centered at 1.4 and 1.8 ppm for protons attached to backbone (aliphatic) carbons whereas two more are centered at 6.5 and 7.1 ppm for aromatic protons. These numbers are very close to the ¹H NMR values obtained for **P1**, viz. ~1.5, 6.5 and 7.1 ppm. The newly observed shoulders at 1.69 and 7.27 ppm are absent in homopolymer **P1** as well as in pure polystyrene. Since they are only observed in the copolymers of **1** and **26**, thus it is difficult to confirm if they are from unsubstituted styrenic (**26**) fragments or from **1**. Jessop, P. G.; Kozycz, L.; Ghoshouni Rahami, Z.; Schoenmakers, D.; Boyd, A. R.; Wechsler, D.; Holland, A. M. *Green Chem.* **2011**, 13, 619-623.
- (13) Peak number 8 is for -CF₂ and peak number 6 is for -CF₃. Intensity of Peak number 6 was normalized for -CF₂ and then the ratio for 8:6 was calculated.
- (14) Qiu, J.; Matyjaszewski, K. *Macromolecules* **1997**, 30, 5643-5648.
- (15) Teng, H.; Lou, L.; Koik, K.; Koike, Y.; Okamoto, Y. *Polymer* **2011**, 52, 949-953.
- (16) Chen, K.; Harris, K.; Vyazovkin, S. *Macromol. Chem. Phys.* **2007**, 208, 2525-2532.
- (17) Piboonsatsanasakul, P.; Wootthikanokkhan, J.; Thanawan, S. *J. Appl. Polym. Sci.* **2008**, 107, 1325-1336.
- (18) Kroeger, A.; Deimede, V.; Belack, J.; Lieberwirth, I.; Fytas, G.; Wegner, G. *Macromolecules* **2007**, 40, 105-115.

Chapter 7

General conclusions and future recommendations

The research in this thesis is focused to create foundation for engineering of *the self-assembled membrane and electrodes for PEMFC* from smaller building blocks namely polymerizable fluorosurfactant (**1**) and related compounds.

The design of the polymerizable fluorosurfactant, and the synthetic routes were based on availability of the starting precursor compounds, reactivity of the functional groups to modify them to desirable structure, and stability and the ability of the polymerizable group to undergo polymerization by conventional ways. Sulfinatodehalogenation reaction and copper mediated cross-coupling reactions were studied separately to generate the $-\text{SO}_3^-$ as well as styryl groups.

Compounds **1** and **2** were synthesized using the starting compound, sodium 5-iodooctafluoro-3-oxapentanesulfonate. Coupling of aromatic bromides to it by a copper mediated cross-coupling was the most suitable pathway. The presence of a sulfonate moiety did not interfere with this reaction. Styryl functionalized polymerizable fluorosurfactant **1** was synthesized in two steps, first coupling of the starting fluorocarbon sulfonate to 4-bromobenzaldehyde and second the conversion of the aldehyde moiety into the styryl group by a Wittig reaction.

The micellization properties of **1** and **2** were studied. Both surfactants are perfectly soluble in water at room temperature unlike several other fluorinated sulfonic acid salt surfactants. This enhanced solubility of **1** and **2** is due to the hybrid character of, and the presence of bulky aromatic moieties in the surfactant tails. Both surfactants form spherical micelles in their

water solutions. Both display comparable cmc values, surface tension values at cmc. The Gibbs energy of micellization of **1** and **2** are in the range of -24 to -26 kJ mol⁻¹. The aggregation numbers are low and in the range of 25 to 35. Micelle formation is largely driven by entropy changes where the dependence of the Gibbs energy of micellization on temperature follows a U-shaped relation.

The phase behavior of **2**-water mixture at high surfactant concentrations shows two lyotropic phases between 63 to 84 wt% [**2**]. An unusual supramolecular columnar (C_s) phase made up by self-assembly of “Leek” shaped aggregates was observed between 63 and 70 wt% [**2**] and a lamellar (L_α) phase was observed from 70 to 84 wt% [**2**]. The “Leeks” were shown to be formed by wrapping up of the **2**-water bilayers. The molecules of **2** were arranged into partially interdigitated or tilted or both fashions in the LLC phases.

Compound **1** easily undergoes polymerization by free radical method to give homo and copolymers with model comonomer, **3** and styrene. It is proposed on the basis of the GPC results and the signals in the second “only solvent” elution run, that due to strong interactions of ionic groups and fluorocarbon moieties, the obtained molecular weights of homopolymer of **1** are of the aggregates of **1**. Homopolymer of **3** was found to be insoluble in most of the polar as well as nonpolar solvents. The presence of water molecules inside the ionic clusters of the polymers was confirmed by FTIR. ¹⁹F NMR experiments revealed that the large compositional drifts with respect to the comonomer feed ratios occurred during the polymerization and there is inhomogeneity within the polymer samples. Thermal stability of copolymers of **1** with styrene was found to be the best among all polymers studied. Cryo-TEM on homopolymer of **1**-water solution revealed that the polymer forms elongated worm-like micelles with ~5 nm diameter and length of up to 400 nm. These micelles are proposed to be formed by the lateral self-assembly of 2-3 extended polymer chains of P1.

We propose that the further direction of this research would be to synthesize polymerizable fluorosurfactant with longer fluorocarbon spacers, and with fluorinated polymerizable moieties on them. Preparing and studying micellar phases of **1** and **2** with water and third component e.g. fluorocarbon oil could be interesting to obtain desired bicontinuous microstructured phases. Synthesizing and investigating block copolymers of **1** with appropriate comonomers can also be a possible direction to create self-assembled nanostructured PEMFC membranes and electrodes.

Summary

The purpose of this thesis is to create foundation to make improved electrodes and membranes for PEMFC. The research described in it dealt with the synthesis of the basic building blocks i.e. polymerizable fluorosurfactant (**1**) and non-polymerizable analogue (**2**) and study of their self-assembly properties. Similarly (co)polymerization behavior of **1** and the polymer properties are described.

The design of the polymerizable fluorosurfactant, **1** and the synthetic routes to obtain the desired functionalities and molecules are discussed in Chapter 1. The reaction pathways to create SO_3^- as well as styryl groups are described.

The syntheses of compounds **1** and **2** are described in Chapter 3. The key reactions viz. the copper mediated cross-coupling reactions to attach fluorocarbon molecules to aromatic moieties and the Wittig reactions to obtain styryl functionalities are described.

The micellization properties of **1** and **2** are deliberated in Chapter 4. Unlike, several fluorinated sulfonic acid salt surfactants, both surfactants were soluble in water at room temperature. This is due to their hybrid character and the presence of bulky aromatic moieties in the surfactant tails. Both display comparable cmc values ~ 30 mM, with spherical shaped micelles. The Gibbs energy of micellization of **1** and **2** are in the range of -24 to -26 kJ mol $^{-1}$. The micelles were characterized by low aggregation numbers, in the range of 25 to 35. Entropy driven micelle formation was observed and a U-shaped relation was observed between the Gibbs energy of micellization and experiment temperatures.

The LLC phase behavior of **2**-water mixtures is described in Chapter 5 and two lyotropic phases in the range of 63 to 84 wt% [**2**] were identified and studied. An unprecedented supramolecular columnar (C_s) phase made up by self-assembly of “Leek” shaped aggregates was observed in the concentration regime, 63 and 70 wt% [**2**] and a lamellar (L_α) phase was observed from 70 to 84 wt% [**2**]. The “Leeks” were shown to be formed by wrapping up of the **2**-water bilayers. Interdigitated and/or tilted assembly of **2** molecules was suggested in both LLC phases based on SAXS data analysis.

The homo and copolymers of compound **1** with model comonomer, **3** and styrene prepared by free radical method are discussed in Chapter 6. The strong interactions of ionic groups and fluorocarbon moieties of Poly**1** seem to cause difficulties in the molecular weight determination by GPC. Homopolymer of **3** is insoluble in most of the polar as well as nonpolar solvents. ^{19}F NMR experiments revealed that there are inhomogeneities within the polymer samples because of the large compositional drifts with respect to the comonomer feed ratios occurred during the polymerization. Thermal stabilities of all polymers were slightly better to the thermal stability of polystyrene. Cryo-TEM Poly**1**-water solution revealed the formation of elongated worm-like micelles with ~5 nm diameter and length of up to 400 nm. These micelles were suggested to be formed by the lateral self- assembly of 2-3 extended polymer chains of Poly**1**.

Sammenvatting

Het doel van dit proefschrift is het ontwerpen, creëren en elementaire bouwstenen voor de bouw van zelf-geassembleerde nanogestructureerde elektroden en membranen voor PEMFC te bestuderen. Het onderzoek beschreven over de synthese van polymeriseerbare fluor (**1**) en de niet-polymeriseerbare analoge (**2**) en de studie van hun zelf-assemblage eigenschappen. Evenzo worden de (co)polymerisatie gedrag van **1** en de polymeereigenschappen beschreven.

Het ontwerp van de polymeriseerbare fluorstof, **1** en de synthetische routes om de gewenste functionaliteiten te verkrijgen en moleculen worden besproken in hoofdstuk 1. De reactiepaden maken-SO₃⁻ en styryl groepen worden beschreven.

De syntheses van verbindingen **1** en **2** zijn beschreven in Hoofdstuk 3. De sleutel reacties weten. de koper gemedieerde cross-coupling reacties fluorocarbon moleculen hechten aan aromatische groepen en de Wittig reactie te verkrijgen styryl functionaliteiten beschreven.

De micellering eigenschappen van **1** en **2** zijn overlegd in hoofdstuk 4. In tegenstelling tot verschillende gefluoreerde oppervlakteactieve sulfonzuurzout, beide oppervlakte waren oplosbaar in water bij kamertemperatuur. Dit komt door het hybride karakter en de aanwezigheid van volumineuze aromatische groepen in het surfactant staarten. Beide verbindingen **1** en **2** geven vergelijkbare waarden cmc ~ 30 mM en vorm bolvormige micellen. De energie van Gibbs micellering van **1** en **2** in het traject van -24 tot -26 kJ mol⁻¹. De micellen werden gekenmerkt door lage aggregatie getallen in het bereik van 25 tot 35. Entropie aangedreven micelvorming en een U-vormige relatie waargenomen tussen de energie van Gibbs micellering en experiment temperaturen waargenomen.

De LLC fasegedrag van **2**-water mengsels wordt beschreven in hoofdstuk 5 en twee lyotrope fasen in het bereik van 63 tot 84 wt% **2** geïdentificeerd en onderzocht. Een ongekende supramoleculaire zuilvormige (C_S) fase gevormd door zelf-assemblage van "Leek" vormige aggregaten waargenomen in de concentratie regime tussen 63

en 70 wt% **2** en een lamellaire (L_α) fase werd waargenomen 70 tot 84 wt% **2**. De "Leek" bleken te worden gevormd door het wikkelen uit de 2-dubbellagen water. Een interdigitated en / of gekanteld samenstel van twee moleculen werd Zowel voor LLC fasen gebaseerd op SAXS gegevensanalyse.

Homo-en copolymeren van verbinding **1** met het model van de geperfluoreerde comonomeer werden **3** of styreen bereid door vrije radicalen methode, en worden besproken in hoofdstuk 6. De sterke onderlinge compatibiliteitsproblemen van ionische groepen en fluorocarbon groepen van poly**1** ernstig belemmerd het molecuulgewicht bepaald door middel van GPC. Homopolymeer of **3** is onoplosbaar in de meeste polaire en niet-polaire oplosmiddelen. ^{19}F NMR experimenten bleek dat er inhomogeniteiten in het copolymeer bereid uit monsters **1** en **3** door de grote samenstelling afwijkingen ten opzichte van de comonomeer verhoudingen voeder tijdens de polymerisatie. Thermische stabiliteiten van alle polymeren werden iets beter dan de thermische stabiliteit van polystyreen. Cryo-TEM Poly**1**-wateroplossing bleek de vorming van langgerekte wormachtige micellen met ~ 5 nm diameter en lengte van 400 nm. Deze micellen werden voorgesteld worden gevormd door de laterale zelfassemblage van 2-3 verlengde polymeerketens van Poly**1**.

Acknowledgements

Without the support, guidance and vigor from my supervisors, colleagues, friends and family, I could not have finished this PhD research successfully. I am highly grateful to them.

First, my heartfelt gratitude goes to my promoter, Stephen Picken and copromotor, Wolter Jager. I am really fortunate to have you as my mentors and supervisors.

Wolter, doing chemistry in the lab was made much easier because of you and thanks to the organic chemistry exercises, you insisted me to do. The frequent discussions, your critical comments on my work and writings have taught me immensely. Stephen, you were always available and keen to enlighten my knowledge. Your advices and ideas on molecular designs were so crucial that they have been implemented in this work. Your way of thinking is amazing, that helped to solve some intriguing queries in this research.

In true sense, without both of your guidance and care, this PhD thesis could not have seen the light of day.

Next, I would like to cordially thank Ger Koper, Gaby Janssen, Ernst Sudhölter, Eduardo Mendes, and, Kristina Djanashvili for being amenable and for the expertise they provided to bolster this work. Ger, your pizza lectures were “delicious” and quite helpful while studying surfactant properties. I especially acknowledge your travel to Brussels just for the discussion of the paper. Ernst, discussions with you were very vital, especially in the final phase of this work. It was nice to be the part of NOC group. Eduardo, I learnt a lot from you and I appreciate your enthusiasm for explaining the complicated polymer physics. Kristina, your contributions to this work are indispensable. Doing NMR experiments and their interpretation was made so much simple because of you, thanks a lot for that. I would like to further acknowledge Jan, Rienk for occasional discussions and support you provided while working in SAS lab. Gaby, your critical remarks on the work, suggestions and valuable inputs on scientific writings were very much helpful. You organized our meetings meticulously. I also thank Andreas Schmidt-Ott for kindly accepting to become the reserved jury member for the PhD defense.

During this work, two new collaborations were made with the research groups outside the Netherlands. Special mentions and thanks to Prof. Dganit Danino from Israel and Prof. Bruno Ameduri. Dganit, this thesis consists of some important results obtained from your lab. Collaborating with you has been exceptionally prolific. I am very grateful for all your assistance and inputs for the manuscript on the LLC phases. Bruno, thank you very much for your support for the scientific proposal, for becoming the reviewer for the defense as well as for giving me the postdoctoral opportunity in Montpellier.

There are several people from NSM, NOC and, SAS groups who helped, contributed to this thesis and who made my PhD life enjoyable, whom I am highly indebted to. All the technical experts, who responded quickly and helped me in every stage of this work, are greatly cherished. Gerard, Ben, Piet, Marcel, Lars, Mark, and Louw, you made working in ChemE very easy by prompt service and help. Gerard, your help for the fuel cell practicum was vital. Ben, Piet and, Marcel, many thanks to you for all the assistance and resources you gave when I needed them very much. I sincerely value your patience and persistence to my frequent characterization requests.

The secretarial staff of ChemE has been very efficient. Wil, Karin, Astrid, Marjan, because of you, several official procedures, filling out forms, travel bookings could never scare me. Wil and Karin, I am truly obliged to you for being extremely helpful throughout all PhD years. It would have been very difficult in the final phase of my PhD to deal with various official procedures.

Several PhD and postdoc colleagues whose help have been invaluable to my PhD research. Krishna, Job, Stefan, Antonia, Thelma, Hayley, Dainius, Cristian, Christoph, Xiaoyan, Aurelie, Marta, Arek, Feng, Natalia, Arjend, please accept my sincere gratitude for everything you did for me.

Krishna, you have been a great precious friend and colleague to me. I do not remember of a time during my PhD when I asked for some help from you and you didn't provide it. Job, and Christoph your contributions in this research are of great importance. Job, your critical remarks on the manuscript on micellization made a big difference to its quality.

There are some friends and colleagues who filled my life during as well as after working hours with big rejoice. Murthy, Venkatesh, Chetan, Somnath, Madan, Amol, Nirmal, Ahson, Girish, Sameer, Sudam, Kedar, Jaweed, Kaustubh, Sachin and, Supriya, thank you for all the fun and your assistance. It will be difficult to forget enjoyable moments that I have spent with you.

I would also like to thank Prof. Frank Wuerthner, Andreas Lohr and the group members from Wuerzburg. Frank, I learnt some interesting organic chemistry in your lab. Thank you for the opportunity that you provided me. It created the base for my future research.

I greatly obliged to people from Brussels, Bruno van Mele, Guy van Asche, Gil Scheltjens and group members. Bruno and Guy, it was a great learning experience to be in your group. Cordial thanks for all the assistance. Gil, it would have been quite difficult without your help.

My research career started at National Chemical Laboratory, India. Several people at NCL have shaped my research career, mentored me, given me assistance at several occasions and are very good friends of mine. I owe them a lot. The list consists of, although not in a particular order: Dr. Ashish Lele, Dr. K. Guruswamy, Dr. Premnath, Dr. Prakash Wadgaonkar, Aarti, both Abhijeets, Amit, Ankush, Chandrashekhar, Ganapathy, Grace, Nilesh, Prakash, Shailesh, Samir, Sanket, Vikrant, Vipin, Wasif and many others whose names I might have forgotten.

Lele sir, your assistance when I was in the final stages to complete this thesis, is deeply admired. Guru and Premnath, thank you for giving me opportunity to work with you. I have learnt so much from both of you. Guru, the way you motivated me during NCL days is wonderful. Wadgaonkar sir, special thanks to you for all the assistance. Abhijeet, Amit, Ankush, Chandu, Samir, Wasif, Vijay, Prafulla, Gokul and Rahul, I cherish your long lasting friendship, love and support.

From my Masters, I would like to thank Prof. Maldar, Prof. Lonikar, Prof. More, Dr. Ankolekar and Dr. Ghanwat for making me capable to take on the research career.

आई, बाबा आणि कौस्तुभ, तुमचे patience आणि प्रेम यामूळेच मी ईथवर पोचू शकलो आहे. प्रिय माधवी, तुझ्याशिवाय हा thesis आणि जीवन दोन्हीही अपूर्णच राहिले असते! चि. वेदिनी, तुझ्या हसण्या खिदळण्यामुळे सगळेच सुंदर होते. आई, दादा आणि सुमीत, या सर्वांमध्ये तुमचा support अतिशय महत्वाचा ठरला आहे. शेवटी, अविमामा आणि अंजलीमामी, तुमचा ऋणनिर्देश केल्याशिवाय thesis complete होणार नाही.

Curriculum Vitae

Mohan Wadekar was born on April 9, 1979 in Satara, India. After completing his education up to Bachelors in Science with major subject as Chemistry, he became highly interested in polymer materials. For that reason, he moved to Solapur to do a Masters in Polymer Chemistry at Post Graduate Teaching center, Shivaji University. Since September 2001 until February 2005, he worked at National Chemical Laboratory, Pune, as a Project assistant II. His work initially involved “the study of molecular structure-properties relationship of polyolefins” and later “synthesizing nanodimensional polymeric as well as inorganic metal particles in soft lyotropic liquid crystalline phases of nonionic surfactants”. Later he worked at Wuerzburg Universtiy in Germany until February 2006, on the organic synthesis and properties study of merocyanine dyes.

In June 2006, he got an opportunity to start a PhD in Nano-Structured Materials group, TUDelft, the Netherlands on the project of “Self-Assembled Nanostructured electrodes for PEMFCs”. In Delft, his work has been focused on the synthesis of polymerizable fluorosurfactants and related molecules. He has investigated surfactant properties as well as the polymerization behavior of them. Later, he did a postdoctorate on “the synthesis and thermal characterization of plasma polymer coatings” in Vrije Universiteit Brussel, Belgium. From December 2012, he is going to work at University of Montpellier II, France for his second postdoctorate and work there on fluorinated polymers.

Publications

1. Wadekar *et al* "Thermal characterization of plasma polymerized allylmethacrylate in a dielectric barrier discharge reactor" manuscript under preparation.
2. Wadekar, M. N. Djanashvili, K.; Mendes, E.; Abezgaus L.; Danino, D.; Jager, W. F.; Picken, S. J. "Supramolecular and interdigitated self-assembly of anionic fluorinated surfactants in lyotropic liquid crystalline phases" manuscript under preparation.
3. Wadekar, M. N.; Boekhoven, J.; Jager, W. F.; Koper, G. J. M.; Picken, S. J. "Micellization behaviour of aromatic moiety bearing hybrid fluorocarbon surfactants" *Langmuir* **2012**, 28, 3397-3402.
4. Wadekar, M. N.; Jager, W. F.; Sudhölter, E. J. R.; Picken, S. J. "Synthesis of a polymerizable fluorosurfactant for the construction of stable proton conducting membrane" *J. Org. Chem.* **2010**, 75, 6814-6819. (Most read from JOC in year 2010).
5. Wadekar, M. N.; Jager, W. F.; Kowlgi, K. N. K.; Koper, G. J. M.; Janssen, G. J. M.; Lebedeva, N. P.; Picken, S. J. "Polymerizable Fluorosurfactants to Improve Performance of PEMFC Electrodes" *Abstracts of Papers, 238th ACS National Meeting, Washington DC, USA, August 2009*, POLY-092 (**Preprint**, Oral).
6. Wadekar, M. N.; Pasricha, R.; Gaikwad `A. B.; Kumarswamy, G. "Polymerization in surfactant liquid crystalline phases" *Chem. Mater.* **2005**, 17, 2460-2465.
7. Kumaraswamy, G.; Wadekar, M. N.; Agrawal, V. V; Pasricha, R. "Polycondensation in liquid crystalline phases of nonionic surfactants. Kinetics and morphology" *Polymer* **2005**, 46(19), 7961-7968.
8. Wadekar, M. N.; Pasricha, R.; Gaikwad, A. B.; Kumarswamy, G. "Polymerization in surfactant lyotropic liquid crystalline phases" *MACRO 2004, Thiruvananthapuram, India, December 2004* (Preprint, oral).